11-8-2016

Phasor Measurement Unit Data-based States and Parameters Estimation in Power System

Hossein Ghassempour Aghamolki
University of South Florida, hossein1@mail.usf.edu

Phasor Measurement Unit Data-based States and Parameters Estimation in Power System

by

Hossein Ghassempour Aghamolki

A dissertation submitted in partial fulfillment
of the requirements for the degree of
Doctor of Philosophy
Department of Electrical Engineering
College of Engineering
University of South Florida

Major Professor: Zhixin Miao, Ph.D.
Tapas Das, Ph.D.
Lingling Fan, Ph.D.
Fangxing Li, Ph.D.
Wilfrido Moreno, Ph.D.

Date of Approval:
October 24, 2016

Keywords: State Estimation, PMU, Kalman Filter, Second Order Conic Programming, Semi-Definite Programming Cut

DEDICATION

To my lovely wife and my parents

ACKNOWLEDGMENTS

First of all, I would like to express my sincere gratitude to my advisor Dr. Zhixin Miao for his help, guidance, training and support.

Second, I would like to thank Dr. Lingling Fan for her unlimited help and guidance during my research and project work. I would also like to thank the other committee members, Dr. Tapas Das, Dr. Fangxing Li and Dr. Wilfrido Moreno, for their encouragement and constructive comments toward significant improvement of my dissertation.

I owe my thanks to my recent and former colleagues from the smart grid power system lab, in particular Vahid Rasouli, Mohemmed Alhaider, Javad Khazaei, Lakanshan Prageeth Piyasinghe for the discussions, help and enjoyable atmosphere in the lab.

Last but not the least, I would like to especially thank my wife, Saeedeh Hosseini, for all of her sacrifices, endless love and outstanding support during my studies. I would also like to extend my thanks to my parents, Nikzad Ghassempour and Golkhanom norozi, for all of their support and encouragement in my life.

TABLE OF CONTENTS

LIST OF TABLES

LIST OF FIGURES

ABSTRACT

The dissertation research investigates estimating of power system static and dynamic states (e.g. rotor angle, rotor speed, mechanical power, voltage magnitude, voltage phase angle, mechanical reference point) as well as identification of synchronous generator parameters. The research has two focuses:

i Synchronous generator dynamic model states and parameters estimation using real-time PMU data.

ii Integrate PMU data and conventional measurements to carry out static state estimation.

The first part of the work focuses on Phasor Measurement Unit (PMU) data-based synchronous generator states and parameters estimation. In completed work, PMU data-based synchronous generator model identification is carried out using Unscented Kalman Filter (UKF). The identification not only gives the states and parameters related to a synchronous generator swing dynamics, but also gives the states and parameters related to turbine-governor and primary and secondary frequency control. PMU measurements of active power and voltage magnitude, are treated as the inputs to the system while voltage phasor angle, reactive power and frequency measurements are treated as the outputs. UKF-based estimation can be carried out at real-time. Validation is achieved through event play back to compare the outputs of the simplified simulation model and the PMU measurements, given the same input data. Case studies are conducted not only for measurements collected from a simulation model, but also for a set of real-world PMU data. The research results have been disseminated in one published article.

In the second part of the research, new state estimation algorithm is designed for static state estimation. The algorithm contains a new solving strategy together with simultaneous bad data detection. The primary challenge in state estimation solvers relates to the inherent non-linearity and non-convexity of measurement functions which requires using of Interior Point algorithm with no guarantee for a global optimum solution and higher computational time. Such inherent non-linearity and non-convexity of measurement functions come from the nature of power flow equations in power systems.

The second major challenge in static state estimation relates to the bad data detection algorithm. In traditional algorithms, Largest Normalized Residue Test (LNRT) has been used to identify bad data in static state estimation. Traditional bad data detection algorithm only can be applied after state estimation. Therefore, in case of finding any bad datum, the SE algorithm have to rerun again with eliminating found bad data. Therefore, new simultaneous and robust algorithm is designed for static state estimation and bad data identification.

In the second part of the research, Second Order Cone Programming (SOCP) is used to improve solving technique for power system state estimator. However, the non-convex feasible constraints in SOCP based estimator forces the use of local solver such as IPM (interior point method) with no guarantee for quality answers. Therefore, cycle based SOCP relaxation is applied to the state estimator and a least square estimation (LSE) based method is implemented to generate positive semi-definite programming (SDP) cuts. With this approach we are able to strengthen the state estimator (SE) with SOCP relaxation. Since SDP relaxation leads the power flow problem to the solution of higher quality, adding SDP cuts to the SOCP relaxation makes Problems feasible region close to the SDP feasible region while saving us from computational difficulty associated with SDP solvers. The improved solver is effective to reduce the feasible region and get rid of unwanted solutions violate cy-

cle constraints. Different Case studies are carried out to demonstrate the effectiveness and robustness of the method.

After introducing the new solving technique, a novel co-optimization algorithm for simultaneous nonlinear state estimation and bad data detection is introduced in this dissertation. ℓ_1-Norm optimization of the sparse residuals is used as a constraint for the state estimation problem to make the co-optimization algorithm possible. Numerical case studies demonstrate more accurate results in SOCP relaxed state estimation, successful implementation of the algorithm for the simultaneous state estimation and bad data detection, and better state estimation recovery against single and multiple Gaussian bad data compare to the traditional LNRT algorithm.

CHAPTER 1

INTRODUCTION

1.1 Background

Nowadays, our society's life depends on the critical infrastructures such as electric power systems, telecommunication networks, and water distribution networks. Steady growth in size, complexity, level of uncertainty, and unpredicted behavior of such systems, make the designing, monitoring, and controlling of the systems become more and more challenging every day. All of these critical infrastructures operation relies on the electric power system. Therefore, secure and relatable operation of power systems are essential for modern societies.

Continuously maintaining the balance between power generation and consumption is the main objective for the power system operation and control. Traditionally, (SCADA) system with the low-density sampling rate and nonsynchronous data are used for monitoring and control of the system. SCADA system consists of an SCADA control center and Remote Terminal Units (RTU). Traditional SCADA system can only be used for static estimations because of its limitations which are:

- Data refresh rate is around 2 to 5 seconds.
- Measurement signals are not synchronized.
- It is an offline estimation, and the results aren't reliable.

After 1965 Northeast blackout (Fig. 1.1), a federal commission was appointed to investigate the reasons which caused the blackout. One of the critical reasons found by the federal

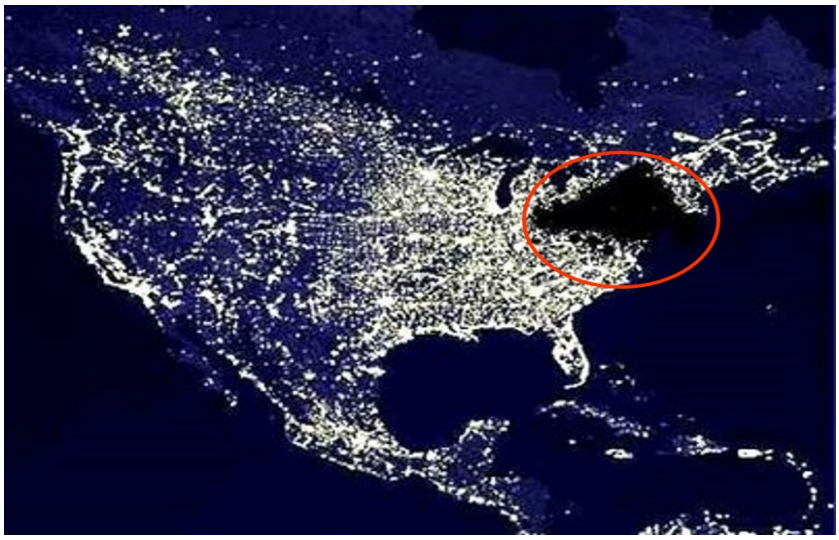

Figure 1.1. Famous 1965 northeast blackout

commission was that the absence of real-time knowledge within the utilities. Consequently, one of their suggestions to avoid the same problem in the future was establishing a real-time measurement system [1]. This was the starting point for the utilities to reform SCADA system and replace it with wide area measurement and control(WAMC) system and using real-time state estimation algorithm.

1.1.1 Phasor Measurement Unit (PMU)

The Phasor Measurement Unit (PMU) is a device capable of measuring synchronized time-stamped voltage and current phasor in power system. PMU using synchronized signal from GPS (global positioning satellite) to create same time phasor measurement sampling with time-stamped. Time synchronization allows synchronized real-time measurements of multiple remote measurement points on the grid. The resulting measurement is known as a synchrophasor. PMUs are considered to be one of the most important measuring devices in the future of power systems [2].

Fig. 1.2 shows the block diagram of hardware in a PMU device [3]. Anti-aliasing filter has been used to filter out frequencies above Nyquist rate from the input waveform. The GPS one pulse per second is converted into a sequence of high-speed timing pulses used in the waveform sampling by the phase locked oscillator. The microprocessor has the responsibility to execute the DFT phasor calculations. Finally, the phasor is time-stamped and uploaded to a collection device known as a data concentrator [3].

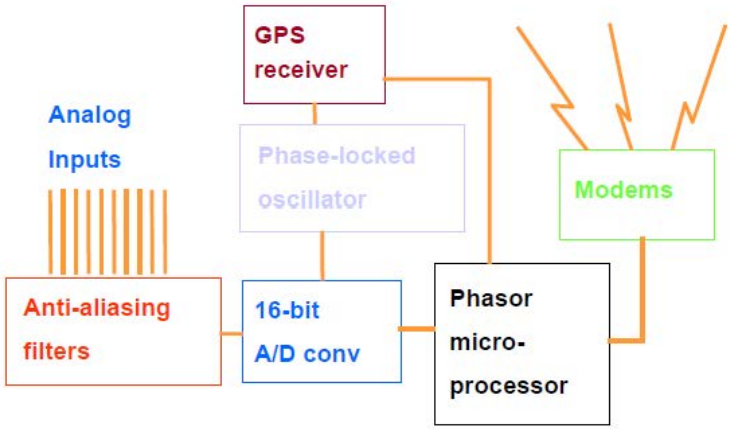

Figure 1.2. Hardware block diagram of a PMU

PMU has a wide range of applications in power system. Some of its applications are as follows:

- Wide area visualization and monitoring
- Real-time angle and frequency monitoring
- Inter-area oscillation detection and analysis
- Proximity of voltage stability
- Online state estimation

- Fast frequency regulation
- Transmission fault location estimation
- Parameters estimation and dynamic model validation

In summary, the benefit of PMU in power system is to improve the monitoring and control of the grid by providing a real-time accurate snapshot of the system state at any time. PMU high sampling rate which can be up to 60 samples per second, enables dynamic phenomena to be observed and thus online state estimation, contingency analysis, and load flow algorithms can be applied to determine states of the power system at any time. Determining state variables of the system can lead to understanding the current environment and being able to accurately anticipate future problems and to be able to implement effective preventive actions. Furthermore, a precise snapshot of the system which provided by one microsecond accuracy of GPS signal highly improves post-disturbance analysis which helps to analyze the vulnerability of the system for any future incidents.

1.1.2 Wide Area Measurement and Control

In recent years, phasor measurement units (PMUs) equipped with GPS antennas have been widely used to monitor different points of power grids. PMU allows 6-60 Hz measurement data to be sent to the control center. Therefore, a large quantity of information obtained from power system can be employed for system monitoring and control. Wide area measurement system consists of PMUs, advance communication technology, data management tools, and operational infrastructure that used to monitor and control of large, complicated power grids. Fig. 1.3 shows the WAMC structure [4]. As it can be seen, PMUs measure the voltage and current phasor at different points of the system and send the data to the control center by using standard protocols such as IEEE C37-118. The control center is equipped with the database software which can save received data. After data process-

ing procedure gathered data would be used in phasor data applications such as real-time monitoring, state estimation, on-line power flow and etc.

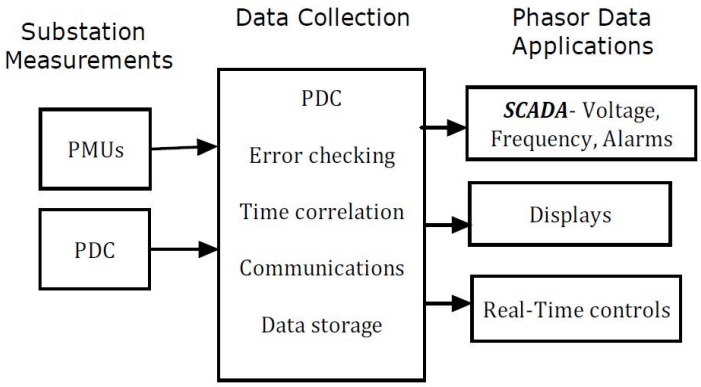

Fig. 7. Wide area measurement system using PMUs

Figure 1.3. Wide area measurement and control system using PMU

1.2 State and Parameter Estimation in Power System

1.2.1 State Estimation in Power System

As it has been discussed, it is critical for power grid operators to have the knowledge about the state of the system at any time in order to grantee reliable and efficient operation of the system. Therefore, state estimation techniques were developed in the 1970s. At that time, traditional SCADA system only had the capability of low sampling rate measurements (from seconds to minutes). Therefore, only centralized steady state system model was used for implementing state estimation. That is why power system state estimation is treated as static state estimates. In traditional SCADA systems, RTUs are gathering the data from widely spread locations within the power system which means the data have to be sent from a significant distance to the data center. Therefore, communication problems and data latencies are important problems for traditional SCADA systems. Furthermore, because the

time-stamped is not accurate for RTU measured data and it is independent of RTU locations, it can introduce significant biases in state estimation [5].

Introducing PMUs with GPS common reference signal enables synchronized phasor of voltages and currents to be measured with high-density sampling rate up to 60 samples per second, which makes the dynamic model state estimation possible and thus, enhances power system situation awareness. The objectives of PMU based state estimation are:

- To give accurate states of the power system by filtering, smoothing and bad data elimination from WAMC real-time measurement data.
- To provide a consistent power system security assessment by using online power flow, online contingency analysis, and online frequency and voltage monitoring and control algorithms.
- to obtain the best estimation for states and parameters of the dynamic model of the system.

The power system states are phasor voltages of the buses and their complex power phasor that can be used to determine all the other parameters of the system. Therefore, synchronophasor measurements from PMU devices which contain voltages and currents phasor of specific nodes of the grid are used as the measurement inputs of the state estimator. Also, system configuration provided by topological processor together with the network parameters, is used as other input of state estimator. The estimator uses those inputs to run dynamic state estimation algorithm in order to determine all of the states and unknown parameters of dynamic model as well as the processing results of measurement errors. Fig. 1.4 shows the block diagram of the power system state estimation procedure.

PMU online data can be used for states estimation of the power system as well as parameter estimation of dynamic models. In the better words, dynamic model state and parameter

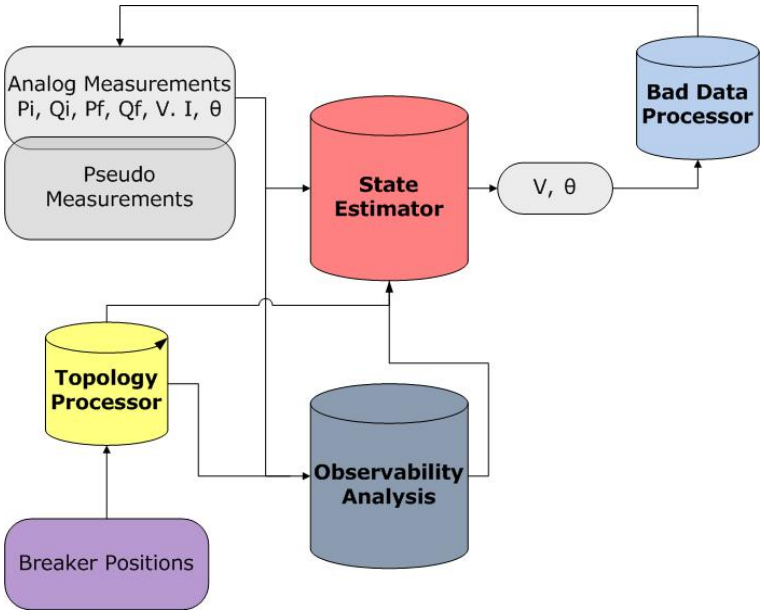

Figure 1.4. PMU-based power system state estimation procedure

estimation can be used to find an equivalent low-order dynamic model for any subsystem of the power grid. Fig. 1.5 shows dynamic model reducing procedures.

There are at least two major systematic methods for parameter estimation: least squares estimation (LSE) and Kalman filter-based estimation. A window of data is required if the LSE method is implementing for the parameter estimation of the dynamic model of the system. On the other hand, Kalman filter-based estimation is carried out at each time step and thus it can be used for online applications. This is also one of the reasons why PMU-based system identification opts for Kalman filter estimation [6–10].

1.2.2 Parameter Estimation in Power System

Provided values for the parameters of the generator by its manufacturers could change over the years due to the factors such as aging and repairs. The difference between provided generators parameters values with their real values in practice could create a serious deviation between the dynamic response of the simulation studies compares to the actual dynamic

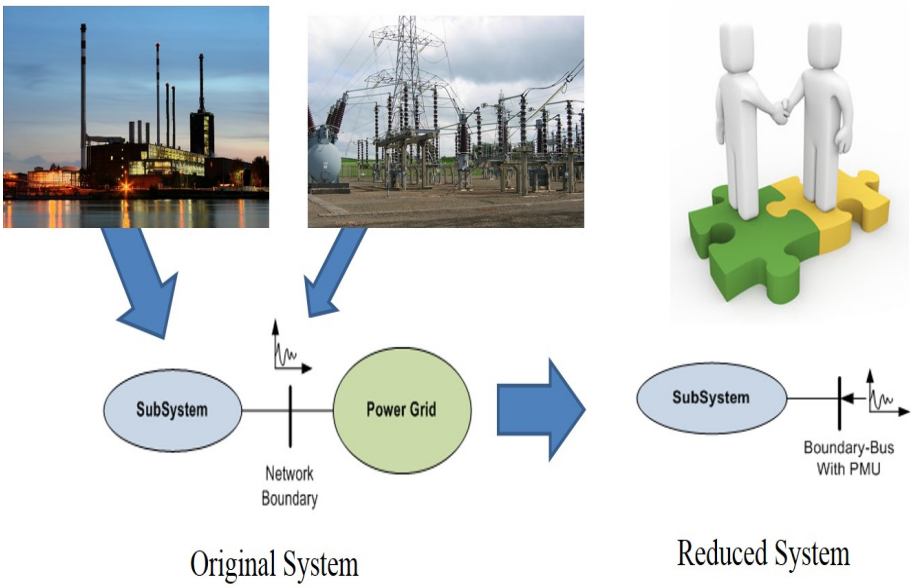

Figure 1.5. PMU-Based online states and parameters estimation for reducing the order of the dynamic model

response of the generator to an event. The WSCC model validation guidelines call for periodic verification of the synchronous machine key parameters. These parameters include machines reactances, time constants, inertia, and stator resistance, among other parameters. Moreover, unit-specific dynamic data should be filed in order to comply with NERC MOD-013 standard. This standard covers power generating systems inclusive of generators (inertia constant, damping coefficient, direct and quadrature axes reactances and time constants), excitation systems, voltage regulators, turbine-governor systems, power system stabilizers. Currently, the generating unit is brought off-line and is subject to tests in order to provide the data required by NERC [11]. Therefore, the research work of this dissertation has a practical application in the real-world system. Our proposed method in this research helps companies to provide generator data required by NERC MOD-013 while the generator is online.

1.3 Statement of the Problem

The purpose of this dissertation is to investigate both static and dynamic state estimation in power system in order to produce efficient computing methods for conducting state estimation and online parameter identification. In particular, the dissertation goals are:

- To investigate the benefits of PMU data and wide area measurement in state estimation
- To develop a new algorithm for online state and parameter estimation of the synchronous generator. In parameter estimation, not only electromechanical dynamics related states and parameters but also turbine-governor dynamics, primary and secondary frequency control parameters will be estimated.
- To implement dynamic state and parameter estimation algorithm for the real-world PMU data in order to demonstrate the feasibility of the proposed UKF estimation approach for system identification using real-world PMU data.
- To explore new algorithm for static state estimation solver to develop faster and more reliable solving technique. Traditionally Gauss-Newton algorithm is used to solve state estimation problem. The algorithm can only find local optimization point and needs significant computation time due to the non-convexity of the problem.
- To investigate new robust state estimation algorithm for simultaneous state estimation and bad data identification.

1.4 Outline of the Dissertation

The dissertation is organized as follows:

- Chapter 1 introduces the importance of state estimation and the effect of PMU device and wide area measurement system on both static and dynamic state estimation algorithms

- Chapter 2 presents a detailed literature survey on the various problems tackled in this dissertation. The chapter highlights the limitations and assumptions of such research and points out to specific objectives to be attained by this dissertation providing an incremental contribution to the established research in the literature.

- Proposed algorithm for dynamic state estimation and parameter identification of synchronous generator is introduced in chapter 3. The chapter introduces Unscented Kalman Filter algorithm and its implementation for dynamic state estimation and parameter identification in sections 3.3and 3.4 respectively. Also, implementation of the proposed algorithm for the real-world PMU data obtained from anonymous busbar of the MISO system have been shown in section 3.5.3.

- Chapter 4 presents state estimation standard formulation and its related relaxations. The relation between the feasible region of each relaxation is introduced, and new cycle based relaxation is investigated in this chapter. Section 4.6 presents joint co-optimization algorithm for simultaneous state estimation and bad data identification. New convex solver for nonlinear state estimation is introduced in section 4.7 with using LSE based SDP cuts for SOCP relaxation of SE problem. Finally, case studies in this chapter show the effectiveness and robustness of joint co-optimization algorithm.

- Chapter 5 concludes the dissertation with the main results drawn from the research and proposes future works by extending the research of both static and dynamic state estimation to improve proposed algorithms.

CHAPTER 2

REVIEW OF RELEVANT LITERATURE AND RESEARCH

2.1 Static State Estimation

Static state estimation (SSE) is the algorithm which uses measurement data from a snapshot of the power system to produce a reliable estimation of the transmission line flow and voltage of the buses. Since measurement data usually contains some errors and noises, SSE should be able to identify those errors and uncertainties in its algorithm. Measurement errors come from a form of the metering communication error, uncertainties in some of the parameters of the power system, bad data due to the noises, transients, and metering accuracy, and topology error related to the structure of the power system in a specific snapshot. Therefore, SSE algorithm consists of three steps: 1) mathematic formulation of the measurement function with respect to the topology of the network and measurement variables; 2) optimization algorithm to find state vector; 3) bad data detection and topology error to ensure the reliability of the estimation. One of the most known SSE algorithms is least square estimation (LSE). LSE will be discussed in the following section.

2.1.1 Least Square Estimation

LSE minimizes the sum of squares of the difference between measured and calculated values. The least squares criterion is a computationally convenient measure of fit. It corresponds to maximum likelihood estimation when the noise is normally distributed with equal variances [12]. Consider a linear system model represented by function $f(x, \beta)$ where x is

system inputs and β is the unknown parameters to be estimated. Assume a set of m data points $(x_1, y_1), (x_2, y_2), ..., (x_m, y_m)$ for n unknown parameters are available from measurements which $m \geqslant n$. Based on system model we will have:

$$y = f(x, \beta) + noise \tag{2.1}$$

Therefore, system error and the sum of the squares of the errors can be written as 2.2 and 2.3 respectively.

$$r_i = y_i - f(x_i, \beta) \qquad for \quad (i = 1, 2, ..., m.) \tag{2.2}$$

$$S = \sum_{i=1}^{m} r_i^2 \tag{2.3}$$

LSE objective is to minimize S and it happens when the gradient is zero. Also, since the system is linear ($\frac{\partial r_i}{\partial \beta_j} = -X_{ij}$), the normal equation for solving LSE problem can be written as 2.4.

$$\sum_{i=1}^{m} \sum_{k=1}^{n} X_{ij} X_{ik} \hat{\beta}_k = \sum_{i=1}^{m} X_{ij} y_i \qquad for \quad (j = 1, 2, ..., m) \tag{2.4}$$

Finally, if we use matrix format, equation 2.4 can be rearranged to 2.5.

$$(X^T X)\hat{\beta} = X^T y \tag{2.5}$$

In nonlinear systems, the derivatives $\frac{\partial r_i}{\partial \beta_j}$ are functions of both inputs x_i and the parameters β_i. So the gradient equation does not have a closed solution. Therefore, iterative method and Taylor's expansion have to be used to solve the estimation problem. By assuming Jacobian matrix as function of constants, the independent variable, and the parameters and by using Taylor expansion, the derivatives of error will be $\frac{\partial r_i}{\partial \beta_j} = -J_{ij}$. Consequently, the normal equation in matrix form can be written as 2.6.

$$(J^T J)\Delta\beta = J^T \Delta y \tag{2.6}$$

2.1.2 Least Absolute Value Estimation

LAV minimizes the sum of absolute values of the difference between measured and calculated values. LAV corresponds to maximum likelihood estimation when the error has the Laplace distribution. Consider a linear system model represented by function $f(x, \beta)$, where x is system inputs and β is the unknown parameters to be estimated. Assume a set of m data points (x_1, y_1), (x_2, y_2), ..., (x_m, y_m) for n unknown parameters are available from measurements which $m \geqslant n$. Based on system model we will have:

$$y = f(x, \beta) + noise \tag{2.7}$$

Therefore, system error and the sum of the absolute values of the errors can be written as 2.8 and 2.9 respectively.

$$r_i = y_i - f(x_i, \beta) \qquad for \quad (i = 1, 2, ..., m.) \tag{2.8}$$

$$S = \sum_{i=1}^{m} |r_i| \tag{2.9}$$

Unlike least square algorithm, the least absolute value can not be solved with an analytical solving method. Therefore, an iterative method requires for solving LAV problems. Also since the cost function of LAV contains absolute function, it's not a continuous function and cannot be solved by linear programming. However, it's well known that we can solve the problem using linear optimization method by introducing two positively bounded variables to the cost function of LAV. Therefore, the problem can be represented as follows:

$$\min \sum_{i=1}^{m} (r_i + s_i) \tag{2.10}$$

$$\text{s.t.} \quad y_i - f(x_i, \beta) + r_i - b_i = 0 \tag{2.11}$$

$$r_i \geq 0, \quad b_i \geq 0, \quad for\ i = 1, ..., m \tag{2.12}$$

Introducing above constraints force the minimization problem to become equal to the cost function in 2.9. Since this version of the problem does not have the absolute value function, it can be solved by any linear programming package.

2.2 Dynamic State Estimation

The dynamic state estimation (DSE) relies on the knowledge of the previous step state values in order to determine the current state of the system. Therefore, unlike static state estimation which belongs to the maximum likelihood estimation, dynamic state estimation is an example of Bayesian estimation where recursive algorithms such as Kalman Filtering are used to estimate states of the system. The accuracy of DSE depends on the sampling rate of the measurements. the low sampling rate of the traditional SCADA system was not allowed dynamic of the system to be captured and thus, DSE could not be implemented

based on those measurement data. Introducing PMU with the high sampling rate between 30-60 Hz, allowed Kalman Filter algorithm to be implemented for dynamic state estimation. Next section investigates Kalman filter estimation algorithm for dynamic state estimation in power system.

2.2.1 Kalman Filter and Extended Kalman Filter

One of the most widely used algorithm for dynamic state estimation is Kalman Filter. Kalman Filter is a recursive algorithm that uses prediction-correction steps process to estimate unknown states and parameters of the system. At each time step, given the previous step's information, Kalman filter estimation will provide the state information of the current step and the relating covariance of the state. Usually, a prediction step estimates the information based on the dynamic model only, and a correction step corrects the information based on the current step's measurements. Kalman Filter has some advantages over LSE [13]:

- The Kalman filter equations provide an extremely convenient procedure for digital computer implementation.
- Kalman Filter is posed in a general framework that one can easily analyze the behavior of the estimates in this framework.
- Kalman Filter has found its greatest application to nonlinear systems.

Kalman Filter (KF) was originally implemented for linear systems, but by using the Extended KF (EKF) algorithm, it can be applied to nonlinear systems as well. If the level of nonlinearity is not harsh, the performance of the EKF is acceptable because of its simple structure as well as its popularity. Assume state model of the system in k time step can be shown as 2.14.

$$x_k = A_k x_{k-1} + q_{k-1} \tag{2.13}$$

$$y_k = H_k x_k + r_k \tag{2.14}$$

where q and r are the procedure noise and measurement noise respectively. In prediction step, EKF calculates an estimation of the states at time step k and its relevant covariances from previous step's measurements. 2.16 shows the prediction step equations.

$$\hat{x_k^-} = A_k \hat{x}_{k-1} \tag{2.15}$$

$$P_k^- = A_{k-1} P_{k-1} A_{k-1}^T + Q_{k-1} \tag{2.16}$$

In correction step, EKF updates predictions by observing measurements output and calculating Kalman Filter gain. 2.19 shows the equations for updating estimation results.

$$K_k = P_k^- H_x^T(\hat{x}_k^-.k)[H_x(\hat{x}_k^-.k) P_k^- H_x^T(\hat{x}_k^-.k) + R_k]^{-1} \tag{2.17}$$

$$\hat{x}_k = \hat{x}_k^- + K_k(y_k - h(\hat{x}_k^-.k)) \tag{2.18}$$

$$P_k = P_{k-1}^- + K_k H_x(\hat{x}_k^-.k) P_k^- \tag{2.19}$$

2.2.2 Unscented Kalman Filter (UKF)

EKF and LSE have some limitations which can affect state estimation results. The most important limitations for LSE and EKF are [13]:

- LSE and EKF use the first order Taylors expansion for linearizing the system. In some cases, the accuracy of the results are not satisfying.

- In both algorithms, the Jacobian matrices need to exist so that the transformation can be applied. Therefore, Jacobian Matrix singularity may cause convergence problem.
- In many cases, the calculation of Jacobian matrices can be a very difficult and complex process.

Unscented Kalman Filter (UKF) overcomes the limitations of LSE and EKF algorithms. UKF is a Monte-Carlo simulation method. In the UKF procedure, the probability distribution is approximated by a set of sigma points. the dynamic process of these sigma points will be computed based on the nonlinear estimation model. Probability distribution information of the dynamic process will then be evaluated. Fig. 2.1 shows the difference between actual, EKF and UKF sampling procedure [14]. Detail investigation regarding UKF algorithm for state estimation will be discussed in upcoming chapters.

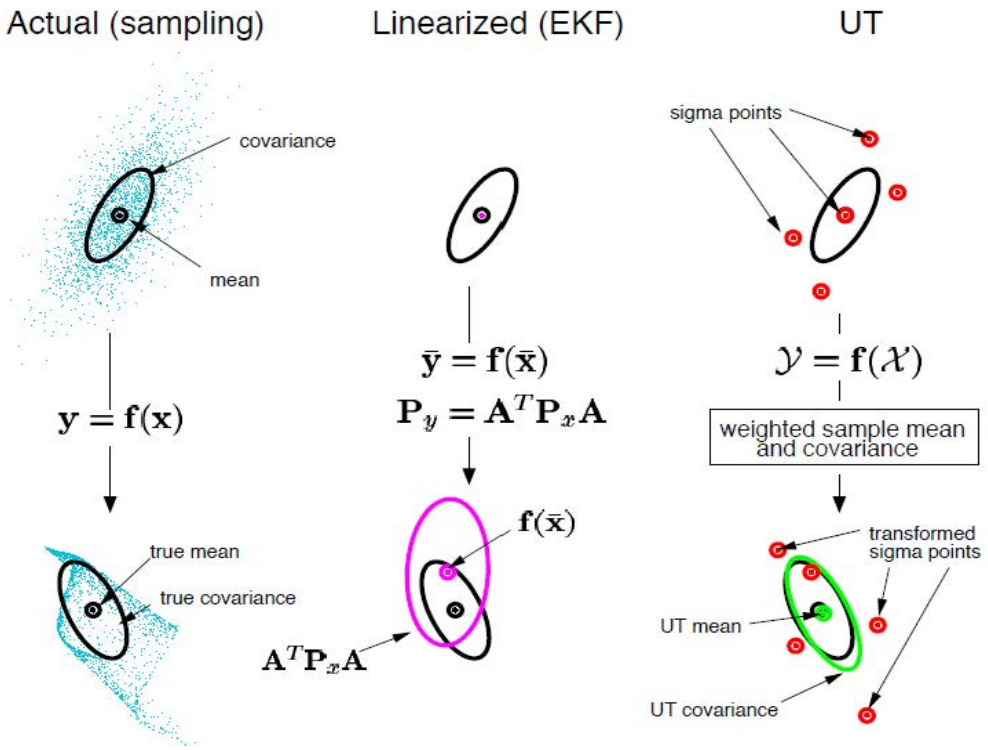

Figure 2.1. Example of the UT for mean and covariance propagation. a) actual, b) first-order linearization(EKF), c) UT.

2.3 Scope of the Work

The advent of PMU equipped with GPS antenna provides voltage-current phasors and frequency with a high-density sampling rate up to 60 Hz. These phasor measurements, transmitted with the time stamps, can help control systems to have an accurate picture of the state of the power system. Using PMU has opened new possibilities for complicated state estimation algorithms with more accurate results. Therefore, in rest of our research, we are focusing on the developing of a new algorithm for dynamic and static state estimation as well as parameter identification of synchronous generator in order to find better solutions for reliable and efficient real-time operation of power system.

2.3.1 PMU-based Dynamic States and Parameters Estimation

One of the important applications of PMU in power system operation comes from dynamic model parameters and state estimation. Because dynamic estimation deals with the dynamic oscillations in a range of 0.1 to 3 Hz, traditional SCADA measurement system with low sampling rate could not be used in dynamic states estimation and synchronous generator parameters identification. Having PMU's high sampling rate voltage and current measurements, make it possible to capture dynamic states of the system and estimate all the unknown parameters needed for reliable and efficient operations of the power system. Besides, PMU data can make the dynamic model calculation much easier by simplifying high orders dynamic model of any unknown subsystem.

2.3.1.1 Literature Review

Synchronous generator states and parameters estimation has been investigated in the literature. Based on the scope of the estimation, some only investigate electrical state estimation (e.g. rotor angle and rotor speed) [15, 16], while others estimate both system states

and generator parameters [17–20]. Based on estimation methods, there are at least two major systematic methods for parameter estimation: least squares estimation (LSE) [21–23] and Kalman filter estimation [6–10]. In order to use LSE for parameter estimation of the dynamic model of the system, a window of data is required. On the other hand, Kalman filter can be carried out for each time step. Thus Kalman filter algorithm can be used for online estimation. This is also one of the reasons why PMU based system identification opts for Kalman filter estimation [6–10].

Kalman Filter was originally proposed for the linear systems. Extended Kalman Filter (EKF) is developed to implement on nonlinear systems by using linearization techniques. EKF was first applied by PNNL researchers in dynamic model identification via PMU data [6, 19, 20]. [19] focuses on parameter calibration for a simple generator dynamic model. [20] presents parameter calibration for a multi-machine power system under varying fault locations, parameter errors and measurement noises. In [6], parameter calibration for a more complicated generator model consisting of electromechanical dynamics, electromagnetic dynamics, exciter dynamics, voltage control blocks and power system stabilizer (PSS) was presented. EKF-based simple generator model estimation was also carried out in [7, 8]. Limitations of EKF method has also been investigated in [7].

In the UKF procedure, the probability distribution is approximated by a set of sigma points. the dynamic process of these sigma points will be computed based on the nonlinear estimation model. Probability distribution information of the dynamic process will then be evaluated. UKF overcomes the limitation of the linearization process required by the EKF method with the cost of more computing effort. In [9], UKF is applied for state estimation. Accuracy and convergence for both EKF and UKF are compared. Both papers focus on state estimation only, and parameter estimation was not discussed. In [10], UKF is applied to estimate the following parameters E_q, X'_d and H along with states. A comparison of various Kalman filter methods is documented in [24].

2.3.1.2 Identification of the Problem

Traditionally LSE was used to estimate states and parameters of synchronous generators. Since generator identification algorithms deal with the non-linear equations, iteration based linearization using Taylor's expansion is used for states and parameter estimations. The most important problem associated with the usage of LSE based estimation are:

- LSE estimation needs a window of data for estimation.
- System linearization using Taylor's expansion can affect the accuracy of the results in some cases.
- LSE needs invertible Jacobian matrix to exist. Therefore, Jacobian Matrix's singularity may cause Convergence problem.
- In many cases, the calculation of Jacobian matrices can be a very difficult process

In order to address some of the issues associated with LSE, the Kalman filter algorithm is introduced in literature. Kalman Filter was originally proposed for the linear systems. Thus, Extended Kalman Filter (EKF) is developed to implement on nonlinear systems by using linearization techniques. The advantage of EKF over LSE is that EKF equations provide an extremely convenient procedure for digital computer implementation and it has a great application for nonlinear systems [13]. However, EKF still needs Jacobian matrix and linearization techniques and thus it is limited by the drawbacks associated with those techniques. Using UKF algorithm overcomes linearization limitations and increase the accuracy of the estimation.

Other problem which can be identified in the literature, comes from the lack of frequency system parameter identification and its effect on the on-line estimation of synchronous generator model. Since frequency control system is responsible for responding to the frequency dynamics, it has a direct effect on the accuracy of generator's dynamic model. Therefore,

neglecting frequency control system will introduce process error to the estimation. Finally, implementing UKF algorithm on a real-world PMU data will evaluate the effectiveness of the method and develops a new algorithm to simplify high-order dynamic model of the real-world synchronous generator to the low order classic generator model.

2.3.1.3 Approach

The synchronous generator model identified in the aforementioned papers focuses on the generator electromechanical, electromagnetic and excitation system only. For example, a 4^{th} order transient generator estimation model is assumed in [24]; a subtransient generator estimation model is adopted in [6].

In this dissertation, UKF is implemented to estimate dynamic states and parameters of a low-order synchronous generator model with both primary and secondary frequency control systems. Both simulation data and real-world PMU data are used for case studies. In this research, various techniques are implemented to improve UKF algorithm for this application. The techniques include: (i) parameter conversion to increase parameter detection sensitivity from the measurements; (ii) measurements interpolating to have a higher sampling rate to improve UKF convergence. The case studies demonstrate the feasibility of the proposed UKF estimation approach for system identification using PMU data. Through the proposed estimation method, a complex generator model can be emulated using a low-order generator with frequency controls. The case study on the real-world PMU data demonstrates the capability of the proposed UKF on identifying an equivalent generator. Therefore, This part of our research successfully completed first three tasks introduced in dynamic states and parameters estimations research. The results of this part of research presented in one transaction paper [25].

2.3.2 AC Network Static State Estimation

Static state estimation was first introduced for transmission systems under the name 'power system state estimation (PSSE)' and traditionally used low rate SCADA measurements [26–28]. The main idea of static state estimation is to estimate the most possible states (generally voltage magnitudes and angles of buses) of the systems based on the limited measurements. The main challenge of the PSSE is the limitation of number of measurements in power system. The objective of this part of research is to integrate PMU data with traditional measurements and develop enhanced state estimation.

2.3.2.1 Literature Review

Reliable operation and control of power system depend on the results of state estimation. State estimation problem have been reported in a large number of research works in literatures [15] and [29–52]. Corrupted data usually exist in power system measurements due to limited measurement sensor's accuracy, communication system problems, and cyber attacks. Therefore, state estimator has been equipped with bad data identification algorithms in order to detect such corrupted data and guarantee the accuracy of state estimation. Classic bad data detection algorithms such as *Largest Normalized Residue Test* (LNRT) have been reported in the literature for identifying bad data, [53–55].

LNRT test relies on the state estimation residuals and thus can only be implemented after running state estimation. After any bad datum been detected, state estimation has to be rerun by eliminating that bad datum. Hence, the efficiency and computational time of the LNRT algorithm becomes a major concern.

State estimation problems rely on the set of non-convex measurement functions that come from its corresponding power flow equations. Therefore, non-convex state estimation accuracy can be a very challenging problem, especially for large-scale power systems with

thousands of buses and generators. In order to address this challenge, traditionally iterative linearization were used in literature. However, it is clear that such linearization will affect the accuracy of the algorithm and cannot guarantee the global optimality of the solutions. Another solution for the non-convexity problem in SE is the usage of a local optimal solver such as interior point method (IPM) and Newton's algorithm. The final solution of these type of algorithms, are sensitive to the initial guesses and therefore they subject to stuck in local optimal solution and usually cannot reach to the global one.

In recent years, convex relaxation approach is becoming widely popular for solving non-convex power flow optimization. The most famous convex relaxation methods are semidefinite programming relaxation (SDP) and second order conic programming (SOCP). In [56] new SDP state estimator was introduced to overcome inherent non-convexity of state estimation. Although SDP solver can produce quality results and small duality gap, they still have high computational time limitation, especially for large-scale systems. On the other hand, SOCP can be used to reformulate power flow equation and state estimation problem as it explored in [57–59].

In particular in [59], state estimation problem was reformulated by using second order conic programming method. However, SOCP formulation for SE problem still contains two non-convex feasibility constraints and Thus, IPM (interior point Method) solver was used to find local answers for the optimization. Therefore, despite of its effectiveness for IEEE test cases, it still cannot guarantee the global optimality of the solution. Consequently, [60]and [61] suggested strengthening SOCP relaxation by separating its optimal solution from SDP Feasible region.

2.3.2.2 Identification of the Problem

The main problem in static state estimation relates to the bad data detection algorithm. Corrupted data (a.k.a. bad data) can affect the result of SE. Thus, bad data identification is

necessary for state estimation in power system. Largest normalized residue algorithm (LNR) have widely been used for bad data identification in literature. LNR algorithm relies on LSE residuals and therefore, can be implemented only after running SE. So, for any bad data detection, it is needed to rerun the SE again with discarding corrupted datum [62]. Also, in recent years, the risk of cyber attacks have been increased significantly. The research shows that cyber attacks can be unidentified by the traditional bad data detection schemes in case the attack would be able to cause multiple corrupted measurements. Consequently, new co-optimization algorithm has to be designed for state estimation and bad data detection.

Traditionally, non-convex Gauss-Newton algorithm has been used to solve SE iteratively. However, Newton method is a local solver with no guarantee for a global solution. Introducing co-optimization for state estimation and bad data detection, not only changes the objective function of the optimization but also changes the SE optimization structure to be constrained. Thus, a non-convex solver may stick in a local solution. The main problem in state estimation solvers relates to the inherent non-linearity and non-convexity of measurement functions which comes from the nature of power flow equation in power systems. High accuracy (less than 1% noise) in PMU-based measurement data simplifies the usage of the convex algorithm for the static state estimation.

In our research work for static state estimation, SOCP programming is used to improve solving technique for power system state estimator with using linear measurement functions. However, the non-convex feasible constraints in such estimator forced the use of local solver such as IPM (interior point method) with no guarantee for global answers. Therefore, cycle based SOCP relaxation applied to the state estimator and a least square estimation (LSE) based method is implemented to generate semidefinite programming (SDP) cuts in order to strengthen the state estimator (SE) with SOCP relaxation. Since SDP relaxation provides a tighter bound for power flow problem , adding SDP cuts to the SOCP relaxation, makes the Problems feasible region close to the SDP feasible region while saving us from computational

difficulty associated with SDP solvers. The improved solver is effective to reduce the feasible region and get rid of unwanted solutions violated cycle constraints. Case studies are carried out to demonstrate the effectiveness and robustness of the method.

2.3.2.3 Approach

A joint co-optimization algorithm for nonlinear state estimation and bad data detection is introduced in this dissertation. The proposed algorithm uses the sparse matrix characteristic to identify bad data detection. However, since sparse matrix based co-optimization is implemented for linear system state estimation in literature, our recently developed LSE based SDP cuts algorithm have been implemented for state estimation with SOCP relaxation to make the joint co-optimization possible for nonlinear state estimation.

Convex relaxation approach, especially second order conic programming (SOCP), draw more research interests in recent years. In this dissertation, SOCP programming was used to build power system state estimator with linear measurement functions. However, the non-convex feasible constraints in estimator with linear measurement function, forced the use of a local solver such as IPM (interior point method) with no guarantee for a global solution. In order to improve static estate estimation technique, cycle based SOCP relaxation applied to the state estimator and a least square estimation (LSE) based method from [63] is implemented to generate semidefinite programming (SDP) cuts in order to strengthen the state estimator (SE) with SOCP relaxation. Since SDP relaxation provides a tighter bound for power flow problem, adding SDP cuts to the SOCP relaxation, makes the Problems feasible region close to the SDP feasible region while saving us from computational difficulty associated with SDP solvers. The implemented method is effective to reduce the feasible region and get rid of unwanted solutions violate cycle constraints.

Numerical case studies demonstrate more accurate results in SOCP relaxed state estimation, successful implementation of the algorithm for the simultaneous state estimation and

bad data detection and better state estimation recovery against single and multiple Gaussian bad data compare to the traditional LNRT algorithm.

2.4 Contribution of the Dissertation

This dissertation investigates both static and dynamic state estimation algorithms using PMU data. Specifically, the contributions of the dissertation include:

- Not only electromechanical dynamics related states and parameters, but also turbine-governor dynamics, primary and secondary frequency control parameters will be estimated. Estimation related to frequency control based on PMU data has not been seen in the literature. This dissertation will address this topic for the first time. Particularly, we will estimate the following parameters and states: inertia constant H, damping factor D, internal voltage E_q, transient reactance x'_d, mechanical power input P_m, Droop regulation R, turbine-governor time constant T_r, and secondary frequency control integrator gain K_i.

- Event playback method [6] is used in this paper to validate the identified low-order model. For validation, estimated parameters will be used to create a dynamic simulation model. Then event playback will be used to inject the same inputs to the dynamic simulation model. The output signals from the simulation will be compared with the PMU measurements.

- Identify the issues facing the application estimation techniques on real PMU data and real-world PMU data-based model identification will be implemented to demonstrate the effectiveness of the proposed estimation model.

- Introducing a new formulation of simultaneous AC network state estimation and bad data identification. The constrained optimization problem is further relaxed using SOCP relaxation technique.

- Implementing an LSE based SDP cutting plane method to solve the SOCP relaxed problem. This solver leads to more accurate results of state estimation as well as bad data identification.

CHAPTER 3

DYNAMIC STATE ESTIMATION AND MODEL IDENTIFICATION

3.1 Note to the Reader

Portions of these results have been previously published (as a 1st author in [25]). The results are utilized with permission of the publisher.

3.2 Introduction

Traditional SCADA system can not capture the system dynamics. In recent years, WAMC (wide Area Measurement And Control) system using phasor measurement units (PMUs) equipped with GPS antennas have been largely used. The advent of phasor measurement units (PMUs) equipped with GPS antenna provides voltage-current phasors and frequency with a high-density sampling rate up to 60 Hz. These phasor measurements transmitted with time stamps can help control systems have an accurate picture of the power system. States and dynamic model estimation are necessary for a safe and reliable operation of power system.

The goal of this section of the dissertation is to apply UKF for parameter and state estimation for a synchronous generator model consisting of electromechanical dynamics and frequency control. Contributions of this part of research are summarized in the following paragraphs.

- Not only electromechanical dynamics related states and parameters, but also turbine-governor dynamics, primary and secondary frequency control parameters will be es-

timated. Estimation related to frequency control based on PMU data has not been seen in the literature. Particularly, we will estimate the following parameters and states: inertia constant H, damping factor D, internal voltage E_q, transient reactance x'_d, mechanical power input P_m, Droop regulation R, turbine-governor time constant T_r, and secondary frequency control integrator gain K_i. Some parameters are difficult to estimate due to nonlinearity. Parameters conversion is adopted in this research in order to make estimation easier.

- Event playback method [6] will be used to validate the identified low-order model. For validation, estimated parameters will be used to create a dynamic simulation model. Then event playback will be used to inject the same inputs to the dynamic simulation model. The output signals from the simulation will be compared with the PMU measurements.

- Lastly, real-world PMU data model identification will be carried out to identified equivalent dynamic model of the unknown part of the power grid in order to simplify the complexity order of dynamic model of the power system network.

3.3 Basic Algorithm of UKF

Characterizing the output of the nonlinear system faced with a stochastic input is very difficult. In order to solve the problem, the system can be linearized first, and the stochastic output of the linearized model is used then. This approximation works in some cases, but inaccurate estimation has been reported as well. The Unscented Transformation (UT) is a nonlinear transform that provides a good characterization of the output of a nonlinear system subject to a stochastic input. Considering m_x as the mean and p_x as the covariance of $n \times 1$ stochastic vector x, UT approaches the approximated mean and covariance of the output of a known nonlinear function $y = f(x)$. This can be done by defining a set of

sigma points $\sigma_x^i \quad i = 0, 1, 2, ..., N$ with the same mean and covariance as vector x, then transforming sigma points by function y will lead to a set of projected sigma points, σ_y^i. Weighted sample mean and covariance of the σ_y^i can be considered as a good approximation of mean and covariance of nonlinear function y.

Kalman Filter (KF) was originally implemented for linear systems, but using the Extended KF (EKF) it has been applied to nonlinear systems as well. If the level of nonlinearity is not harsh, the performance of the EKF is acceptable because of its simple structure as well as popularity. EKF has been used as one of the most interesting nonlinear state estimators so far. Combining UT and KF will result in Unscented Kalman Filter (UKF) which is mostly the discrete KF in which the mean value and covariance updates are derived by UT approach. Discrete KF uses the first two statistical moments and updates them with time. A brief summary of the UKF is included below.

A continuous nonlinear dynamic system is represented by the following equations.

$$\begin{cases} \dot{x}(t) = \overline{f}[x(t), u(t), v(t)] \\ y(t) = h[x(t), u(t), v(t)] + w(t) \end{cases} \tag{3.1}$$

where, $x(t)$ is the vector of state variables, $y(t)$ is the vector of output variables, $u(t)$ is the vector of input variables, $v(t)$ is the non-additive process noise, and $\omega(t)$ is additive measurement noise. Considering the time step of Δt, (3.1) can be written as (3.2) in the discrete time domain:

$$\begin{cases} x_k = x_{k-1} + \overline{f}[x_{k-1}, u_{k-1}, v_{k-1}]\Delta t \\ \quad\;\; = f[x_{k-1}, u_{k-1}, v_{k-1}] \\ y_k = h[x_k, u_k, v_k] + w_k \end{cases} \tag{3.2}$$

The state x_k is considered as a random variable vector with an estimated mean value of $\hat{x}_k$ and an estimated covariance of P_{x_k}. Vector ψ_k is considered as a set of unknown model parameters. For simplification, ψ_k can also be treated as states. Then new state vector is $X_k = \begin{bmatrix} {x_k}^T & {\psi_k}^T \end{bmatrix}^T$. The state-space model in (3.2) is reformulated as:

$$\begin{cases} X_k = f[X_{k-1}, u_{k-1}, v_{k-1}] \\ y_k = h[X_k, u_k, v_k] + w_k \end{cases} \tag{3.3}$$

Kalman filter is a recursive estimation algorithm. At each time step, given the previous step's information, such as the mean of the state $\hat{X}_{k-1}$, the covariance of the state $P_{X_{k-1}}$, Kalman filter estimation will provide the state information of the current step, *i.e.*, the mean of the state $\hat{X}_k$ and the covariance of the state P_{X_k}. Usually, a prediction step estimates the information based on the dynamic model only, and a correction step corrects the information based on the current step's measurements. There are several references for UKF algorithm in literatures. For rest of this section, [64] are used as the reference for all UKF algorithm's equations.

Unscented Kalman filter (UKF) is a Monte-Carlo simulation method. A set of sigma points will be generated based on the given information: mean and covariance of the states. Sigma points vectors will capture the mean and covariance of distribution of the state variable X.

The set of sigma points is denoted by χ^i and their mean value represented by $\hat{X}$ while their covariance represented by P_X. For n number of state variables, a set of $2n+1$ points are generated based on the columns of matrix $\sqrt{(n+\lambda)P_x}$. As shown below, at $k-1$ step, $2n+1$ sigma points (vectors) are generated. Based on the information of the sigma points of the next step, the mean and the covariance of the states will be computed.

$$\begin{cases} \chi_{k-1}^{0} = \hat{X}_{k-1} \\ \chi_{k-1}^{i} = \hat{X}_{k-1} + \left[\sqrt{(n+\lambda)P_{X_{k-1}}}\right]_i , \quad i = 1, ..., n \\ \chi_{k-1}^{i+n} = \hat{X}_{k-1} - \left[\sqrt{(n+\lambda)P_{X_{k-1}}}\right]_{i+n} , \quad i = 1, ..., n \end{cases} \tag{3.4}$$

where λ is a scaling parameter ($\lambda = \alpha^2(n+\kappa) - n$), α and κ are positive constants.

In the *prediction* step, prediction of the next step information will be carried out for all these sigma points. UKF will use weights to calculate the predicted mean and covariance. The associated weights can be written as below:

$$\begin{cases} W_{m_0} = \frac{\lambda}{(n+\lambda)} \\ W_{c_0} = \frac{\lambda}{(n+\lambda)} + (1 - \alpha^2 + \beta) \\ W_{m_i} = \frac{1}{2(n+\lambda)} , \quad i = 1, ..., 2n \\ W_{c_i} = \frac{1}{2(n+\lambda)} , \quad i = 1, ..., 2n \end{cases} \tag{3.5}$$

where β is a positive constant, W_{m_i} is used to compute the mean value, and W_{c_i} is used to compute the covariance matrix. α, κ and β are the Kalman Filter parameters which can be used to tune the filter.

Scaling parameter β is used to incorporate prior knowledge of the distribution of $x(k)$ and for Gaussian distributions $\beta = 2$ is optimal [65]. The scaling parameter α is a positive value used for an arbitrary small number to a minimum of higher order effects. For choosing α, two laws have to be taken into accounts. First, for all choices of α, the predicted covariance must be defined as a positive semidefinite. Second, The order of accuracy must be preserved for both the mean and covariance [66]. See [65] and [66] for more detail insight regarding the effect of scaling parameter α on UKF tuning.

κ is a scaling factor that controls how far away from the mean we want the points to be. A larger kappa will choose points further away from the mean, and a smaller kappa will choose points nearer the mean. Based on (3.5) it can also be seen that when κ gets larger not only the sampled sigma points goes further away from the mean, but also the weight of those samples gets smaller. In the other word, by choosing larger κ samples are chosen further and further away from the mean with less weight assigned to those samples. Therefore, choosing appropriate κ will reduce higher order errors of Tylor's series for predicting the mean and covariance of the states of the system.

It is shown in [67] and [68], that if $x(k)$ is Gaussian, it is more appropriate to choose κ in a way that $n+\kappa = 3$. However, if the distribution of $x(k)$ is different, then we have to use a different approach for choosing κ. A detailed discussion regarding UKF parameters can be found in [67], [69] and [68].

The predicted sigma points at the k-th step (χ_k^-), the mean ($\hat{X}_k^-$) and the covariance ($P_{X_k}^-$) of the k-th step state are described in (3.6). Note the superscript $^-$ denotes a prior state.

$$\begin{cases} \chi_k^{i-} = f(\chi_{k-1}^i, u_{k-1}), i = 0, \cdots, 2n \\ \hat{X}_k^- = \sum_{i=0}^{2n} W_{m_i} \chi_k^{i-} \\ P_{X_k}^- = \sum_{i=0}^{2n} W_{c_i} \left(\chi_k^{i-} - \hat{X}_k^-\right) \left(\chi_k^{i-} - \hat{X}_k^-\right)^T \end{cases} \tag{3.6}$$

Subsequently, the predicted measurement sigma points γ_k^- can be generated by finding the predicted sigma points χ_k^- through the measurement equation (3.7).

$$\gamma_k^{i-} = h(\chi_k^{i-}, u_k), i = 0, \cdots, 2n \tag{3.7}$$

Consequently, the weighted mean of the predicted measurement $\hat{y}_k^-$ and the corresponding covariance matrix $P_{y_k}^-$ as well as the cross-correlation matrix $P_{X_k y_k}^-$ can be computed as shown in (3.8).

$$\begin{cases} \hat{y}_k^- = \sum_{i=0}^{2n} W_{mi} \gamma_k^{i-} \\ P_{y_k}^- = \sum_{i=0}^{2n} W_{ci} (\gamma_k^{i-} - \hat{y}_k^-)(\gamma_k^{i-} - \hat{y}_k^-)^T + R \\ P_{X_k y_k}^- = \sum_{i=0}^{2n} W_{ci} (\chi_k^{i-} - \hat{X}_k^-)(\gamma_k^{i-} - \hat{y}_k^-)^T \end{cases} \tag{3.8}$$

In the *correction* step, UKF then *updates* the state using Kalman gain matrix K_k. The mean value $\hat{X}_k$ and covariance matrix P_{X_k} (superscript $^-$ denotes a prior state) are expressed as follows.

$$\begin{cases} K_k = P_{X_k y_k}^- (P_{y_k}^-)^{-1} \\ \hat{X}_k = \hat{X}_k^- + K_k \left[y_k - \hat{y}_k \right]^T \\ P_{X_k} = P_{X_k}^- - K_k P_{y_k}^- K_k^T \end{cases} \tag{3.9}$$

There are existing general Kalman filter Matlab toolboxes available. In this research, we use a general EKF/UKF toolbox developed by Helsinki University [70]. Specific models of PMU data-based synchronous generator estimation are described in the next section and coded in the toolbox.

3.4 Implementation of UKF for Dynamic Parameter Estimation

In the proposed estimation model, a synchronous generator is considered as a constant voltage source behind an impedance. The electromechanical dynamics can be described by the following swing equation [71].

$$\begin{cases} \frac{d\delta(t)}{dt} = \omega_s(\omega(t) - \omega_0) \\ \frac{d\omega(t)}{dt} = \frac{1}{2H}(P_m - P_g(t) - D(\omega(t) - \omega_0)) \end{cases} \tag{3.10}$$

where $\delta(t)$, $\omega(t)$, ω_0 and ω_s are the rotor angle in radius, rotor speed in pu, synchronous speed in pu and base speed (377 rad/s), respectively. Rewriting the dynamic equations in the discrete form, we will have:

$$\begin{cases} \delta_k = \delta_{k-1} + (\omega_{k-1} - \omega_0)\omega_s \Delta t \\ \omega_k = \omega_{k-1} + \frac{\Delta t}{2H_{k-1}}(P_{m_{k-1}} - P_{g_{k-1}} - D_{k-1}(\omega_{k-1} - \omega_0)) \end{cases} \tag{3.11}$$

where Δt is the sample period.

The PMU measured data can be separated into two groups. One group is treated as the input signals to the dynamic model, and the other group is treated as the outputs or measurements. A PMU provides five sets of data at a generator terminal bus: voltage magnitude (V_g), voltage phase angle (θ), active power (P_g), reactive power (Q_g), and frequency (f). The PMU data contains only the positive sequence in this application based on the assumption that the system is operated under balanced conditions. Based on the swing equation, the state vector of the system is defined as $x_k = [\delta_k \;\; \omega_k]^T$. If we treat the parameters (unknown mechanical power P_m, inertia constant H and damping coefficient D) of the model as state variables, the augmented state vector will be $X_k = [\delta_k \;\; \omega_k \;\; P_{m_k} \;\; H_k \;\; D_k]^T$.

In this research work, we will use terminal voltage magnitude (V_g) and generator exported power (P_g) as the input signals, the terminal voltage phasor angle (θ) together with the reactive power are treated as the output signals. The relationship between input and output signals can be written as follows.

$$\begin{cases} P_g = \frac{E_q V_g}{x'_d} \sin(\delta - \theta) \\ Q_g = \frac{E_q V_g \cos(\delta - \theta) - V_g^2}{x'_d} \end{cases} \tag{3.12}$$

From (3.12) we can write:

$$\begin{cases} E_q V_g \sin(\delta - \theta) = P_g x'_d \\ E_q V_g \cos(\delta - \theta) = \sqrt{(E_q V_g)^2 - (P_g x'_d)^2} \end{cases} \tag{3.13}$$

Based on (3.13), the output signals can be expressed by the input signals and state variables as follows.

$$\begin{cases} \theta_{g_k} = \delta_k - \tan^{-1}\left(\frac{P_{g_k} x'_{d_k}}{\sqrt{(E_{q_k} V_{g_k})^2 - (P_{g_k} x'_{d_k})^2}}\right) \\ Q_{g_k} = \frac{\sqrt{(E_{q_k} V_{g_k})^2 - (P_{g_k} x'_{d_k})^2} - V_{g_k}^2}{x'_{d_k}}. \end{cases} \tag{3.14}$$

3.4.1 Primary and Secondary Frequency Control

Power system is faced with load change all the time because the power network is a dynamic system which is changing due to different operating point conditions. When the load is suddenly changed, the power balance between electrical power output and mechanical power input of the generator will be lost. Such an unbalance in power equation of the generator changes the Kinetic energy stored in the rotating system. Reducing the Kinetic energy causes turbine speed and consequently the frequency of the system to fall and vice versa. If changing the frequency continues, the generators synchronization will be lost, and the system will be collapsed. To avoid such a scenario, the frequency of the system has to be kept constant near its nominal value. The turbine governor has to be used to adjust turbine input valve for changing mechanical power input of the generator which will finally bring the rotor speed to a new steady-state in order to keep the frequency fixed.

In Fig. 3.1, R is the speed regulation constant, $\frac{1}{R}$ is named as the droop gain, and T_r is the turbine-governor time constant. A turbine-governor usually has the speed regulation of 5

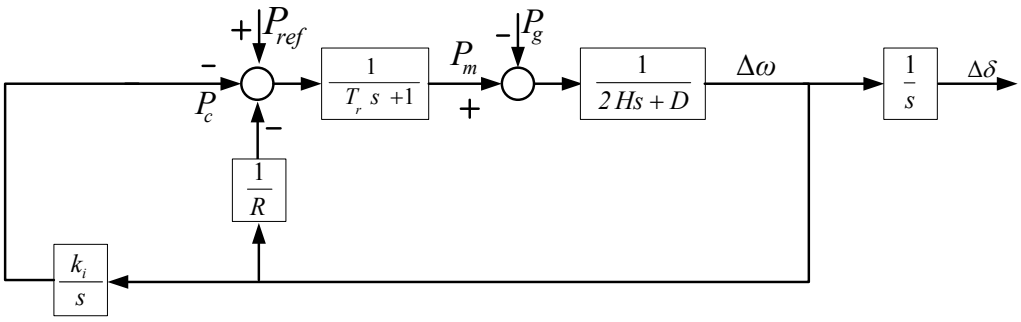

Figure 3.1. Synchronous generator model including primary and secondary frequency control.

to 6 percent from zero to the full load condition. The primary control is a negative feedback from rotor speed with droop gain to the turbine block. The secondary control is a negative feedback with PI controller to track the rotor speed change and tune the reference power input of the generator. Fig 3.1 shows the block diagram of generator models. Additional dynamic equations are as follows after considering the frequency controls.

$$\frac{dP_m}{dt} = \frac{1}{T_r}\left(P_{\text{ref}} - P_c - P_m - \frac{1}{R}(\omega - \omega_0)\right) \tag{3.15}$$

Rewriting in the discrete form, we have:

$$P_{m_k} = P_{m_{k-1}} + \frac{\Delta t}{T_r}\left(P_{\text{ref}} - P_{c_{k-1}} - P_{m_{k-1}} - \frac{1}{R}(\omega_{k-1} - \omega_0)\right) \tag{3.16}$$

Similarly, the secondary frequency control can be written as:

$$P_{c_k} = P_{c_{k-1}} + (\omega_{k-1} - \omega_0)K_{i_{k-1}}\Delta t. \tag{3.17}$$

The state vector of the system is now defined as $x_k = [\delta_k \quad \omega_k \quad P_{m_k} \quad P_{c_k}]^T$. If we treat the parameters of the model as state variables, the augmented state vector will be $X_k =$

$[\delta_k \ \ \omega_k \ \ P_{m_k} \ \ P_{c_k} \ \ R_k \ \ K_{i_k} \ \ H_k \ \ D_k]^T$. The complete generator estimation model is presented as follows.

$$\begin{cases} \delta_k = \delta_{k-1} + (\omega_{k-1} - \omega_0)\omega_s \Delta t \\ \omega_k = \omega_{k-1} + \frac{\Delta t}{2H_{k-1}}(P_m - P_{g_{k-1}} + D_{k-1}(\omega_{k-1} - \omega_0)) \\ P_{m_k} = P_{m_{k-1}} + \frac{\Delta t}{T_{r_k}}\left(P_{\text{ref}} - P_{c_{k-1}} - P_{m_{k-1}} - \frac{1}{R_k}(\omega_{k-1} - \omega_0)\right) \\ P_{c_k} = P_{c_{k-1}} + (\omega_{k-1} - \omega_0)K_{i_{k-1}}\Delta t \\ R_k = R_{k-1} \\ K_{i_k} = K_{i_{k-1}} \\ H_k = H_{k-1} \\ D_k = D_{k-1} \\ T_{r_k} = T_{r_{k-1}} \end{cases} \tag{3.18}$$

The model will be adapted for PMU data-based estimation to enhance the convergence of the UKF algorithm. Some parameters will be converted to new parameters in the estimation process. Parameter conversion has also been adopted in the literature [10].

3.4.2 Model Validation

Kalman Filter uses some of the PMU's measurement data from the real system as inputs while assuming the others as outputs and try to match estimated model output with the output of the real system. In a validation step, estimated parameters are used to build a low order generator dynamic model. Then, event playback is used to validate the result by comparing Estimated model output and actual measurements. Hybrid dynamic simulation was proposed in [72]and [18] for model validation using PMU data.

Hybrid dynamic simulation injects some of measured PMU data to the to a dynamic simulated model as inputs so one can compare the model output with the actual measured data. Figure 3.2 describes the model validation procedure. In this procedure, terminal voltage magnitude and active power measurement are used as inputs to playback into the estimated system.

Then voltage angle and reactive power measured from simulation playback are compared with the actual measurement of the system. In This method, the external system is represented as an infinite bus connected to the generator bus with varying voltage magnitude and phase angle. This assumption can be true mostly because, in the real implementation, the size of the external system is much larger than that of the generator under validation. Thus, the interaction between the generator and external network have a negligible effect on the frequency of the system and terminal voltage. The detail discussion on event playback can be found in [72] and [18].

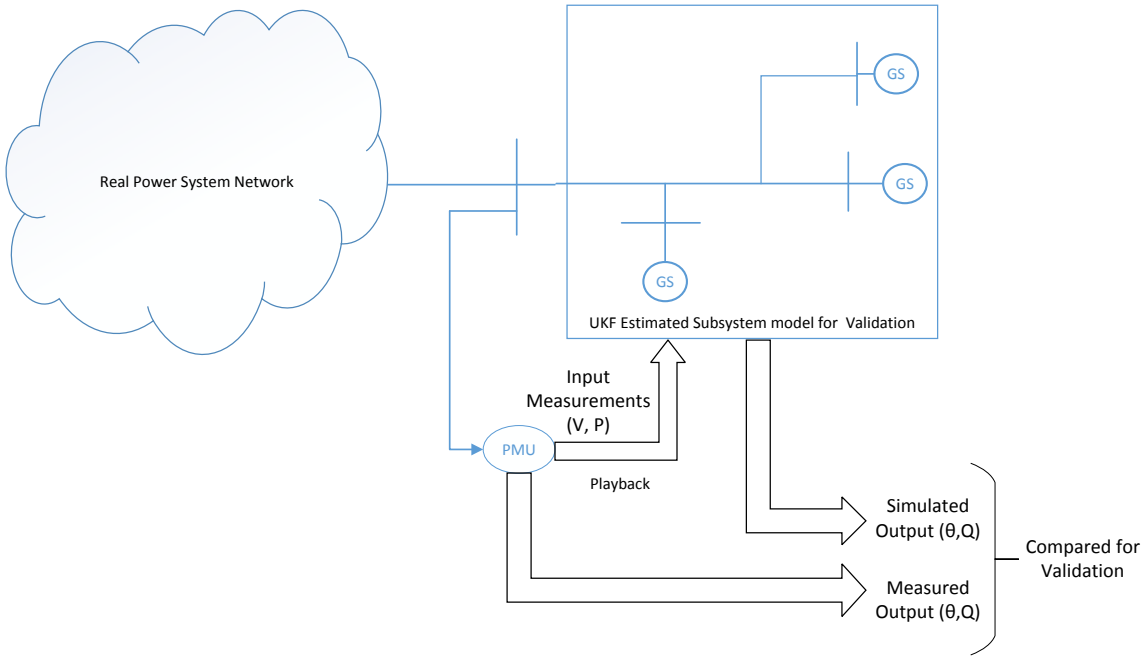

Figure 3.2. Model validation with event playback

3.5 Case Studies

In order to generate PMU data for case study, time-domain simulation data is generated using Matlab/SimPowerSystems. Demos in Matlab/SimPowerSystems includes a classic two-area nine-bus system [71] shown in Fig. 3.3. This system consists of four generators in two areas. Two tie-lines connect these two areas. At $t = 1$ second, a three-phase low impedance fault occurs at Bus 101. After 0.2 seconds, the fault is cleared. A PMU is used to record power, voltage, and the frequency data from Generator 1 terminal bus. The sampling interval is 0.01 second.

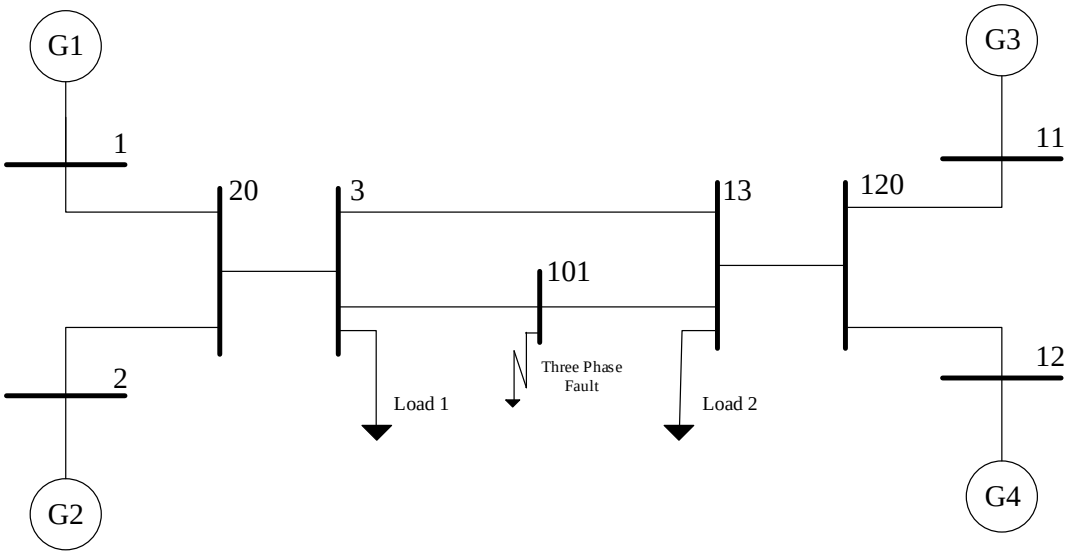

Figure 3.3. The study system.

Three sets of data were recorded (shown in Fig. 3.4) and used to test UKF method. Each set of data will represent a different model for Generator 1 in the simulation studies.

- Set 1: For benchmarking, classical generator model (a constant voltage source behind a transient reactance) is used in the simulation. In this case, the dynamic model used in UKF is exactly the same as the simulation model.

- Set 2: A sub-transient model which includes all damping winding dynamics is used to represent Generator 1 in the simulation. In the estimation model, dynamics related to the flux and damping winding have all been ignored.

- Set 3: The power system stabilizer (PSS), automatic voltage regulator (AVR), and excitation system are added to the sub-transient generator model in this simulation. Adding PSS, AVR, and excitation system adds transients to the internal voltage of generator (E_q). In the estimation model, E_q is assumed to be constant.

In addition, turbine-governor, primary and secondary frequency control models same as those in the estimation model have been considered in Matlab/SimPowerSystems-based simulation. The generator parameters can be found in Table 3.1.

At least two initial guesses for each parameter will be used to demonstrate that UKF can converge to the same estimation.

3.5.1 Parameter Conversion

In the process of UKF tuning, we found that direct estimation of R, T_r and H leads to decreased rate of algorithm convergence. From (3.18), it can be anticipated that the state variables ω and P_m are linearly related to the $\frac{1}{2H}$, $\frac{1}{R}$ and $\frac{1}{T_r R}$ respectively. Therefore, a small change in R, T_r and H results in big fluctuations in P_m and ω. In other words, the output measurements have an insignificant sensitivity to the parameters R, T_r and H, which makes the filter tuning very difficult.

To address this issue, parameters $G = \frac{100}{2H}$, $J = \frac{1}{T_r R}$ and $N = \frac{1}{T_r}$ will be estimated. These changes would help the convergence of the UKF algorithm significantly, mostly because the direct relation of parameters and state variables, decreases the order on non-linearity of the dynamic model. With such changes, also ignoring the damping coefficient (D), (3.18) can be rewritten as (3.19).

$$
\begin{cases}
\delta_k = \delta_{k-1} + (\omega_{k-1} - \omega_0)\omega_s \Delta t \\
\omega_k = \omega_{k-1} + \frac{G_{k-1}}{100}(P_m - P_{g_{k-1}})\Delta t \\
P_{m_k} = P_{m_{k-1}} + N_{k-1}(P_{\text{ref}} - P_{c_{k-1}} - P_{m_{k-1}})\Delta t \\
\qquad\qquad\qquad\qquad - J_{k-1}(\omega_{k-1} - \omega_0)\Delta t \\
P_{c_k} = P_{c_{k-1}} + (\omega_{k-1} - \omega_0)K_{i_{k-1}}\Delta t \\
G_K = G_{k-1} \\
M_K = M_{k-1} \\
J_K = J_{k-1} \\
K_{i_k} = K_{i_{k-1}}
\end{cases}
\tag{3.19}
$$

In the literature, V, θ, P, and Q of PMU data are used as an input-output for Kalman Filter [7, 10, 19]. However, in this section, frequency control parameters are to be estimated. Based on our experience, without frequency measurements from the generator terminal bus, convergence of the estimation is problematic. Therefore, the frequency of generator terminal bus is recorded and used as an output of the estimated model.

We also make a simplifying assumption that the frequency measured at the generator terminal bus is equivalent to the rotor speed (ω). The output signals can be written by input signals and state variables in the discrete form as follows.

$$
\begin{cases}
\theta_{g_k} = \delta_k - \tan^{-1}\left(\frac{P_{g_k} x'_{d_k}}{\sqrt{(E_{q_k} V_{g_k})^2 - (P_{g_k} x'_{d_k})^2}})\right) \\
Q_{g_k} = \frac{\sqrt{(E_{q_k} V_{g_k})^2 - (P_{g_k} x'_{d_k})^2} - V_{g_k}^2}{x'_{d_k}} \\
f_k = \omega_k
\end{cases}
\tag{3.20}
$$

Table 3.1. Generator parameters used in MATLAB/SIMPOWER simulations

Parameters	Set 1	Set 2	Set 3
E_q (pu)	1.0567	1.8537	1.8537
x'_d (pu)	0.3	0.3	0.3
x''_d (pu)	–	0.25	0.25
x'_q (pu)	–	0.55	0.55
x''_q (pu)	–	0.25	0.25
$T_{do}{}'$ (pu)	–	8	8
$T_{do}{}''$ (pu)	–	0.03	0.03
$T_{qo}{}'$ (pu)	–	0.4	0.4
$T_{qo}{}''$ (pu)	–	0.05	0.05
P_{ref} (pu)	0.778	0.779	0.779
H (pu. sec.)	6.5	6.5	6.5
R (pu)	0.1	0.1	0.1
T_r (sec.)	0.1	0.1	0.1
K_i	50	50	50
AVR Gain(K_a)	–	–	200
AVR T_a	–	–	0.001
Exciter K_e	–	–	1
Exciter T_e	–	–	0
PSS K_p	–	–	30
PSS T_w	–	–	10
PSS lead lag 1 T_{num}	–	–	0.05
PSS lead lag 1 T_{den}	–	–	0.02
PSS lead lag 2 T_{num}	–	–	3
PSS lead lag 2 T_{den}	–	–	5.4

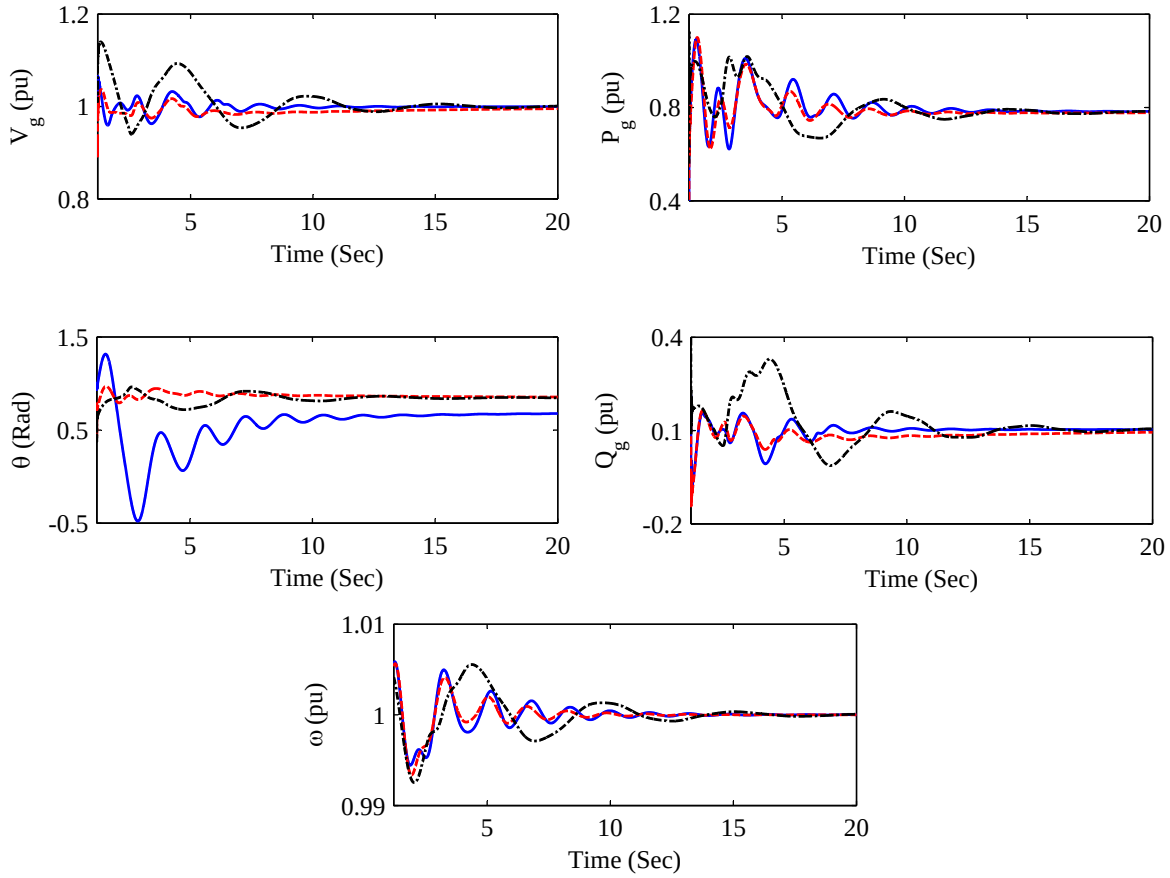

Figure 3.4. Three sets of PMU data generated from Matlab/SimPower systems simulation. Blue solid lines: Set 1; Red dashed lines: Set 2; Black dot-Dashed: Set 3.

For this estimation model, E_q, P_{ref}, x'_d are assumed known. In the UKF algorithm, P is the covariance matrix of the state variables, X_0 is the initial guess of the augmented state vector and P_0 is the initial guess for the covariance matrix P. Estimation accuracy is not sensitive to the initial guess of parameters or state variables. Initial guess for covariance matrix (P_0) will influence the convergence rate. Therefore, fine tuning of P_0 is needed. Q is the covariance matrix of the process noise and kept constant for all three sets of data. Table 3.2 shows the initial guess for X_0 and P_0 as well as diagonal elements of process noise matrix Q. R is the covariance matrix of the output measurement noise ($R = \text{diag}\begin{pmatrix} 10^{-15} & 10^{-15} & 10^{-15} \end{pmatrix}$).

Table 3.2. Initial values for parameters estimation of generator with primary and secondary frequency control

X_0	All Sets	P_0	Set 1	Set 2	Set 3	Q	All Sets
δ	0	P_{11}	0.1	0.1	0.1	Q_{11}	10^{-5}
ω	1	P_{22}	10^{-5}	$1e^{-5}$	10^{-5}	Q_{22}	10^{-11}
P_m	0.8	P_{33}	0.1	0.1	0.1	Q_{33}	10^{-9}
P_c	0	P_{44}	10^{-5}	$1e^{-5}$	$1e^{-5}$	Q_{44}	10^{-9}
G	1	P_{55}	10^{-4}	$1e^{-4}$	80	Q_{55}	10^{-4}
J	10	P_{66}	240	35	76	Q_{66}	10^{-12}
N	1	P_{77}	6.3	3.4	10	Q_{77}	10^{-6}
K_i	10	P_{88}	77	64	20	Q_{88}	10^{-4}

3.5.2 Simulation Results

Fig. 3.6-3.9 shows the estimation of states compared to the simulation one. As it can be seen, because same classic generator model is used for both estimation and simulation model, the rotor angle estimation exactly matches with the simulated rotor angle with benchmark model in Set 1 scenario. However, in set 2 and set 3 scenarios, there is a difference between simulated generator model and the estimated ones. Sub-transient generator model is used in the simulation while classic generator model is employed in estimation. Therefore, there is a discrepancy between the estimation and simulation of angle rotor in set 2 and set 3 though

the dynamic trends match each other well. In order to explain this discrepancy, We have to compare the classical model of the generator versus the two-axis sub-transient model of the machine. Fig 3.5 shows both models. If we want to express the two-axis model with a classical model equivalent [7] , we can write:

$$E = \sqrt{(E'^{o}_{d} + (x'_{q} - x'_{d})I^{o}_{q})^2) + (E'^{o}_{q})^2} \tag{3.21}$$

In consequence, there is always a constant discrepancy (δ'^{o}) which can be calculated as (3.22) between the estimated rotor angle and a simulated one.

$$\delta'^{o} = tan^{-1}(\frac{E'^{o}_{q}}{E'^{o}_{d} + (x'_{q} - x'_{d})I^{o}_{q}}) - \frac{\pi}{2} \tag{3.22}$$

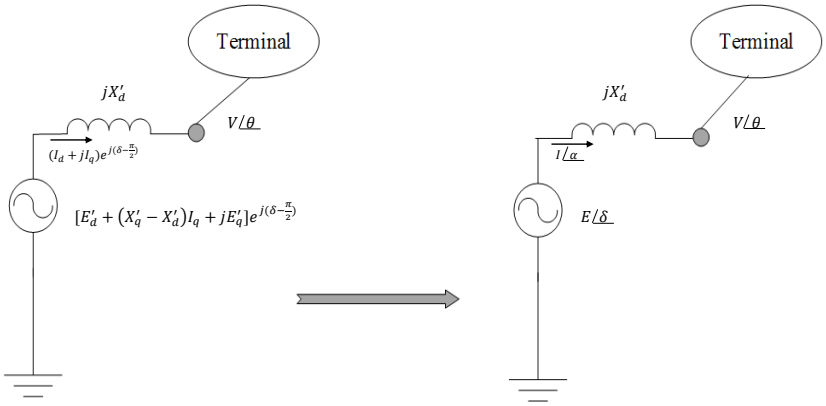

Figure 3.5. Two-axis model of the generator versus its classic model.

Fig 3.10-3.13 show the estimation and simulation result for inertia constant, turbine-governor time constant, droop regulation and frequency loop Integrator constant respectively. It is found that even for a complicated generator model equipped with PSS and AVR, UKF can estimate all parameters and state variables with good accuracy.

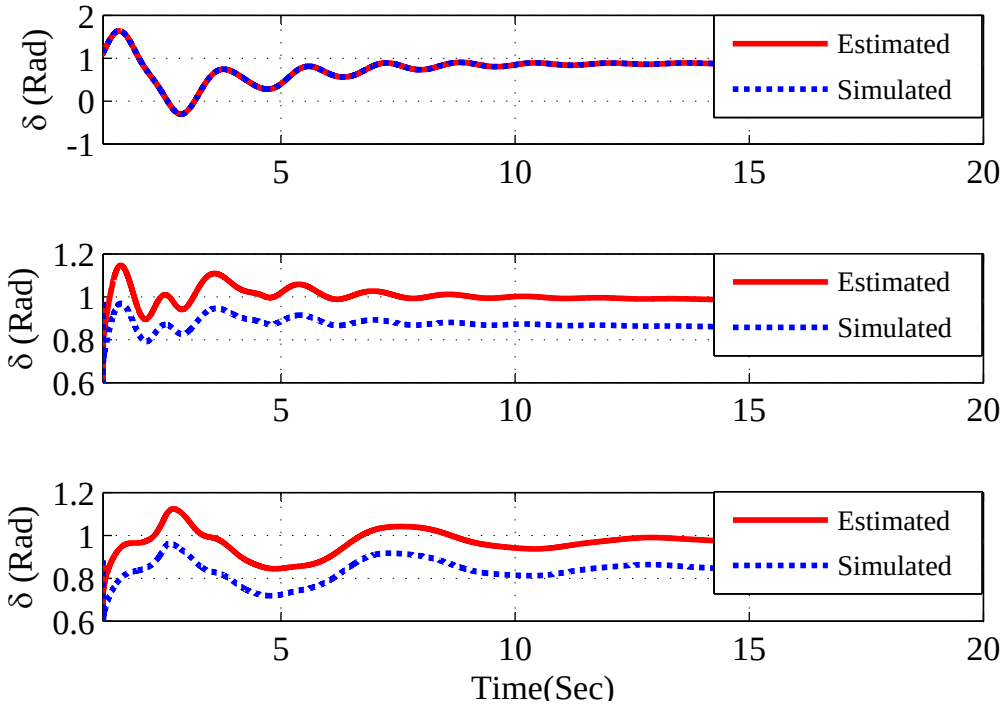

Figure 3.6. Rotor angle estimation and simulation results. Top: Set 1, Middle: Set 2, Bottom: Set 3

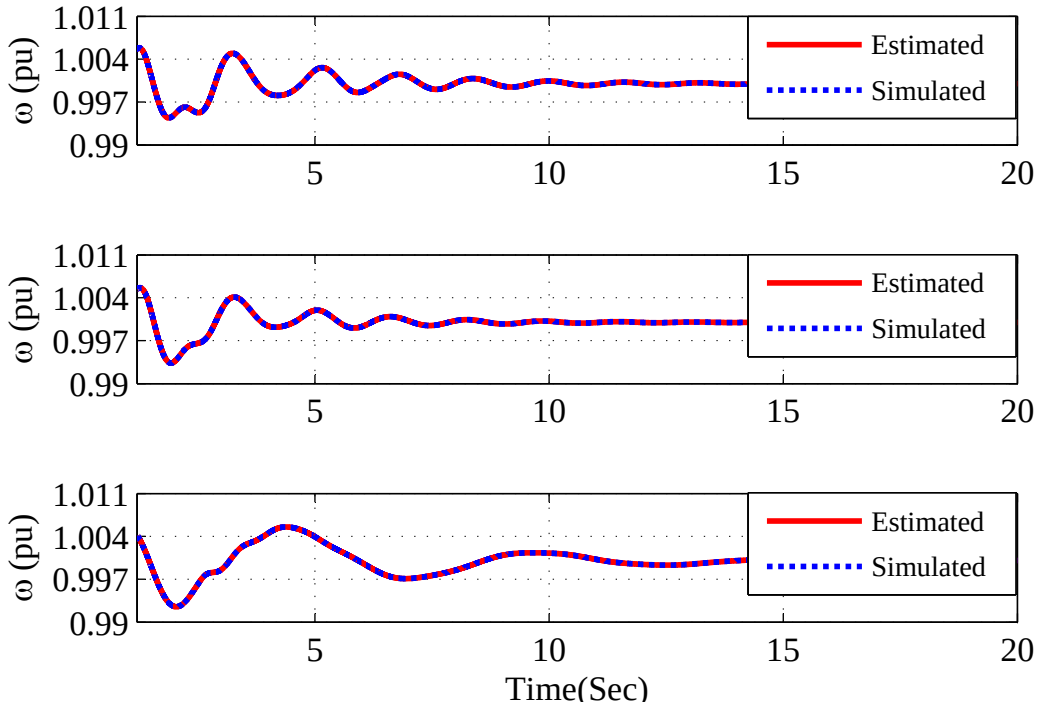

Figure 3.7. Rotor speed estimation and simulation results. Top: Set 1, Middle: Set 2, Bottom: Set 3.

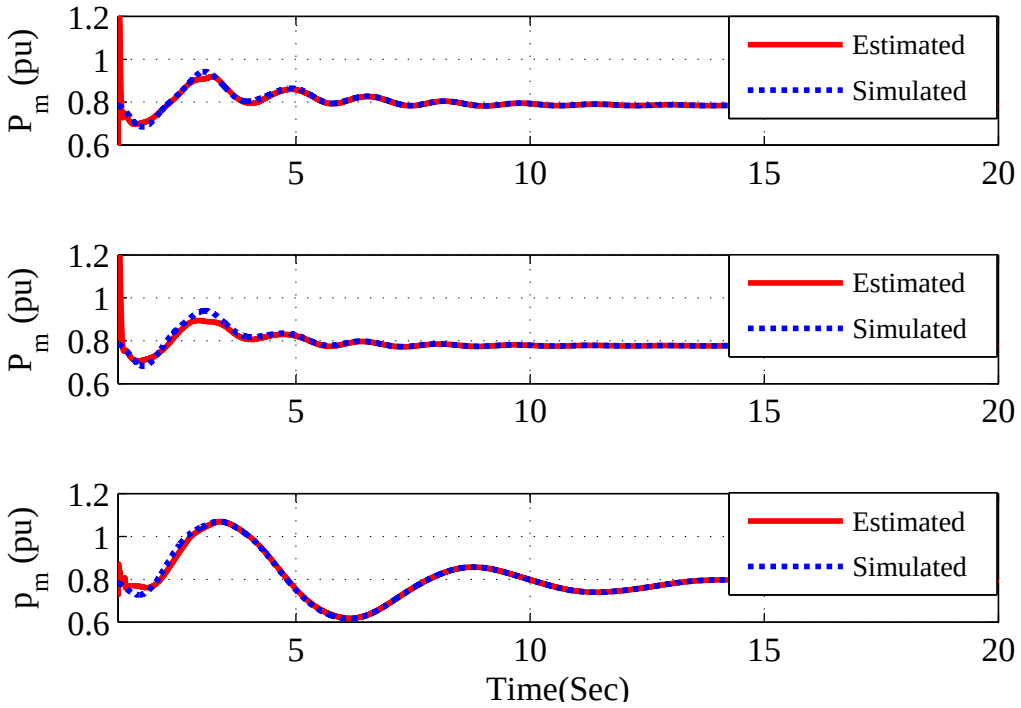

Figure 3.8. Mechanical power estimation and simulation results. Top: Set 1, Middle: Set 2, Bottom: Set 3.

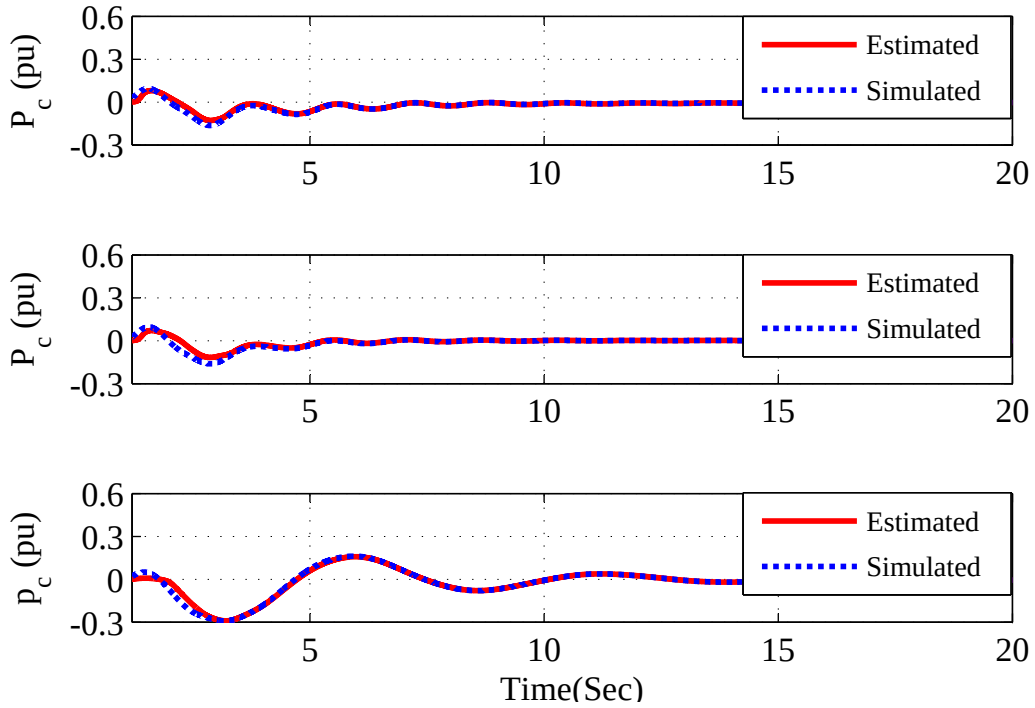

Figure 3.9. Mechanical power reference point estimation and simulation results. Top: Set 1, Middle: Set 2, Bottom: Set 3.

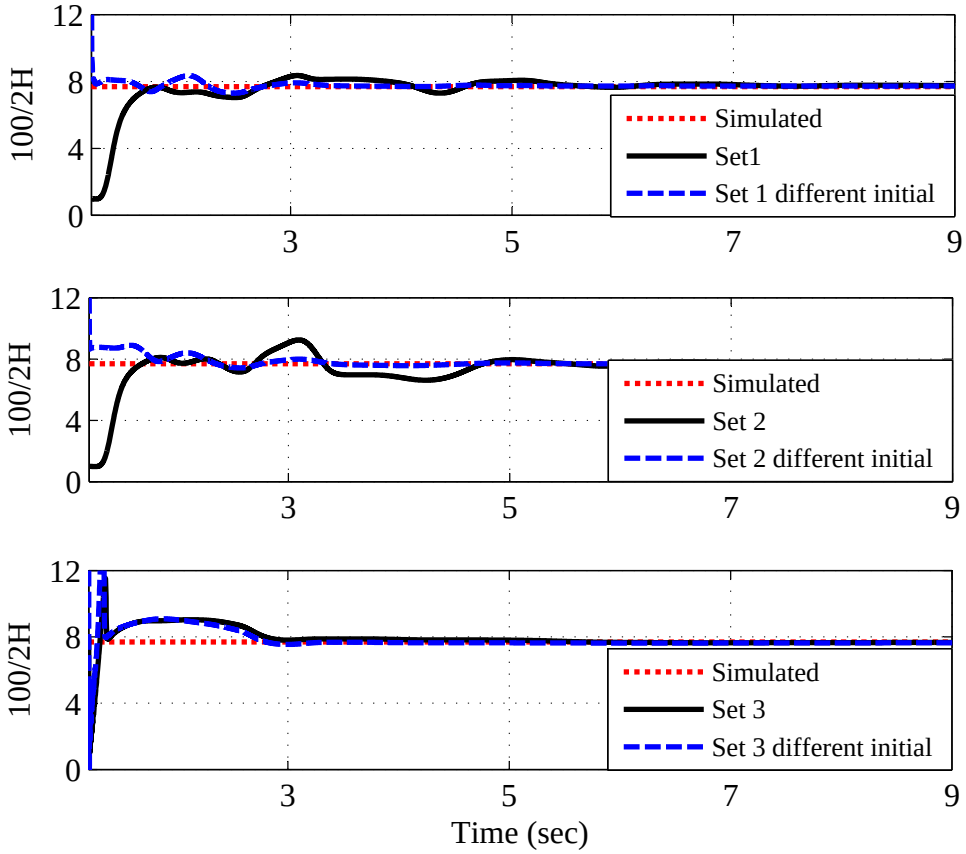

Figure 3.10. Inertia constant estimation and simulation results. Top: Set 1, Middle: Set 2, Bottom: Set 3.

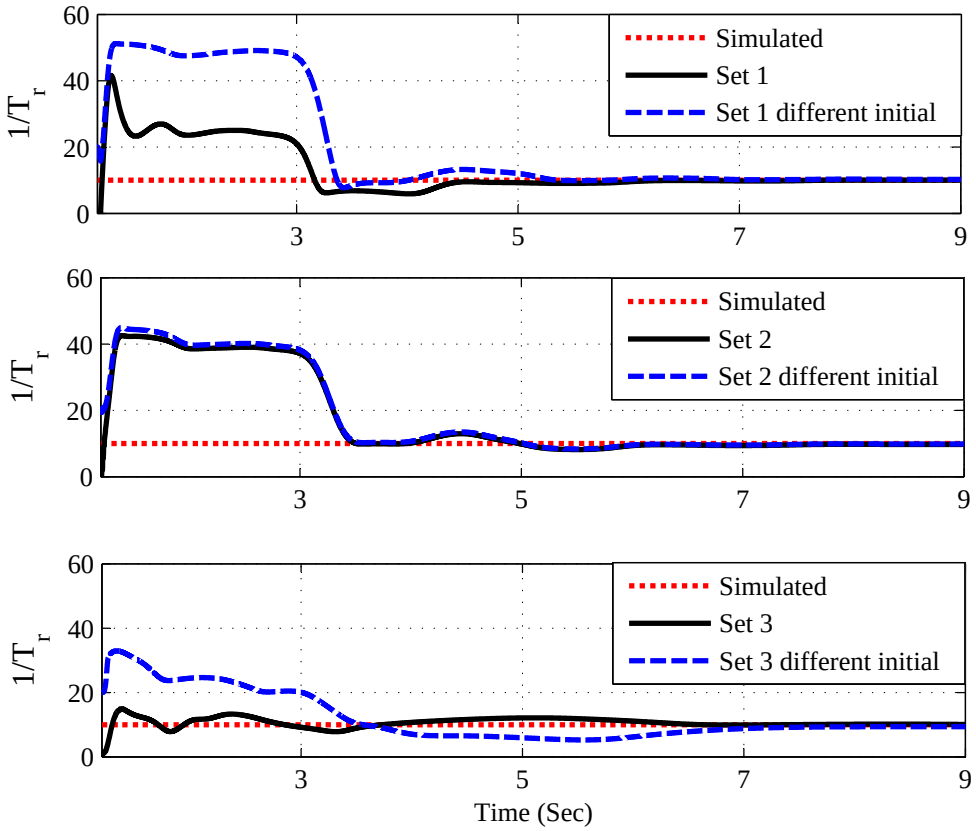

Figure 3.11. Turbine time constant estimation and simulation results. Top: Set 1, Middle: Set 2, Bottom: Set 3.

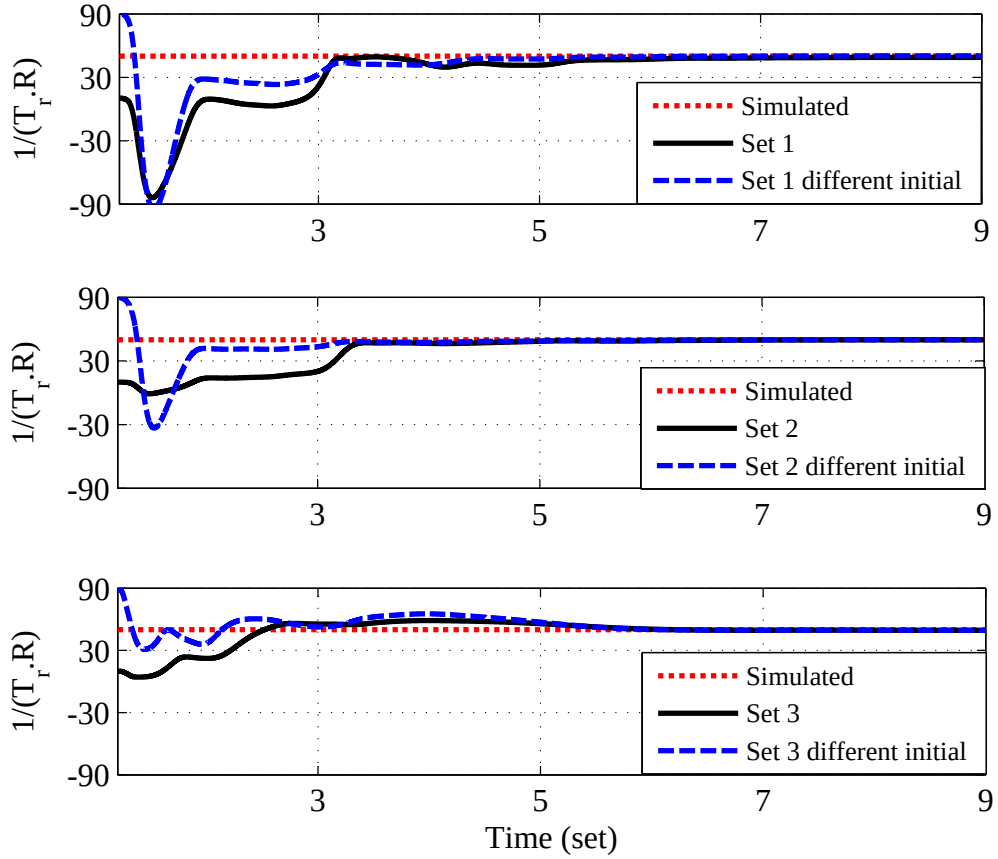

Figure 3.12. Droop regulation estimation and simulation results. Top: Set 1, Middle: Set 2, Bottom: Set 3.

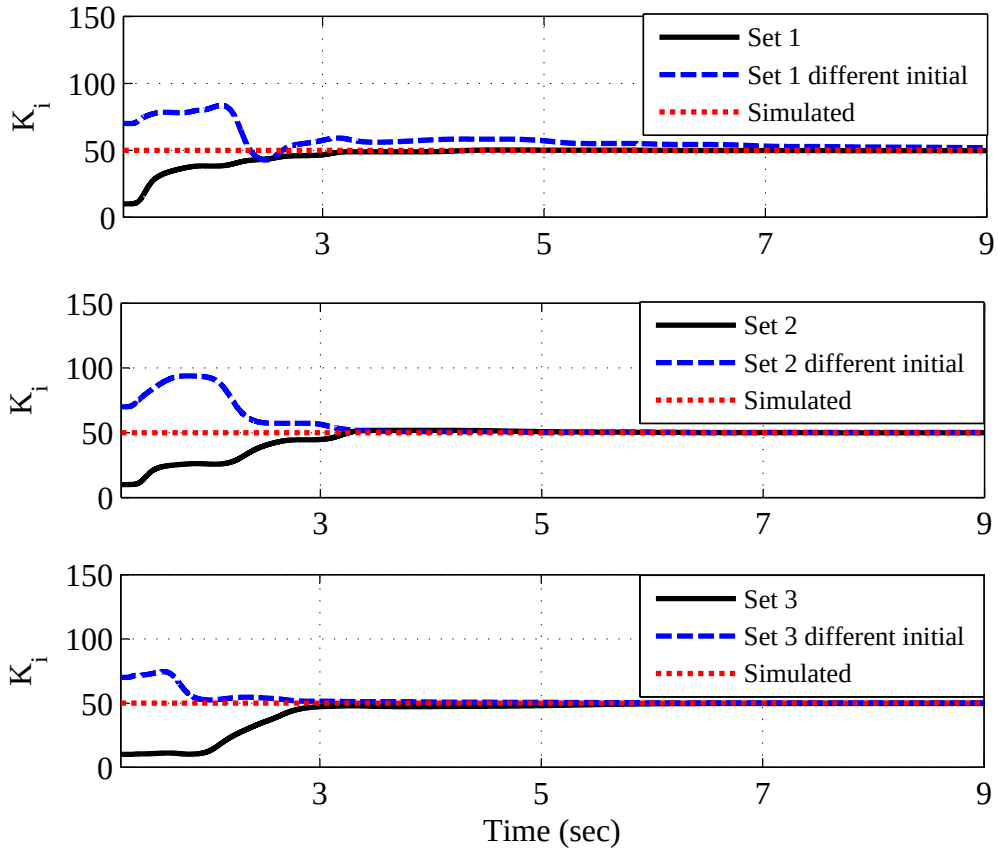

Figure 3.13. Secondary frequency control integrator gain estimation and simulation results. Top: Set 1, Middle: Set 2, Bottom: Set 3.

3.5.2.1 Measurement Noises

In previous scenarios, measurement noises were assumed to be very small (10^{-15}). However, in the real-world applications, the algorithm have to deal with a much higher level of measurement noises. In order to show the effect of such noises on proposed method, three different simulation scenarios were carried out with adding 1%, 2% and 5% Gaussian noises to the Set 3 of the recorded data and the results are compared to the previous parameters estimation. Table 3.5 presents the results for those scenarios. As it would be expected, it can be seen from the table that estimation error increased exponentially with increasing of the measurement noises. Although the error of the estimation was increased with respect to the increasing in the level of measurement noises, the results of the proposed method still show acceptable accuracy for the most of its applications.

3.5.2.2 Model Validation

In the validation step, estimated parameters are used to build a low order generator dynamic simulation model as shown in Fig. 3.1. Then, event playback proposed in [18, 72] is used to validate the estimation model. During event play back, hybrid dynamic simulation injects the inputs (measured PMU data) to the low-order dynamic simulation model, the output of the model will be captured and compared with the actual measurements.

In the previous sections, although UKF is used to estimate parameters, some parameters such as x'_d and E_q are assumed to be known. Moreover, all the generator model needs to have a damping ratio to stabilize the system. Therefore, in this section, UKF method is adjusted to estimate all the parameters of the model. In other words, transient reactance (x'_d), generator's internal voltage (E_q) and generator's damping ratio (D) are added to the parameters which have to be estimated by UKF method. Thus, the augmented state vector

will be $X_k = [\delta_k \ \omega_k \ P_{m_k} \ P_{c_k} \ G_k \ J_k \ M_k \ K_{i_k} \ x'_{d_k} \ E_{q_k} \ D_k]^T$. The PMU data are presented in Fig. 3.4. Kalman filter's parameter estimation are demonstrated in Figs. 3.14 and 3.15.

Estimated parameters have been used to build a continuous dynamic model of the generator in Matlab/Simulink. Then, input data (active power and voltage magnitude) are fed into the model to generate the outputs. Frequency, the reactive power together with voltage phase angle are compared with the data measurements. Figure 3.16 shows the result of validation. Three sets of models are constructed, one with all parameters included, the second one without considering secondary frequency control (without K_i) and the third one without considering any frequency control system (without R and T_r). As demonstrated in Fig. 3.16, considering the frequency control systems in the estimation model will greatly improve the match between the outputs and the PMU data.

3.5.3 Case Study Based on Real-World PMU Data

In this section, UKF method is applied on the PMU data from an anonymous busbar of the MISO system to estimate parameters of a generator dynamic model. In the real-world applications, the only data available is limited to PMU measurements. Equivalent dynamic models are sought. Therefore, it can be anticipated that for the real-world application, all the parameters of the generator are unknown and have to be estimated by the UKF method. The augmented state vector will be $X_k = [\delta_k \ \omega_k \ P_{m_k} \ P_{c_k} \ G_k \ J_k \ M_k \ K_{i_k} \ x'_{d_k} \ E_{q_k} \ D_k]^T$. The initial guess of the state variables X_0 and its covariance matrix P_0 as well as the covariance matrix for the processing noise are listed in Table 3.4.

Fig. 3.17 shows the PMU data of 40 seconds. The set of data was recorded by PMUs after a generator trip event. The data contain significant noises. Besides, PMUs save the data with a 30 Hz sampling rate. Data starting from 12 seconds to 40 seconds are used for estimation. Note that, in the following figures the starting time is 12 seconds. Experiments show that 30 Hz sampling rate does not yield satisfactory performance of UKF. This finding

concurs with the findings documented in [24] that measurements interpolation is needed to improve the performance of Kalman filters. Our experiments show that the real data have to be interpolated to 100 Hz for the UKF method to converge. Figs. 3.18 and 3.19 present the estimation processes. Table 3.3 documents the final parameters estimation results.

Table 3.3. Parameter estimation for real-world PMU data

H	R	T_r	K_i	D	x'_d	E_q
20.18	0.0176	0.073	1.3448	0.031	0.1947	1.0538

In the next step, the low-order model with estimated parameters was built in Matlab/Simulink. Event playback is used to inject voltage magnitude and active power as inputs. The outputs from the estimated model and the output PMU measurements (frequency, voltage phase angle and reactive power) are compared. Fig. 3.20 shows the validation results. It is observed that despite the high level of noise and unknown dynamic system model structure, comparison of the PMU data with the validation model outputs shows a good degree of match. The real-world PMU data case study demonstrates the feasibility of the proposed estimation model in identifying a generator model.

Table 3.4. Initial state variables and covariance matrices for real-world PMU Data

X_0	values	P_0	values	Q	values
δ	0	$P_{1,1}$	0.1	$Q_{1,1}$	$1e^{-5}$
ω	1	$P_{2,2}$	0.1	$Q_{2,2}$	$1e^{-9}$
P_m	0.8	$P_{3,3}$	$1e^{-4}$	$Q_{3,3}$	$1e^{-9}$
P_c	0.8	$P_{4,4}$	$1e^{-2}$	$Q_{4,4}$	$1e^{-9}$
G	15	$P_{5,5}$	0.1	$Q_{5,5}$	$1e^{-8}$
J	50	$P_{6,6}$	1000	$Q_{6,6}$	$1e^{-5}$
N	20	$P_{7,7}$	0.1	$Q_{7,7}$	$1e^{-6}$
k_i	10	$P_{8,8}$	0.71	$Q_{8,8}$	$1e^{-12}$
D	0	$P_{9,9}$	$1e^{-4}$	$Q_{9,9}$	$1e^{-8}$
x'_d	0.1	$P_{10,10}$	$1e^{-3}$	$Q_{10,10}$	$1e^{-7}$
E_q	0.9	$P_{11,11}$	$1e^{-4}$	$Q_{11,11}$	$1e^{-12}$

Table 3.5. Effect of measurement error on parameter estimation error

scenarios	H		Droop		T_r		K_i	
	Value	Error (%)	Value	Error (%)	Value	Error (%)	Value	Error (%)
Simulation	6.5	0	0.2	0	0.1	0	50	0
0% error	6.4773	0.35	0.1992	0.40	0.1005	0.52	50.0127	0.02
1% error	6.4763	0.37	0.1992	0.40	0.1007	0.67	50.0391	0.08
2% error	6.4411	0.91	0.1989	0.56	0.0990	1.00	49.8697	0.26
5% error	6.8068	4.72	0.1948	2.61	0.1059	5.93	50.4820	0.97

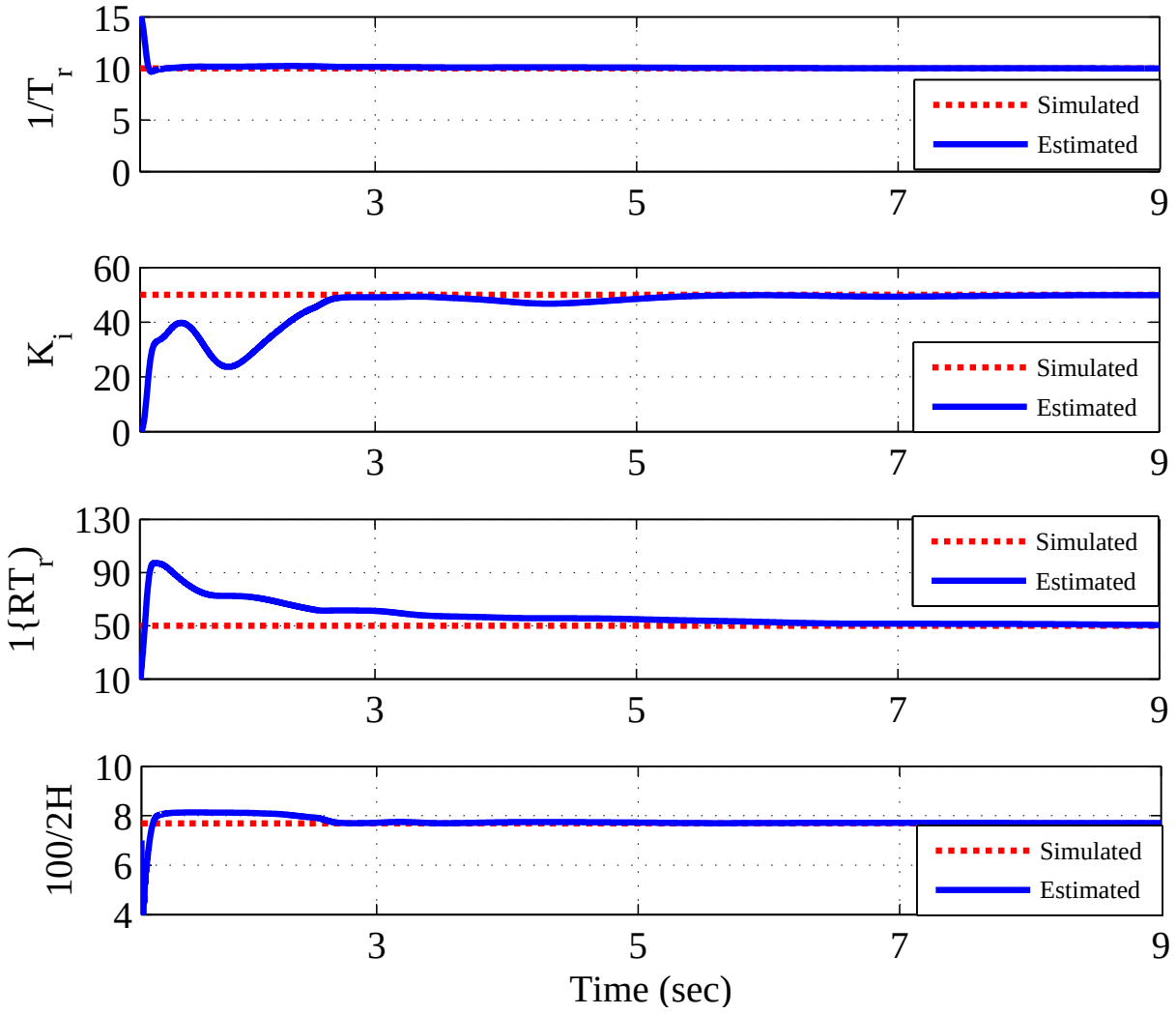

Figure 3.14. Generator parameters estimation and simulation results for set 3.

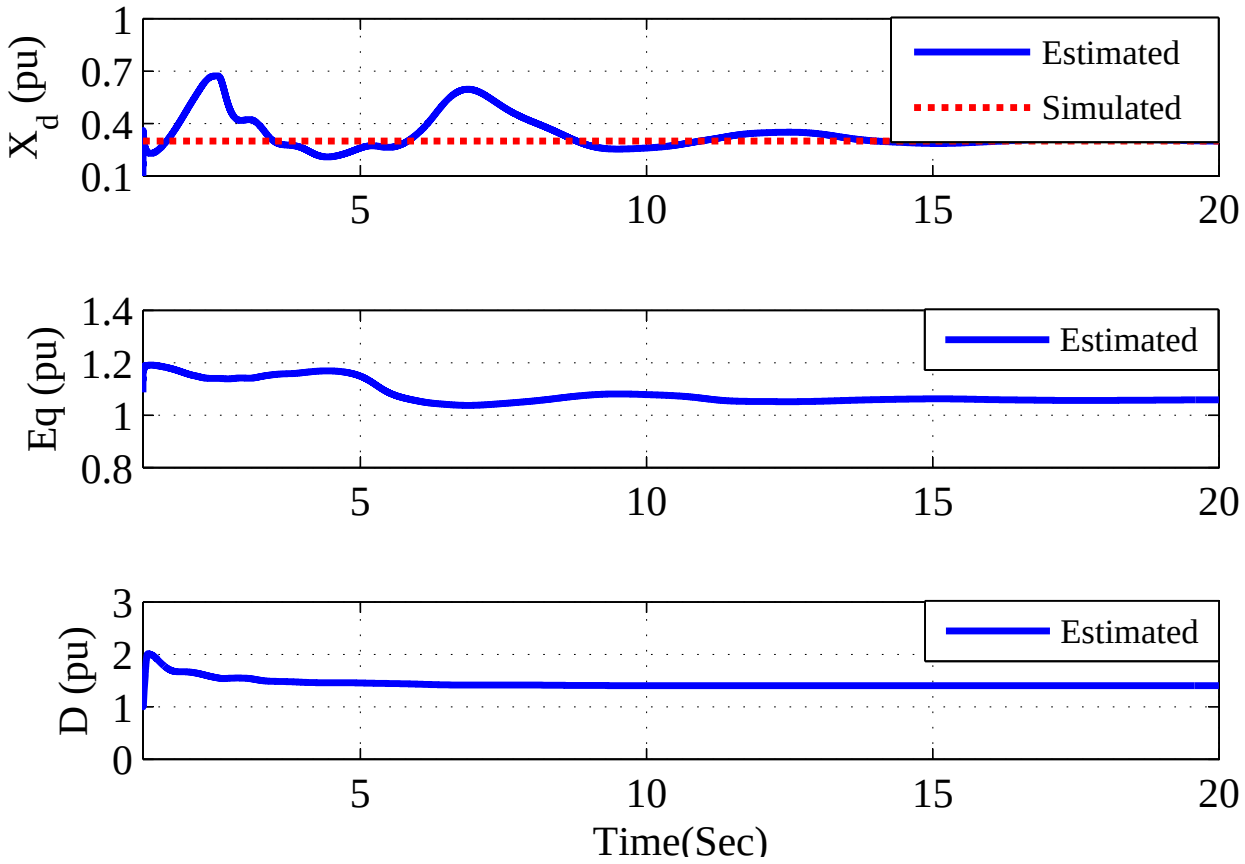

Figure 3.15. Generator parameters estimation and simulation results for set 3.

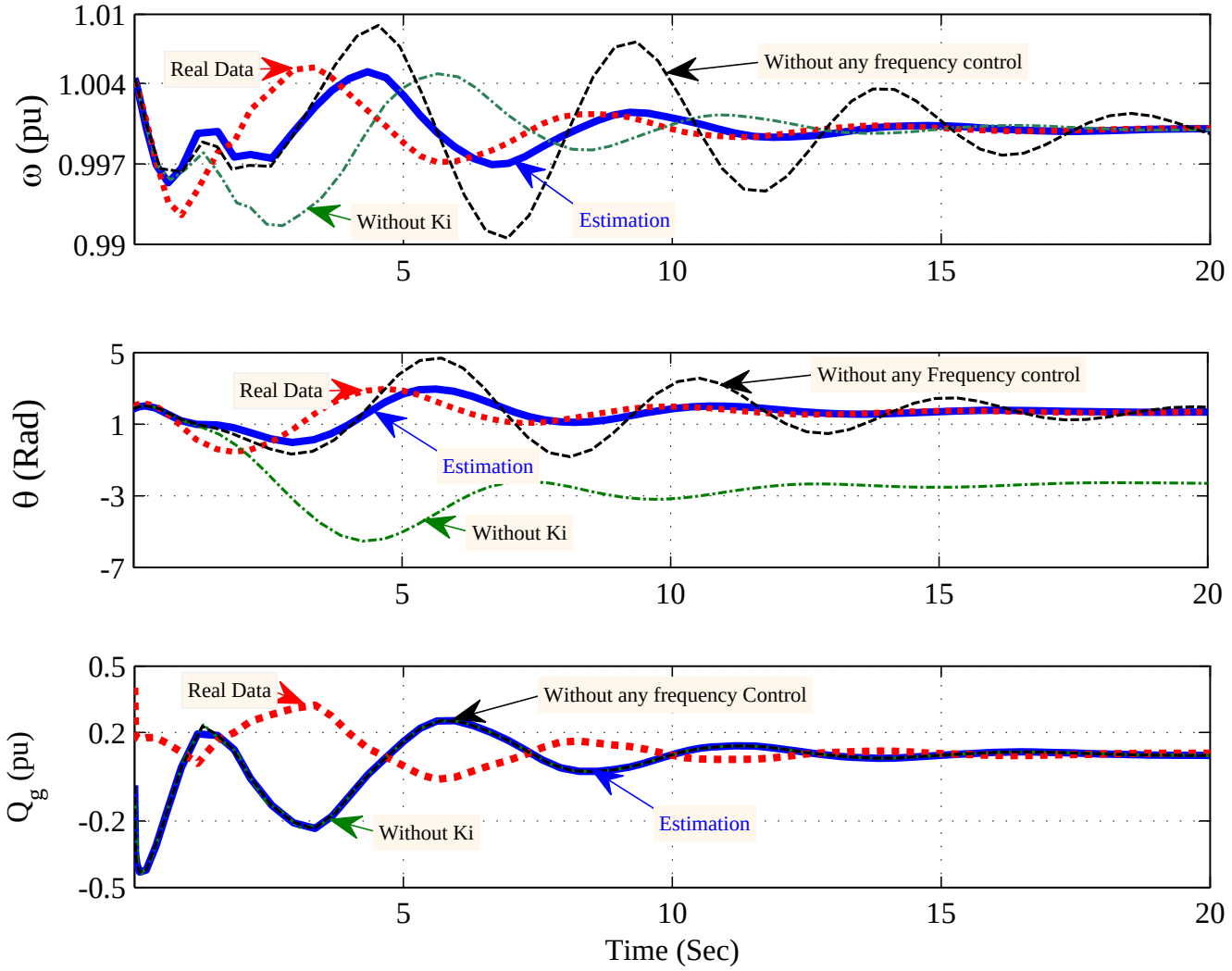

Figure 3.16. Model validation and outputs comparison for set 3. Top: Rotor Speed ω, Middle: Voltage Phase Angle θ, Bottom: Reactive Power Q_g

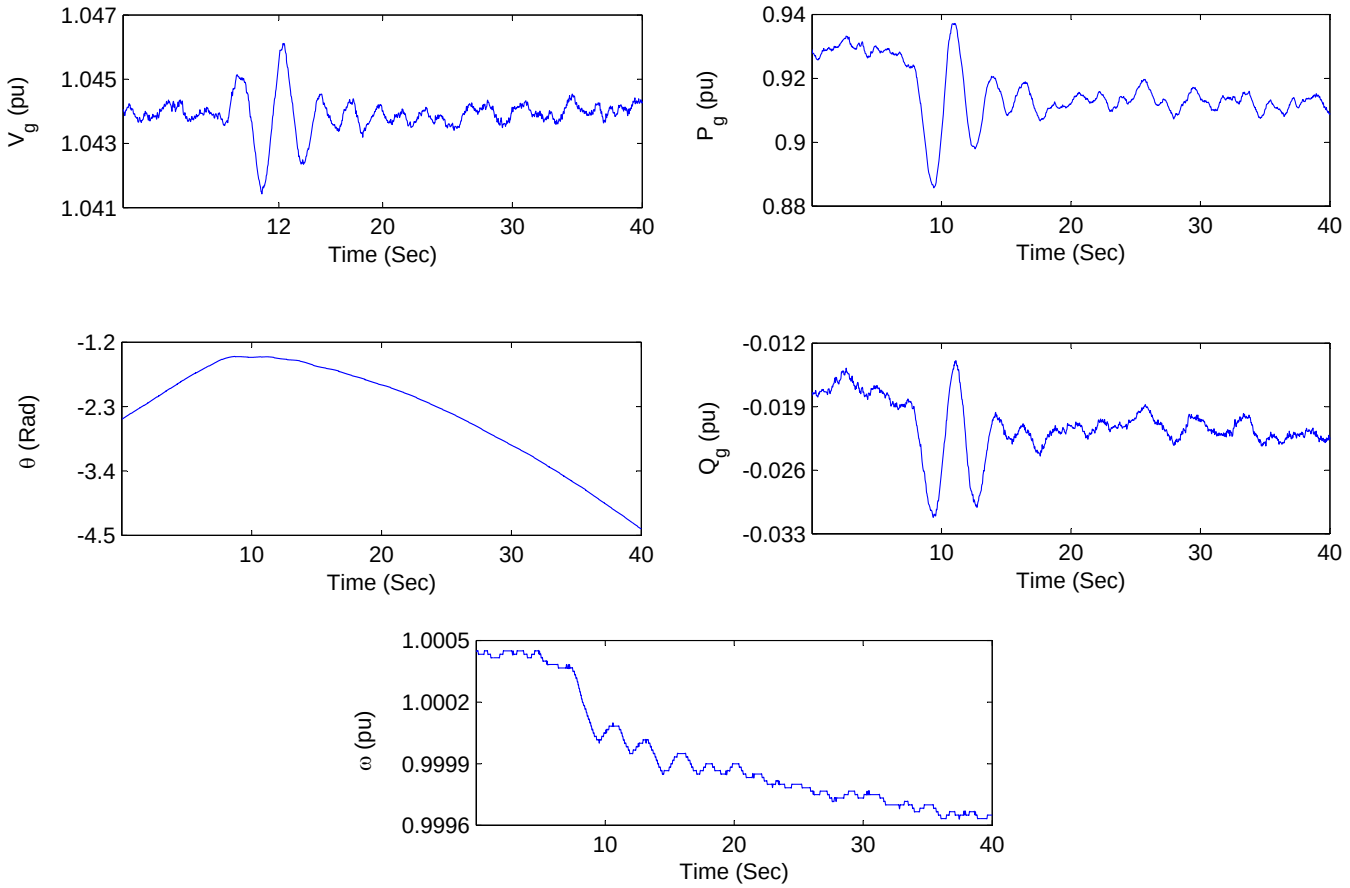

Figure 3.17. Real-world PMU data obtained from a PMU installed at a 500 kV substation. The data has been scaled to pu values, where $S_b = 1000$ MW, $V_b = 500$ kV.

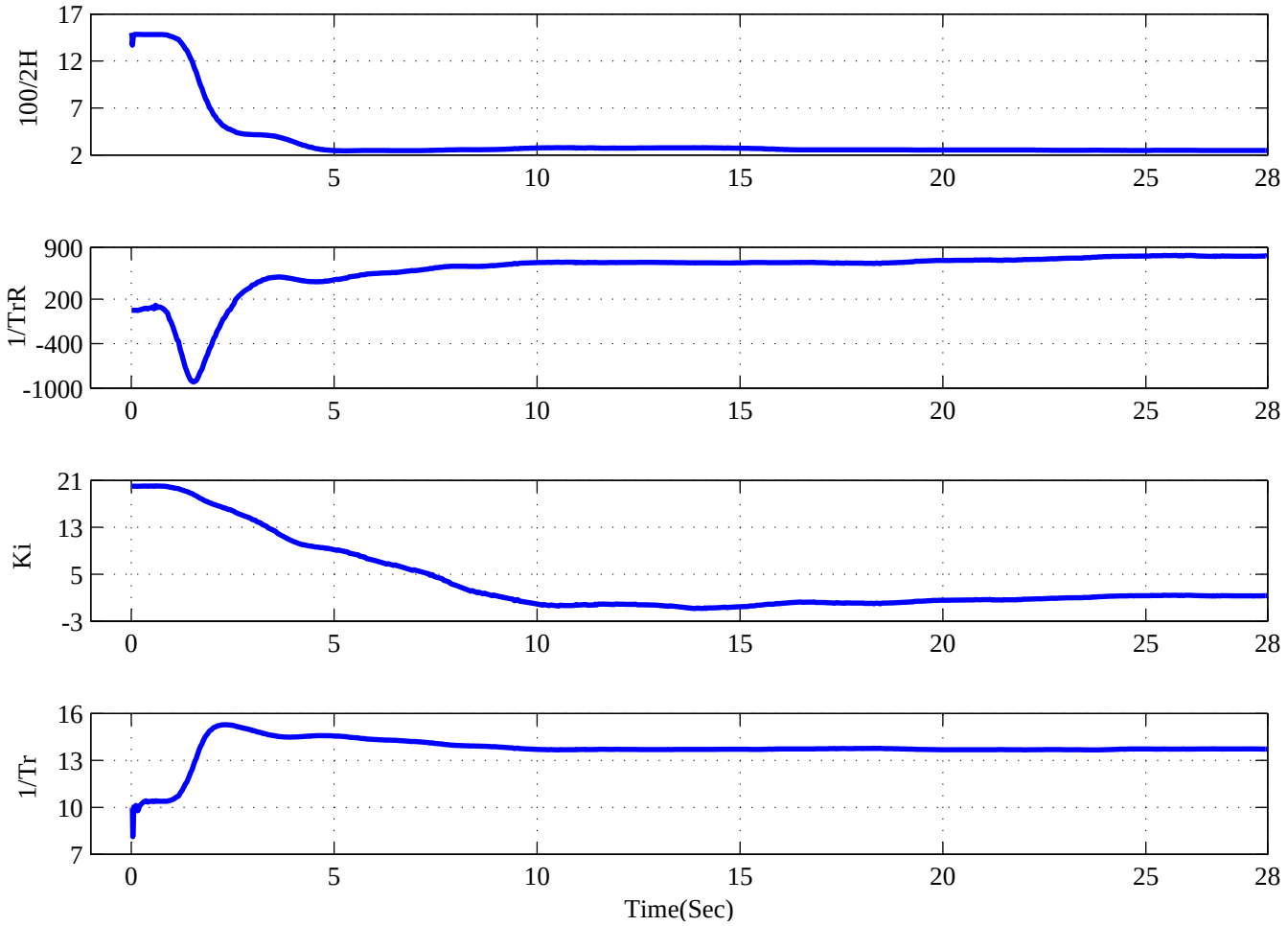

Figure 3.18. Real-world system parameter estimation results.

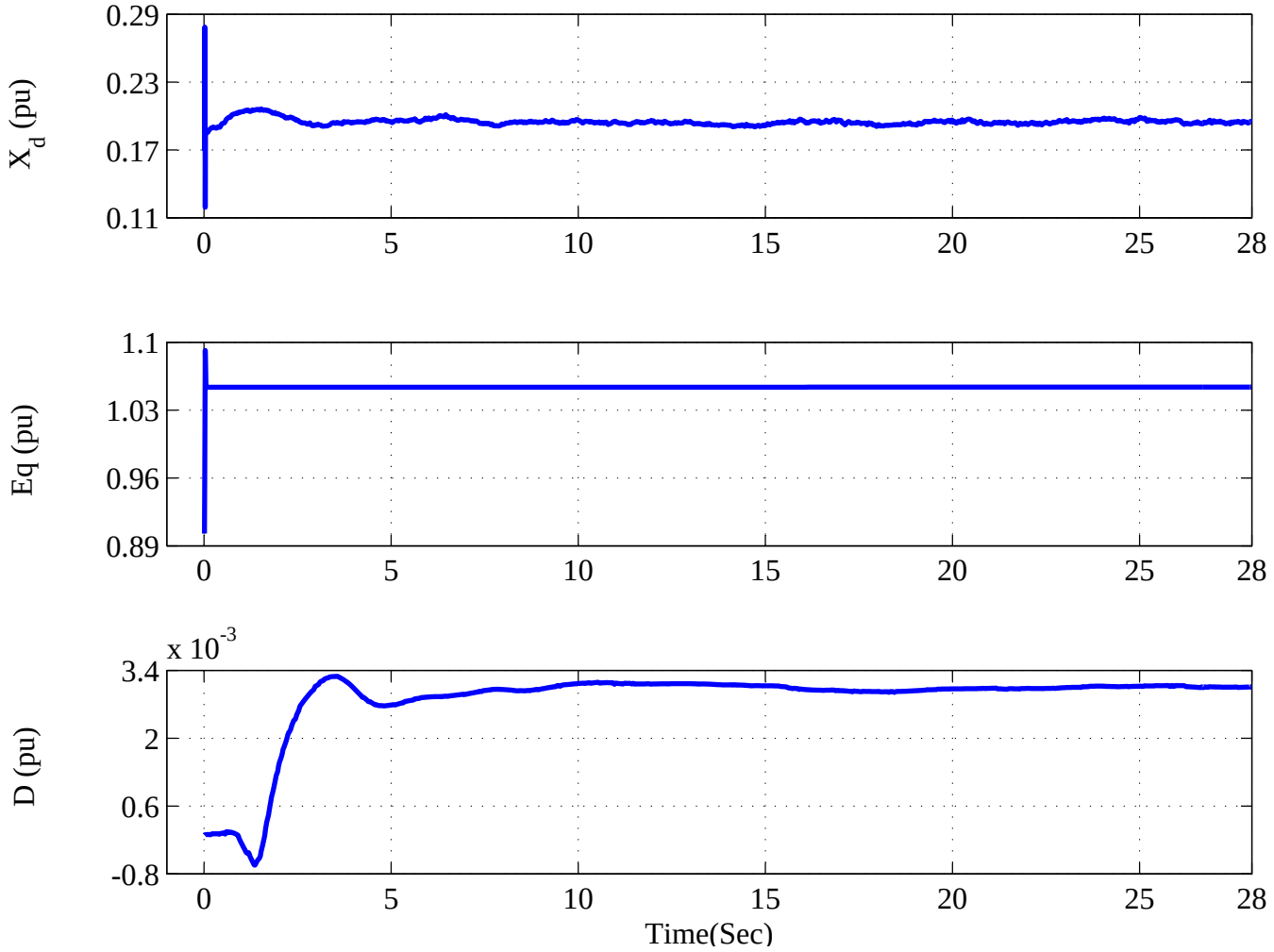

Figure 3.19. Real-world parameter estimation results. Top: x'_d, Middle: E_q Estimation, Bottom: Damping Estimation.

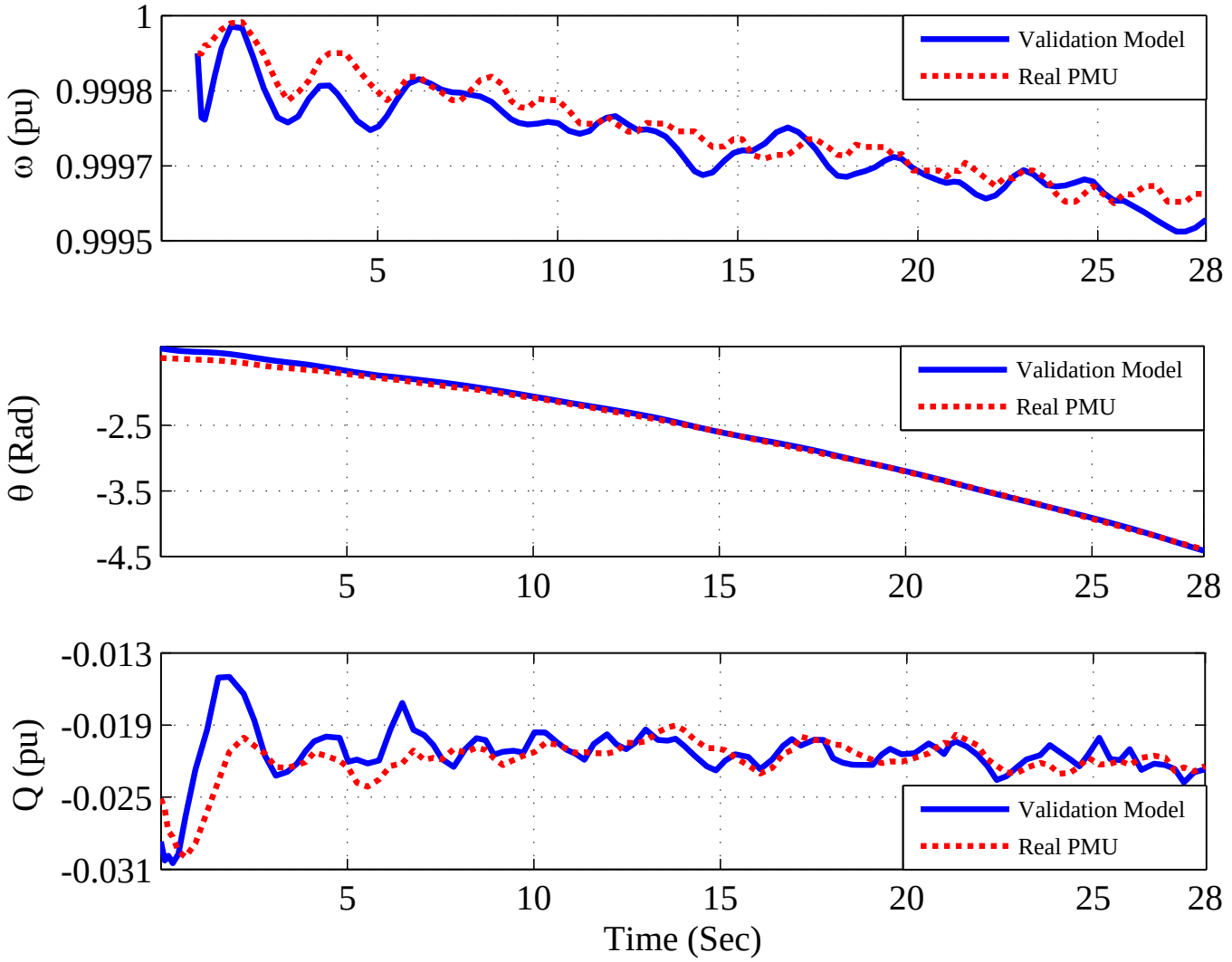

Figure 3.20. Comparison of the real-world measurements and the simplified simulation model outputs. Top: Rotor Speed ω, Mid: Voltage Phase Angle θ, Bottom: Reactive Power Q_g

3.6 Conclusion

UKF is implemented in this section of completed to estimate dynamic states and parameters of a low-order synchronous generator model with both primary and secondary frequency control systems. The proposed method uses voltage magnitude and active power measurements as the inputs, voltage angle, reactive power and frequency as the outputs. The inertia constant, damping coefficient, turbine-governor's time constant, droop regulation as well as secondary frequency integrator unit gain will all be estimated. Both simulation data and real-world PMU data are used for case studies. In this research, various techniques are implemented to improve UKF algorithm for this application. The techniques include: (i) parameter conversion to increase parameter detection sensitivity from the measurements; (ii) measurements interpolating to have a higher sampling rate to improve UKF convergence. In the validation step, a low-order dynamic simulation model is constructed with the estimated parameters. Input data are fed into the model to generate output data. The generated output data will then be compared with the outputs from the measurements.

The case studies demonstrate the feasibility of the proposed UKF estimation approach for system identification using PMU data. Through the proposed estimation method, a complex generator model can be emulated using a low-order generator with frequency controls. The case study on the real-world PMU data demonstrates the capability of the proposed UKF on identifying an equivalent generator model.

CHAPTER 4

ROBUST STATIC STATE ESTIMATION FOR AC NETWORKS

4.1 Note to the Reader

Portions of these results have been submitted for publication (as a 1^{st} author in [73] as well as 3^{rd} author in [63]).

4.2 Introduction

Traditionally, Supervisory Control and Data Acquisition (SCADA) system using non-synchronous data with low-density sampling rate have been used for monitoring and controlling of the system. Such measurements can not capture the system dynamics [74]. Reliable operation and control of power system depend on the results of state estimation. Power system state estimation has been widely investigated in the literature [7,23,25,75,76]. Corrupted data usually exist in power system measurements due to limited measurement sensor's accuracy, communication system problems and cyber attacks. Therefore, state estimator has been equipped with bad data identification algorithms in order to detect such corrupted data and guarantee the accuracy of state estimation. Classic bad data detection algorithms such as *Largest Normalized Residue Test* (LNRT) have been reported in the literature for identifying bad data, [53–55].

LNRT test relies on the state estimation residuals and thus can only be implemented after running state estimation. After any bad datum been detected, state estimation has to be rerun by eliminating that bad datum. Hence, the efficiency and computational time of the

LNRT algorithm becomes a major concern. *Sparse Residual Estimator* (SRE) with ℓ_1-norm optimization was first introduced in [77] for recovering sparse signals from unreliable sensors in the network by using sparse matrix characteristics to create an M-Huber estimator. In [62], SRE application is expanded by using the method for joint linear state estimation and bad data identification for addressing the computing issue associated with the traditional LNRT method. The aforementioned research has focused on linear state estimation. The main goal of this chapter is to introduce an algorithm for simultaneous nonlinear state estimation and bad data identification.

The traditional nonlinear state estimation is formulated as an unconstrained optimization problem and solved by Gauss-Newton iterative method [29]. The requirements of Gauss-Newton method are that the objective function has to be continuous and the problem has to be an unconstrained optimization problem. With l_1-norm constraints introduced in robust estimation, the second requirement cannot be fulfilled. In addition, other types of objective functions (*e.g.*, largest absolute value (LAV)) may not be continuous. In those cases, Gauss-Newton method cannot be applied.

In this chapter, joint state estimation, and bad data detection problem will be formulated as a constrained optimization problem. The traditional power flow constraints are non-convex. There is no guarantee to find global optimum in polynomial time for nonconvex problems. Convex relaxation approach, *e.g.*, semidefinite programming (SDP) relaxations and second-order conic programming (SOCP) relaxations, has been an attractive option to solve non-convex state estimation problems.

In [56, 78], a new SDP state estimator is introduced to overcome the non-convexity of the state estimation problem. Although SDP solvers can produce quality results and small duality gap, they suffer from the high computational time limitation, especially for large-scale systems. On the other hand, SOCP relaxation is superior in terms of computing time. SOCP relaxation has been used to reformulate power flow and state estimation problems

in [57–59]. Compared to SDP relaxation, the feasible region of the SOCP relaxation contains the feasible region of the SDP relaxation for meshed networks. Therefore, SOCP relaxation is termed as a weak relaxation.

Since SOCP relaxation can be weak for the meshed network, [60,61] suggested strengthening SOCP relaxation by separating its optimal solutions from the SDP feasible region. A new least square estimation (LSE)-based SDP cuts for strengthening SOCP relaxation for the optimal power flow problem has been proposed by authors in [63]. In this chapter, the same cutting plane technique is implemented for the SOCP convex problem solving to result in a tighter duality gap.

In summary, the main contributions of this part of research are:

- Introducing a new formulation of simultaneous AC network state estimation and bad data identification. The constrained optimization problem is further relaxed using SOCP relaxation technique.

- Implementing an LSE based SDP cutting plane method to solve the SOCP relaxed problem. This solver leads to more accurate results of state estimation as well as bad data identification.

4.3 Standard Power Flow Equations and its Relaxations

Power flow equations consist of the formulation for power injections of each bus of the system and active and reactive power formulations for transmission line flows.

Using $S_{in} = Y^*(V_i V_i^* - V_i V_n^*)$ and $S_{in} = P_{in} + jQ_{in}$ the polar form of power flow equations can be written as (4.1)-(4.4). Therefore, it can be anticipated that AC power flow problem is a non-linear and non-convex problem.

Power injection equations, i.e.,

$$P_i^g - P_i^d = \sum_{n=1}^{N} |V_i||V_n|(G_{in}\cos(\delta_i - \delta_n) + B_{in}\sin(\delta_i - \delta_n)) \tag{4.1}$$

$$Q_i^g - Q_i^d = -\sum_{n=1}^{N} |V_i||V_n|(G_{in}\sin(\delta_i - \delta_n) - B_{in}\cos(\delta_i - \delta_n)) \tag{4.2}$$

Also, each transmission line's power flow equation can be written as,

$$P_{in} = g_{in}|V_i|^2 - g_{in}|V_i||V_n|\cos(\delta_i - \delta_n) - b_{in}|V_i||V_n|\sin(\delta_i - \delta_n) \tag{4.3}$$

$$Q_{in} = -(b_{in} + \frac{b_{sh}}{2})|V_i|^2 + b_{in}|V_i||V_n|\cos(\delta_i - \delta_n) - g_{in}|V_i||V_n|\sin(\delta_i - \delta_n) \tag{4.4}$$

For writing power flow equations in rectangular form, consider $V_i = e_i + jf_i$. Therefore, one can write $|V_i|^2 = e_i^2 + f_i^2$. The rectangular form of power flow equations which is shown in (4.5)-(4.8), drives by substituting new variables e_i and f_i into the equations (4.1)-(4.4).

$$P_i^g - P_i^d = G_{ii}(e_i^2 + f_i^2) + \sum_{\substack{n=1 \\ n \neq i}}^{N} [G_{in}(e_i e_n + f_i f_n) - B_{in}(e_i f_n - e_n f_i)] \tag{4.5}$$

$$Q_i^g - Q_i^d = -B_{ii}(e_i^2 + f_i^2) - \sum_{\substack{n=1 \\ n \neq i}}^{N} [B_{in}(e_i e_n + f_i f_n) + G_{in}(e_i f_n - e_n f_i)] \tag{4.6}$$

$$P_{in} = g_{in}(e_i^2 + f_i^2) - g_{in}(e_i e_n + f_i f_n) + b_{in}(e_i f_n - e_n f_i) \tag{4.7}$$

$$Q_{in} = -(b_{in} + \frac{b_{sh}}{2})(e_i^2 + f_i^2) + b_{in}(e_i e_n + f_i f_n) + g_{in}(e_i f_n - e_n f_i) \tag{4.8}$$

4.3.1 The SDP Relaxation

SDP relaxation which has been widely reported in literature, is first introduced in [79], [80] and [81]. For applying SDP relaxation, the rectangular form of power flow can be used. Let's define hermitian matrix X (i.e. $X = X^*$) and let it be $X = VV^*$. Based on X definition, one can write equations (4.9)-(4.11).

$$X_{in} = \Re(X_{in}) + j\Im(X_{in}) = V_i V_n^* \qquad \forall (i,n) \in \mathcal{L} \quad (4.9)$$

$$X_{ni} = X_{in}^* = \Re(X_{in}) - j\Im(X_{in}) \qquad \forall (i,n) \in \mathcal{L} (4.10)$$

$$X_{ii} = |V_i|^2 \qquad \forall i \in \mathcal{B} \quad (4.11)$$

By substituting given matrix X, equations (4.5)-(4.8) become linear:

$$P_i^g - P_i^d = G_{ii}X_{ii} + \sum_{\substack{n=1 \\ n \neq i}}^{N} [G_{in}\Re(X_{in}) + B_{in}\Im(X_{in})] \quad (4.12)$$

$$Q_i^g - Q_i^d = -B_{ii}Xii - \sum_{\substack{n=1 \\ n \neq i}}^{N} [B_{in}\Re(X_{in}) - G_{in}\Im(X_{in})] \quad (4.13)$$

$$P_{in} = g_{in}X_{ii} - g_{in}\Re(X_{in}) - b_{in}\Im(X_{in}) \quad (4.14)$$

$$Q_{in} = -(b_{in} + \frac{b_{sh}}{2})X_{ii} + b_{in}\Re(X_{in}) - g_{in}\Im(X_{in}) \quad (4.15)$$

Since $X = VV^*$ and is a hermitian matrix, then equations (4.16) and (4.17) characterize X.

$$X \succeq 0 \tag{4.16}$$

$$rank(X) = 1 \tag{4.17}$$

Using above Semidefinite Programming formulation, we were able to find linear equations for power flow. However, this formulation still is a non-convex problem due to the rank constraint in the equation (4.17). Therefore, discarding rank constraint in the above equation leads to SDP relaxation of the power flow problem which is a convex optimization. Note that, since X components are a complex number the above SDP relaxation belongs to the complex domain.

4.3.2 The SOCP Relaxation

SOCP relaxation can be applied to the SDP model by further relaxation of SDP constraint in 4.16. For doing so, we have to impose positive semidefinite constraints on all the 2×2 submatrices of X for each line of the power network.

$$\begin{bmatrix} X_{ii} & X_{in} \\ X_{ni} & X_{nn} \end{bmatrix} \succeq 0 \qquad \forall (i,n) \in \mathcal{L} \tag{4.18}$$

Because X is a hermitian matrix and based on the Sylvester criterion, (4.18) is equivalent to the following second-order cone constraints [61]:

$$X_{ii}, X_{nn} \geq 0 \qquad \forall i,n \in \mathcal{B} \tag{4.19}$$

$$\Re(X_{i,n})^2 + \Im(X_{in})^2 \leqslant (\frac{X_{ii} + X_{nn}}{2})^2 - (\frac{X_{ii} - X_{nn}}{2})^2 \tag{4.20}$$

It is proven in [82] that the above system of equations is strictly equivalent to the constraint (4.16) for radial power networks. However, in meshed network, SOCP relaxation can

be weak [61]. By looking at the power flow formulations in (4.1)-(4.4), one can find another formulation to implement SOCP relaxation to the power flow problem.

From equations (4.1)-(4.8), we can observe that one of the following forms is responsible for non-linearity and non-convexity of power flow problem: i. $e_i^2 f_i^2 = |v_i|^2$, ii. $e_i e_n + f_i f_n = |V_i||V_n|\cos(\delta_i - \delta_n)$ and iii. $e_i f_n - f_i e_n = -|V_i||V_n|\sin(\delta_i - \delta_n)$. For dealing with those non-linear terms, we can define new variables T and S in a way that $T_{ii} = e_i^2 f_i^2 = |v_i|^2$ for all buses and $T_{in} = e_i e_n + f_i f_n = |V_i||V_n|\cos(\delta_i - \delta_n)$ and $S_{in} = e_i f_n - f_i e_n = -|V_i||V_n|\sin(\delta_i - \delta_n)$ for all lines of the power network. Substituting new variables into the equations (4.1)-(4.8), the new formulation of power flow derives as follows:

$$P_i^g - P_i^d = G_{ii}T_{ii} + \sum_{\substack{n=1 \\ n \neq i}}^{N} [G_{in}T_{in} - B_{in}S_{in}] \tag{4.21}$$

$$Q_i^g - Q_i^d = -B_{ii}Tii - \sum_{\substack{n=1 \\ n \neq i}}^{N} [B_{in}T_{in} + G_{in}S_{in}] \tag{4.22}$$

$$P_{in} = g_{in}T_{ii} - g_{in}T_{in} + b_{in}S_{in} \tag{4.23}$$

$$Q_{in} = -(b_{in} + \frac{b_{sh}}{2})T_{ii} + b_{in}T_{in} + g_{in}S_{in} \tag{4.24}$$

To make alternative formulation to be exact, following relations between the new introduced variables have to be held:

$$T_{in} = T_{ni}, \quad S_{ib} = -S_{ni} \tag{4.25}$$

$$T_{in}^2 + S_{in}^2 = T_{ii}T_{nn} \tag{4.26}$$

Equation (4.26) is a surface of a cone, and above formulation belongs to the SOCP. However, (4.26) is a non-convex constraint and we can further apply SOCP relaxation to alternative formulation by changing this constraint from equality to inequality (i.e. $T_{in}^2 + S_{in}^2 \leqslant T_{ii}T_{nn}$). Note that r elaxed constraint is equivalent to (4.20) in standard SOCP formulation. The above formulation was first introduced in [83] and [57]. Latter shows that The alternative SOCP power flow problem is exact for radial networks. Since the alternative formulation is a strick relaxation of the power flow problem for meshed networks, the optimal solution for this problem may not be feasible, and the relaxation can be weak for the network with cycles. To take care of Kirchhoffs Voltage Law [58] proposed to introduce the following constraints to the alternative formulation of power flow in order to make the formulation be exact for the meshed networks:

$$\delta_n - \delta_i = \tan^{-1}(\frac{S_{in}}{T_{in}}) \tag{4.27}$$

Note that, since the equation in (4.27) contains tangent function, it's a non-convex constraint.

4.3.3 State Estimator with SOCP Relaxation

Voltage magnitudes and angles of each bus of the power network are usually assumed as a state variable. Therefore based on the alternative formulation of the power flow problem in (4.21)-(4.27), state vector x can be defined as:

$$x = [..., T_{ii}, ..., T_{in}, ..., S_{in}, ..., \delta_i, ...]^T \tag{4.28}$$

There are two different methods which widely used for state estimation, Least Square estimation and Least absolute value estimation. LSE minimizes the sum of the squares

of errors between measured values and measurement function. Therefore the cost function for the state estimation problem can be represented by the second norm of the summation of errors between measurement function and measurements. Thus LSE cost function is a quadratic convex problem. i.e.

$$\min \sum_{k=1}^{m} ||h_k^T(x) - z_k||_2^2 \tag{4.29}$$

h_k^T is the kth row of the linear measurement function matrix and z_k is the kth measurements of the system. In compare to the LSE, Least Absolute Value Estimation (LAV) minimizes the sum of absolute errors between measured values and measurement function outputs. The LAV cost function is a non-convex problem due to its absolute function. However, it's well known that we can make the problem convex by introducing two positively bounded variable to the cost function of LAV. Therefore, the problem can be represented as follows:

$$\min \sum_{k=1}^{m} (r_k + b_k) \tag{4.30}$$

$$\text{s.t.} \quad h_k^T(x) - z_k + r_k - b_k = 0 \tag{4.31}$$

$$r_k \geq 0, \quad b_k \geq 0, \quad for\ k = 1, ..., m \tag{4.32}$$

where r_k and b_k are positively bounded variables, introduced for taking care of absolute function.

Based on the measurements type, measurement function takes different forms. If the measurement contains Real and Reactive power injections, measurements function is in the form of equations (4.21) and (4.22).

Also, equations (4.23) and (4.24) represents transmission lines Power flow measurement functions. Furthermore, sometimes the measurements contain transmission lines current magnitudes transformed into the square of measurement current magnitudes and bus voltage magnitudes transformed to the square of the measurement voltage magnitudes as well. In those cases, the measurement functions are in the form of (4.33) and (4.34) respectively.

$$h_k^T(x) = [g_{in}^2 + (b_{in} + \frac{b_{sh}}{2})^2]T_{ii} + (g_{in}^2 + b_{in}^2)T_{nn} - 2[g_{in}^2 + b_{in}(b_{in} + \frac{b_{sh}}{2})]T_{in} - 2(\frac{g_{in}b_{sh}}{2})S_{in} \tag{4.33}$$

$$h_k^T(x) = T_{ii} \tag{4.34}$$

Each mentioned estimation methods restricted to four types of constraints. The first type of constraints which is shown in (4.35) models zero-injection pseudo-measurement. The second type of constraints in (4.36) is inequality constraints, relates to the direction of power flow or power injection and usually uses in conjunction with the current magnitude measurements.

$$h_k^T(x) = z_k \tag{4.35}$$

$$z_k^{min} \leq h_k^T(x) \leq z_k^{max} \tag{4.36}$$

Also adding feasibility constraints in the form of (4.26) and (4.27) can help optimization to converge to the feasible optimal solution. Note that feasibility constraints are non-convex functions. Because of that, we have to apply SOCP relaxation to the state estimation problem as it has been discussed in the previous section. Therefore, applying SOCP relaxation makes equality sign in (4.26) substitute by an inequality sign. Also, angle constraint in

(4.27) will be discarded, and thus SOCP relaxation based state estimator algorithms can be represented by one of the following forms.

Algorithm 1 LSE state estimator with SOCP relaxation

$\min \sum_{k=1}^{m} ||r_k||_2^2$

S.t.

$h_k^T(x) - z_k + r_k = 0$ (form of(4.21)-(4.24)&(4.33)-(4.34))

$h_k^T(x) = z_k$ (zero-pseudo measurements)

$z_k^{min} \leq h_k^T(x) \leq z_k^{max}$

$T_{in}^2 + S_{in}^2 \leq T_{ii} T_{nn}$

Algorithm 2 LAV state estimator with SOCP relaxation

$\min \sum_{k=1}^{m} (r_k + b_k)$

S.t.

$h_k^T(x) - z_k + r_k = 0$ (form of(4.21)-(4.24)&(4.33)-(4.34))

$h_k^T(x) = z_k$ (zero-pseudo measurements)

$z_k^{min} \leq h_k^T(x) \leq z_k^{max}$

$T_{in}^2 + S_{in}^2 \leq T_{ii} T_{nn}$

$h_k^T(x) - z_k + r_k - b_k = 0$

$r_k \geq 0, \quad b_k \geq 0$

4.4 Bad Data Detection Algorithms

Corrupted data usually exist in power system measurements due to limited measurement sensor accuracy, communication system problem and cyber security attacks. Also, sometimes the corrupted data occurs because meters are out of bias or having drifts, the communication system suffers from wrong connections or outage, or the meters subject to the noises from unexpected interferences. Therefore, it is important that state estimator has the ability to detect this corrupted data and eliminates bad data for increasing the accuracy of estimation and guarantees the reliable operation of the power system.

Some of the bad data such as negative voltage magnitude, measurements with the orders of magnitude larger or smaller than it can be, or the significant difference between incoming

and leaving current at a connection node are easy to detect and can be eliminated before running SE algorithm. However, it is not true for all type of bad data, and some bad data are not easy to detect.

For the bad datum which not relates to cyber security attacks, it can be represented by Gaussian distribution with a zero mean. Such bad data can broadly classify as the number of measurements, that contain corrupted data. Therefore, the classification of bad data is as follows:

- Single bad data: Only one of the measurements is corrupted and has a large error in entire system
- Multiple bad data: There are multiple measurements with corrupted data and large error in the system.

Multiple bad data may occur in measurements with residuals with weak or strong correlations. In strongly correlated measurements, the bad data in one will affect the residuals of the others significantly and thus cause some good sensors appears among corrupted measurements. In contrast, weakly correlated measurements, the error of one does not affect the other ones. Also, in strongly correlated measurement residuals, the errors may or may not be confirming which means the errors may or may not consisting with each other [29]. Therefore, multiple bad data can be classified into three groups:

- Non-interacting multiple bad data with weakly correlated residuals.
- Interacting multiple bad data with non-confirming strongly correlated residuals.
- Interacting multiple bad data with confirming strongly correlated residuals.

The performance of traditional tests depends on the type of errors in the system. Therefore, upcoming sections will review the different bad data identification tests and compare their performance in the detection of various types of bad data.

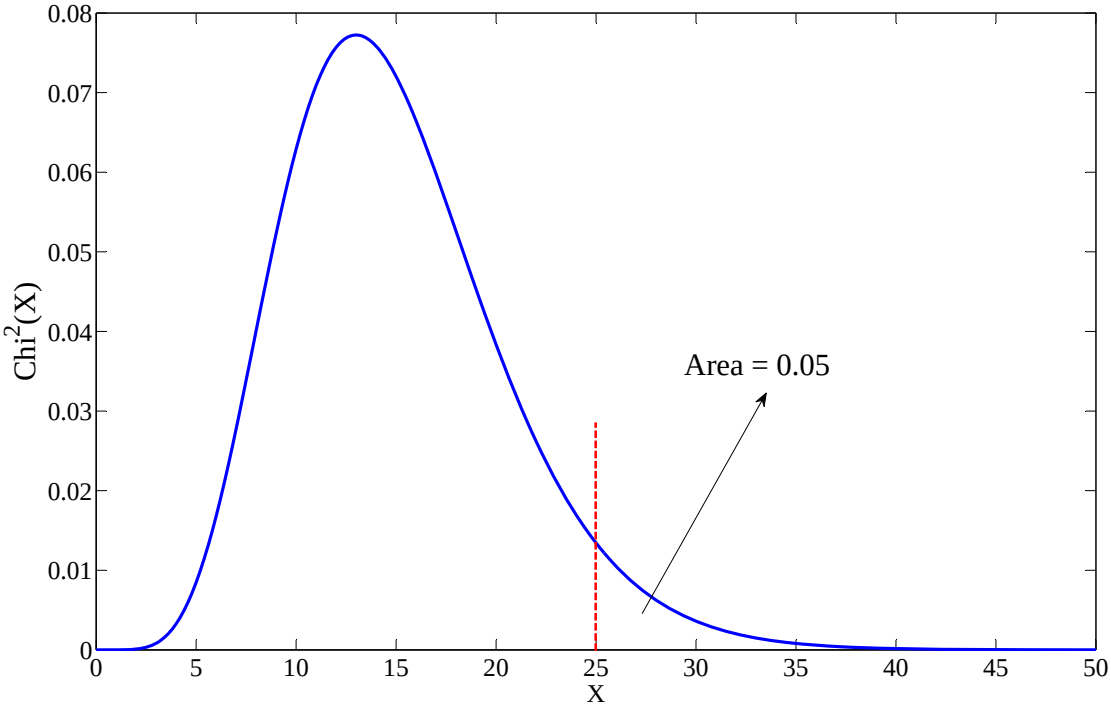

Figure 4.1. χ^2 probability density function with 15 degrees of freedom

4.4.1 Chi-squares χ^2 Distribution Test

Figure 4.1 shows the χ^2-probability density function (p.d.f) with 15 degrees of freedom. The probability of X being larger than a threshold x_t can be calculated by the following equation:

$$PrX \geqslant x_t = \int_{x_t}^{\infty} \chi^2(u)du \tag{4.37}$$

For using χ^2 test for bad data identification, an acceptable probability of error should be considered which usually have been set to 0.05 in literature. Based on chosen error probability, the threshold x_t can be set such that:

$$PrX \geqslant x_t = 0.05 \tag{4.38}$$

Based on equation (4.38) and the degree of freedom which is m(number of measurements) minus n(number of unknown states), the threshold x_t can be obtained from chi^2 p.d.f table.

The threshold represents the largest acceptable value for measurement residuals that will not contain any bad data. In the other word, if a measurement residual exceeds the threshold x_t, with the 95% probability, the measurement contains bad data [29]. Therefore, χ^2 bad data identification test algorithm can be summarized as follows:

Algorithm 3 χ^2-test for bad data identification

Solve the LSE estimation and calculate the residuals ($r_i = \Delta z_i - \Delta \hat{z}_i \ \forall_i$).
Look up the threshold value based on 95% detection confidence and $(m-n)$ degrees of freedom from the χ^2 distribution table $p = Pr(r_i \leqslant \chi^2_{(m-n),p})$
if $r_i \geqslant \chi^2_{(m-n),p}$ **then**
The measurement is suspected to contain bad data.
else
The measurement will be assumed without any bad data.
end if

Based on above algorithm, χ^2-test is inaccurate and may fail to detect bad data in some cases due to the errors by residuals [29]. Therefore, Largest Normalized Residue Test (LNRT) has been introduced in the literature.

4.4.2 Largest Normalized Residue Test (LNRT)

Normalize residual can be calculated by dividing the absolute value of the residuals obtained form LSE estimation by their corresponding diagonal elements of the residual covariance matrix:

$$r_i^N = \frac{|r_i|}{\sqrt{R_i i S_i i}} \ \forall_i \tag{4.39}$$

Based on the above definition, the normalized residue vector has a Standard Normal Distribution. i.e. $r^N \sim N(0,1)$. Therefore, choosing a static threshold based on desired level of detection sensitivity and comparing the normalized residue with chosen threshold

will identify the measurement with data [29]. The LNRT algorithm can be summarized as follows:

Algorithm 4 LNRT algorithm for Bad Data Detection

Calculate the Jacobian matrix H with ($\Delta Z = H\Delta X + U$).
Derive the residual sensitivity matrix $S = I - (H^T R^{-1} H)^{-1} H^T R^{-1}$ (R is the diagonal covariance matrix of the measurement noises).
Calculate residual values ($r_i = \Delta z_i - \Delta \hat{z}_i \ \forall_i$).
Calculate normalized residuals ($r_i^N = \frac{|r_i|}{\sqrt{R_i i S_i i}} \ \forall_i$)
if the largest element in $r_i^N \geq \beta$ **then**
the measurement corresponding to the largest normalized residual is removed, and SE is performed again.
end if

The traditional test such as LNRT can detect single bad data correctly. However, for multiple bad data, LNRT is able to detect non-interacting and non-conforming interacting bad data sequentially. Which means after the SE algorithm should rerun multiple times after detecting every bad data. Besides, for confirming interacting bad data, the LNRT method may fail to identify them. In other words, if the system contains two measurements with confirming interacting residuals, the LNRT test may fail to detect any of them [29].

4.4.3 Hypothesis Test

For addressing the limitations of traditional bad data tests, Hypothesis test has been introduced in literature. The idea behind Hypothesis test is to estimate the measurement errors directly, instead of using derived residuals for the test. The hypothesis test is a general method to accept or reject a statement. The statement is being tested referred to as the Null hypothesis (H_0) and it's complement is referred to as alternative hypothesis (H_1) [29].

For bad data identification, the null hypothesis (H_0) and the alternative hypothesis (H_1) may be chosen as follows:

- H_0: measurement i does not contain bad data.

- H_1: measurement i is corrupted and contain bad data.

Based on above definition, two types of error can be made in accepting or rejecting H_0 [29]:

- Error type I is rejecting H_0 when the measurement does not contain bad data.
- Error type II is rejecting H_1 when the measurement contains bad data.

There are two alternative approaches for choosing the threshold for hypothesis test based on above types of errors. For more detail regarding the hypothesis test please see [29] and [77].

4.5 Proposed Joint State Estimation and Bad Data Identification Algorithm

Nonlinear measurement function can be represented by following equation:

$$z = h(x) + w \tag{4.40}$$

where z is the measurement vector, x is the state variables vector, $h(x)$ is the measurement function coefficient and $win\mathbb{R}^m$ represents noises.

If a corrupted data exists in the measurement, a sparse vector o can be added as an unknown vector which only has non-zero element $o(i)$ if $z(i)$ contains bad data [84], [77], [62]. In this case, the new measurement model can be represented as (4.41).

$$z = h(x) + o + w \tag{4.41}$$

Joint estimation of x and o can reveal states while identifying the corrupted data. [84] shows that relying on the sparsity of o and using above mentioned Hypothesis Test, if a list of τ_0 faulty measurements is expected, ideally a combination of ℓ_0-pseudonorm and ℓ_2-norm

as shown in (4.42) could successfully recover x and o.

$$\begin{aligned} \min_{x \in X, o} \; & ||z - h(x) - o||_2^2 \\ \text{s.t.} \quad & ||o||_0 \; \leq \tau_0 \end{aligned} \tag{4.42}$$

The problem is ℓ_0-pseudonorm in (4.42), which renders NP-hard and makes it computationally impossible to solve the optimization for large scale systems. In order to make the problem computationally efficient, a well-known convex ℓ_1-norm relaxation can be applied to above constraint [84], [62].

$$\begin{aligned} \min_{x \in X, o} \; & ||z - h(x) - o||_2^2 \\ \text{s.t.} \quad & ||o||_1 \; \leq \tau_1 \end{aligned} \tag{4.43}$$

In standard AC state estimation, measurement functions are nonlinear and non-convex as shown in equations (4.1)-(4.4). Therefore in [84] iterative linearization was used to build convex optimization problems at every step.

In this part of the research, we adopt SOCP relaxation to build convex optimization problem with an ℓ_1 norm constraint. Our formulation avoids linearization and can lead to more accurate estimation and identification results. Note that the state variables in our constrained optimization problem are no longer voltage magnitudes and angles, instead they are S and T.

4.6 New LSE Based SDP Cuts for State Estimator with SOCP Relaxation

In this section first, we investigate a new SOCP relaxation of the power flow problem using cycle basis theory and then propose a new LSE based SDP cut to strength SOCP relaxation introduced in previous sections. This section is the first step for improving static state estimation solver.

4.6.1 Cycle Based Relaxation of AC Power Flow

Recently, Kocuk et al. [60] proposed a new cycle based SOCP relaxation for power flow equations. He suggested that instead of using feasibility constraint in (4.27), we can consider a relaxation that guarantees angle differences sum up to 0 modulo 2π over every cycle in a cycle basis. In this way we would able to take care of Kirchhoff's voltage law for every mesh (cycle) in the power network:

$$\sum_{(i,n) \in C} (V_i - V_n) = 0, \qquad \forall C \in \textit{cycle basis} \tag{4.44}$$

A Cycle Basis of a Graph is a set of simple cycles that forms a subgraph in which each vertex has an even degree [85]. For more detail regarding Cycle Basis, please see [86]. Also, the algorithm used for finding the fundamental cycle basis of a graph introduced in the appendix. Since the sum of the angeles in cycle sum up to zero in new cycle base relaxation, one can conclude the following equation:

$$\cos\Big(\sum_{(i,n) \in C} \delta_{in}\Big) = 1 \tag{4.45}$$

If we replace δ angles in (4.45) with their corresponding T and S equivalents based on the equation in (4.27), the cycle constraint can be written as a degree $|C|$ homogeneous polynomial equality relates to the variables T_{ii}, T_{in} and S_{in} [60]. For example, [61] shows that the cycle constraint for a 3-cycle in a cycle basis with $C = \{(1,2),(2,3),(3,1)\}$, can be written as follows:

$$T_{31}T_{23} - S_{31}S_{23} = T_{33}T_{12} \tag{4.46}$$

$$S_{31}T_{23} + T_{31}S_{23} = -T_{33}S_{12} \tag{4.47}$$

For a larger cycle in a Cycle Basis, [60] proposed decomposition procedures to a 3 and 4-cycles by introducing artificial edges and their corresponding variables. In this way, feasibility constraint in (4.27) is relaxed to its equivalent cycle constraints for each cycle in a cycle basis. Although the cycle constraints created by the above procedure are non-convex, but linking the feasible constraint to the cycles in a cycle basis will introduce new inventive ways to strength SOCP relaxation by adding inequality SDP cuts related to each cycle in a cycle basis as we will show in the following section.

4.6.2 Algorithm for Finding Fundamental Cycle Basis

Fundamental Cycle Basis is a set of linearly independent cycles allows every Eulerian subgraph to be expressed as a symmetric difference of basis cycles [85], [86]. One of the applications of Cycle Basis is on applying Kirchhoff's voltage law for an electrical network. Instead of writing mesh equation for all cycles in the electrical network, it has been proven that ([86] and [60]), it's sufficient to apply the Kirchhoff's voltage law for any cycle in cycle basis. In order to find fundamental cycle basis in a graph $G = (V, E)$, first we have to find spanning tree or spanning forest (more than one spanning tree) of the graph, together with the edges which do not belong to that spanning tree.

For finding spanning tree of a graph, Greedy Algorithm has been used in literature. Algorithm 5 shows the steps for finding spanning tree based on Greedy algorithm [87].

For a graph with n nodes and m edges (n buses and m transmission lines for Power network) there are $c = m - n + 1$ fundamental cycles in cycle basis [86]. The algorithm for finding those cycles will be as follows.

If T is a spanning tree of graph G and $e_1, e_2, ..., e_c$ are the remaining edges of G that does not belong to T, then for every remaining edge e we will have one fundamental cycle. In order to find that cycle, remaining edge e will be added to the spanning tree T and will create a cycle in T.

Removing all the leaves from T, will give corresponding fundamental cycle. The above algorithm is shown in Algorithm 6.

Algorithm 5 Finding spanning tree T of a graph $G = (V, E)$

Initially E contains all edges in G
Initially T which will store edges of a spanning tree is empty
while E is not empty **do**
Choose $i \in G$
  if i is not creating loop with other edges in T **then**
Add i to T
  end if
end while

Algorithm 6 Finding fundamental cycle basis

calculate T, e and $c = m - n + 1$
for $i = 1$ to c **do**
add e_i to T
remove all the leaves from T
store the T as a cycle
end for

For example, consider IEEE14 bus system in Fig 4.2. The spanning tree of 14 bus system is shown in Fig 4.3. By comparing T with Fig 4.2, we can find out that the remaining edges which do not belong to T are $e = \{(2,5),(3,4),(4,5),(7,9),(10,11),(12,13),(13,14)\}$.

Now, when we add the e_1 to the T the new T will be as shown in Fig 4.4. Eliminating leaves gives us the first fundamental cycle as it is shown in Fig 4.4. This algorithm will be repeated for all the remaining age in e. The final answer for fundamental cycle basis is shown in Fig 4.5.

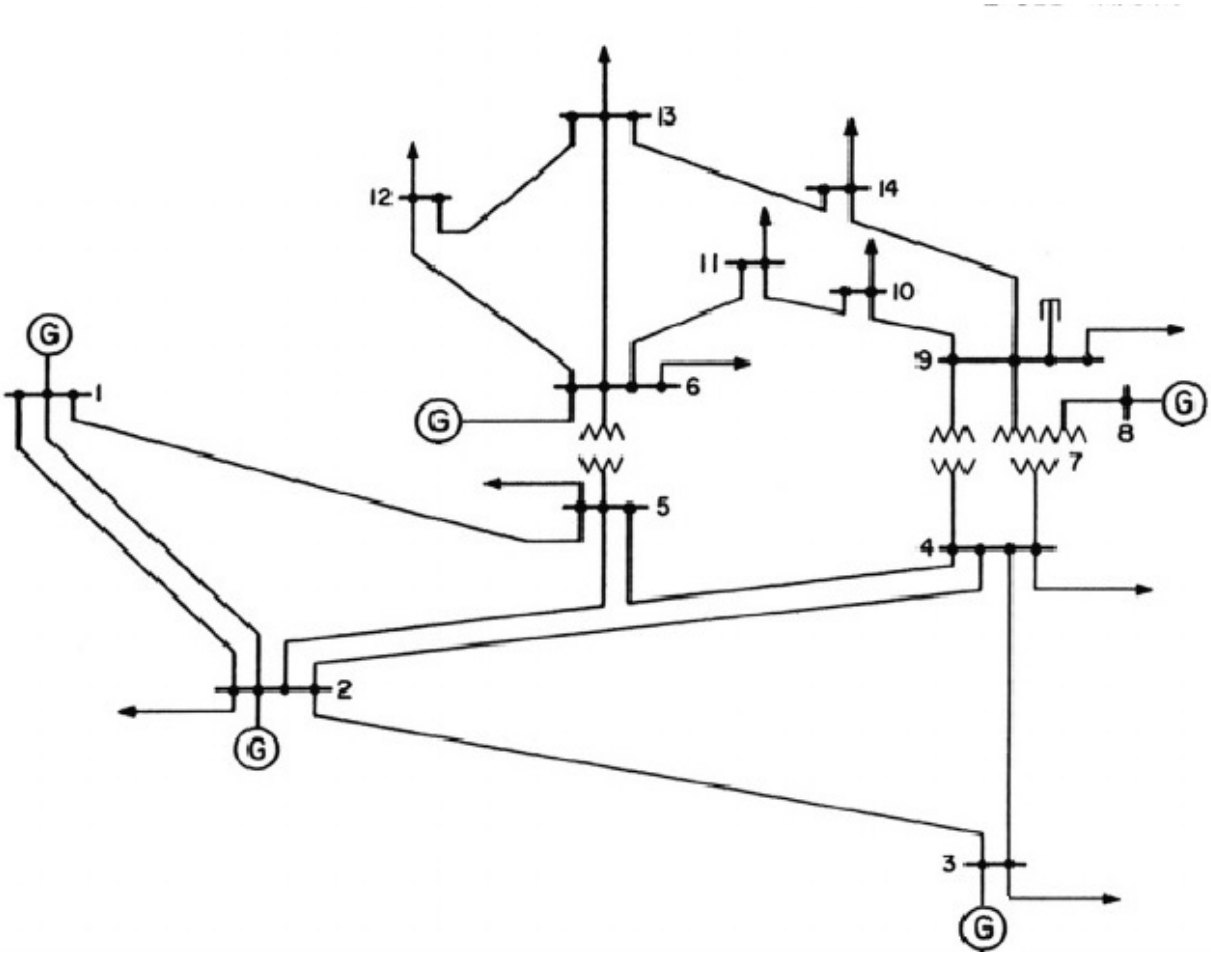

Figure 4.2. IEEE-14 bus system

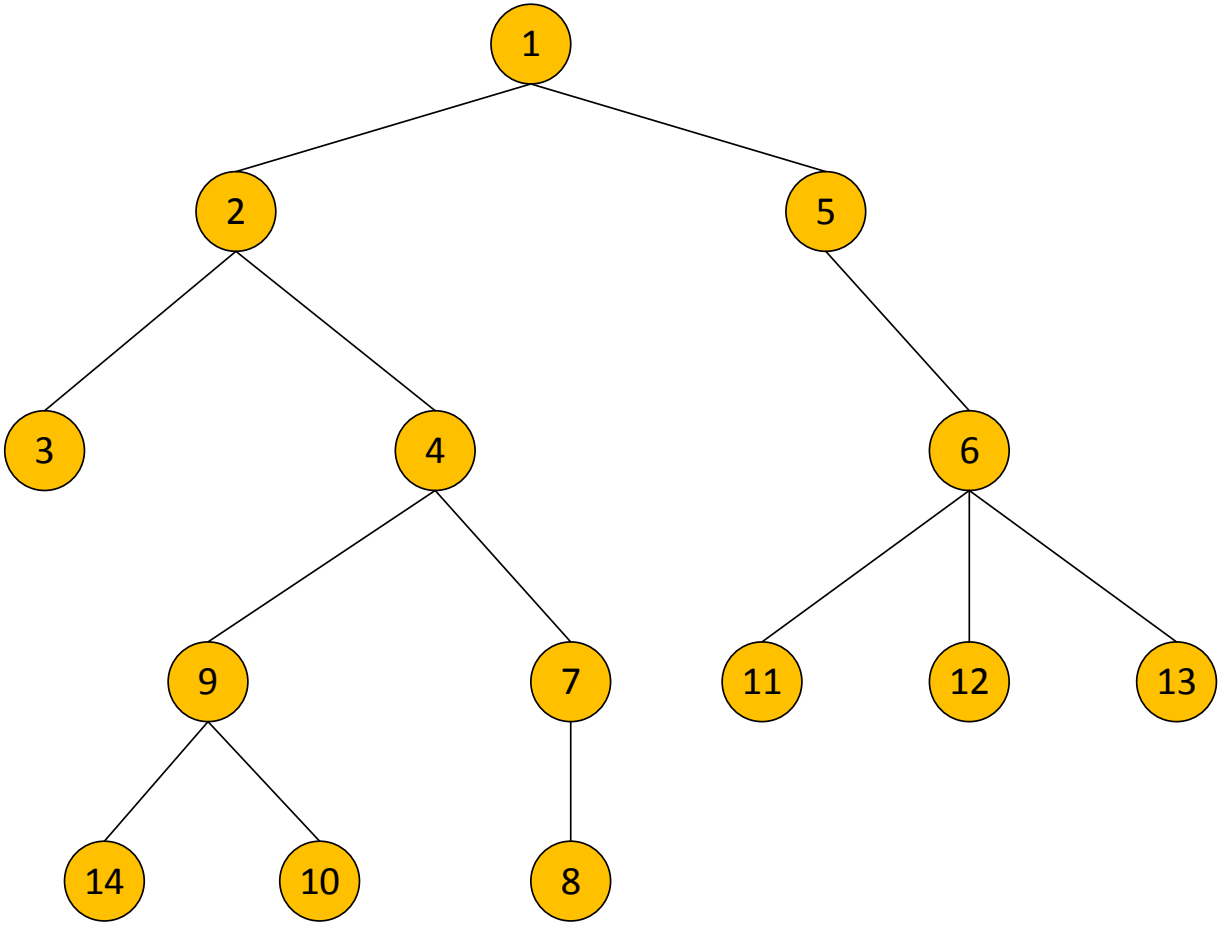

Figure 4.3. Spanning tree T for IEEE-14 bus system

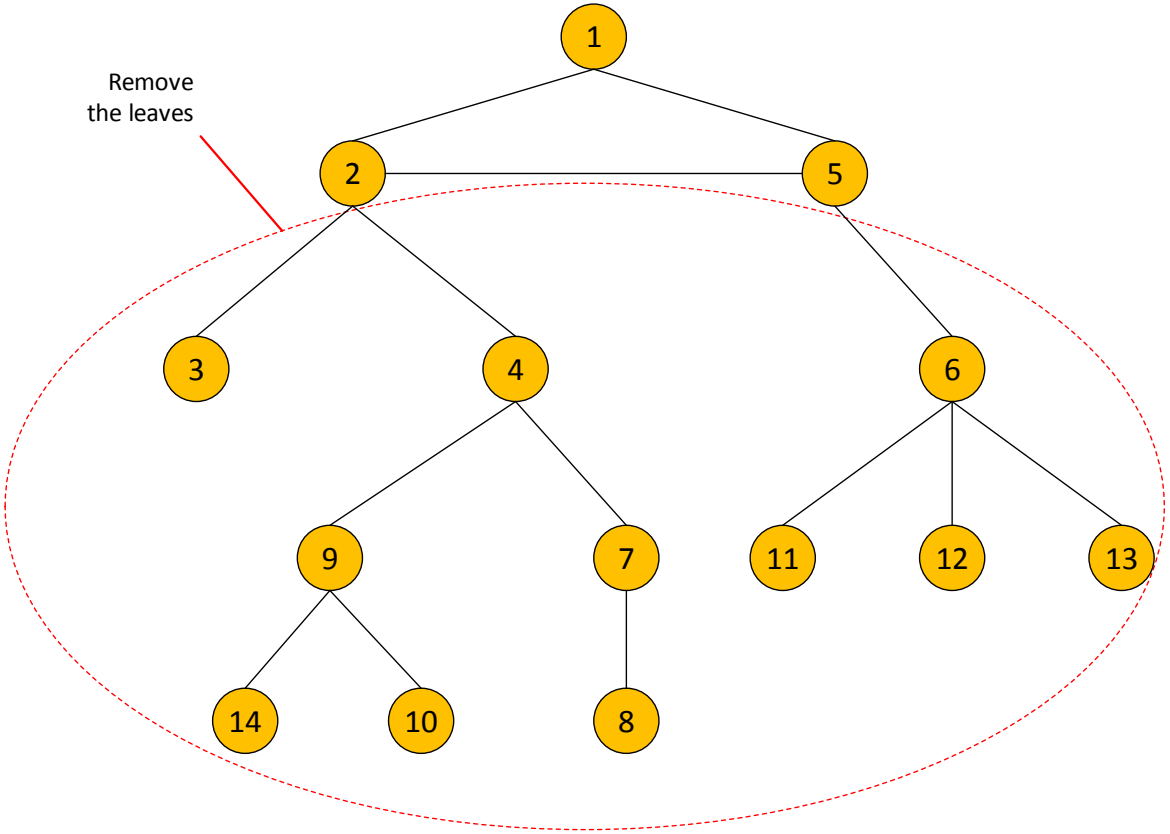

Figure 4.4. Remaining edge (2,5) added to the spanning tree of IEEE-14 bus system

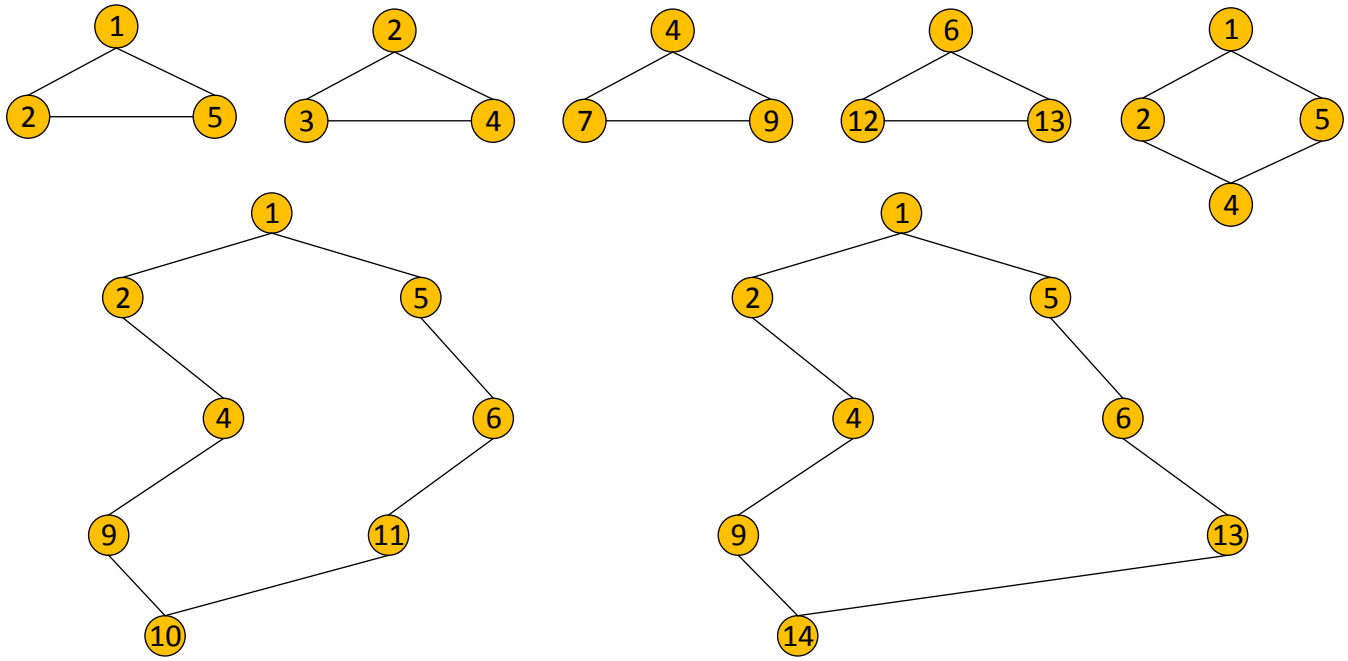

Figure 4.5. Fundamental cycles basis of IEEE-14 bus system

4.6.3 Implementing LSE Based SDP Cuts Algorithm

SOCP relaxation solver can be weak for meshed power network due to discarding the feasibility constraint in (4.27). In the other hand, SDP relaxation is known to produce very tight lower bound and providing quality solution for power flow optimization, but SDP solvers still have scalability issues [61]. For using the benefit of less computationsl time in SOCP relaxation together with the benefit of a tight lower bound in SDP relaxation, SDP cuts are introduced. [63] proposed strengthening SOCP relaxation by adding inequality constraints to separate SOCP answers from SDP feasible region. The SDP cut first introduced in [61] and [60]. For doing so, first, we have to explore the relationship between alternative SOCP relaxation and SDP relaxation. This part of our research is an introduction for improving static state estimation solver to address the non-convexity and non-linearity of SSE. In section 4.3.1 SDP relaxation for power flow was introduced in the complex and real domain. Based on those difinitions, let introduced W as follows:

$$
\begin{aligned}
W &= \left[\begin{array}{c} e_1 \\ \vdots \\ e_n \\ \hline f_1 \\ \vdots \\ f_n \end{array}\right] \left[\begin{array}{ccc|ccc} e_1 & \cdots & e_n & f_1 & \cdots & f_n \end{array}\right] \\
&= \left[\begin{array}{cccc|ccc} e_1^2 & e_1e_2 & \cdots & e_1e_n & e_1f_1 & \cdots & e_1f_n \\ \vdots & \vdots & \vdots & \vdots & \vdots & \ddots & \vdots \\ e_ne_1 & \cdots & \cdots & e_n^2 & e_nf_1 & \cdots & e_nf_n \\ \hline f_1e_1 & f_1e_2 & \cdots & f_1e_n & f_1^2 & \cdots & f_1f_n \\ \vdots & \vdots & \vdots & \vdots & \vdots & \ddots & \vdots \\ f_ne_1 & f_ne_2 & \cdots & f_ne_n & f_nf_1 & \cdots & f_n^2 \end{array}\right]
\end{aligned}
\tag{4.48}
$$

Since $W = [e; f][e^T, f^T]$, then $W \succeq 0$ and $rank(W) = 1$ which is exactly the condition of SDP relaxation in section 4.3.1. Therefore, power flow formulation with SDP relaxation in the real domain can be written as follows:

$$P_i^g - P_i^d = G_{ii}(W_{ii} + W_{i'i'}) + \sum_{\substack{n=1 \\ n \neq i}}^{N} [G_{in}(W_{in} + W_{i'n'}) - B_{in}(W_{in'} - W_{ni'})] \tag{4.49}$$

$$Q_i^g - Q_i^d = -B_{ii}(W_{ii} + W_{i'i'}) - \sum_{\substack{n=1 \\ n \neq i}}^{N} [B_{in}(W_{in} + W_{i'n'}) + G_{in}(W_{in'} - W_{ni'})] \tag{4.50}$$

$$P_{in} = g_{in}(W_{ii} + W_{i'i'}) - g_{in}(W_{in} + W_{i'n'}) + b_{in}(W_{in'} - W_{ni'}) \tag{4.51}$$

$$Q_{in} = -(b_{in} + \frac{b_{sh}}{2})(W_{ii} + W_{i'i'}) + b_{in}(W_{in} + W_{i'n'}) + g_{in}(W_{in'} - W_{ni'}) \tag{4.52}$$

where $i' = i + |\mathcal{B}|$ and $n' = n + |\mathcal{B}|$. By comparing SDP relaxation in(4.49)-(4.52) with alternative SOCP relaxation formulation in (4.21)-(4.24), we can find the relationship between SDP variable W and SOCP variables T and S which showed in (4.53)-(4.55).

$$T_{in} = e_i e_n + f_i f_n = W_{in} + W_{i'n'} \qquad (i,n) \in \mathcal{L} \tag{4.53}$$

$$s_{in} = e_i f_n - e_n f_i = W_{in'} - W_{ni'} \qquad (i,n) \in \mathcal{L} \tag{4.54}$$

$$T_{ii} = e_i^2 + f_i^2 = W_{ii} + W_{i'i'} \qquad i \in \mathcal{B} \tag{4.55}$$

Based on above equations, For every T_{in}, S_{in} and T_{ii}, we can express them to be the Frobenius product related to the matrix W. For example, for a three-bus system with every two buses connected, we have

$$c_{11} = \underbrace{\begin{bmatrix} 1 & 0 & 0 & 0 & 0 & 0 \\ 0 & 0 & 0 & 0 & 0 & 0 \\ 0 & 0 & 0 & 0 & 0 & 0 \\ 0 & 0 & 0 & 1 & 0 & 0 \\ 0 & 0 & 0 & 0 & 0 & 0 \\ 0 & 0 & 0 & 0 & 0 & 0 \end{bmatrix}}_{A_1} \bullet W = \text{Trace}(A_1 W^T) \tag{4.56}$$

where $\bullet$ denotes Frobenious product. For the test system with 3 buses and 3 lines, we will have 12 variables and therefore 12 different A_l.

$$z = \begin{bmatrix} c_{11} & c_{22} & c_{33} & c_{12} & c_{13} & c_{23} & s_{12} & s_{13} & s_{23} \end{bmatrix}^T \tag{4.57}$$

Therefore, for any solution (T^*, S^*) of SOCP relaxation, if exist any symmetric semidefinite W^* that satisfies equations in (4.53)-(4.55), then (T^*, S^*) belong to SDP feasible region and it's an optimal solution for SDP relaxation. If such W^* does not exist, we can separate (T^*, S^*) from SDP feasible region by adding sets of inequality constraints to SOCP relaxation. This procedure proposed in [60] for the first time. Note that finding W in this procedure needs solving SDP optimization with the matrix of the same size of the original SDP relaxation problem which is very time-consuming. Therefore, instead of a full matrix, we can separate the SOCP relaxations over every cycle in a cycle basis. In other words, for any cycle C belongs to cycle basis, we are looking to find corresponding submatrix $\tilde{w}$ of W. This way, the separation will be very efficient and effective. In this case, the SDP set we are looking for can be defined as follows:

$$\left\{ \begin{array}{l} \mathcal{S} := z \in \mathbb{R}^{2|C|} : \exists \tilde{W} \in \mathbb{R}^{2|C| \times 2|C|} \text{ s.t.} \\ \quad -z_l + A_l \bullet \tilde{W} = 0 \quad \forall l \in \mathcal{L}, \quad \tilde{W} \succeq 0 \end{array} \right\} \tag{4.58}$$

[63] proposed a new method to find proper inequality constraints to separate SOCP relaxation results from SDP's feasible region. The philosophy is explained by Fig 4.6.

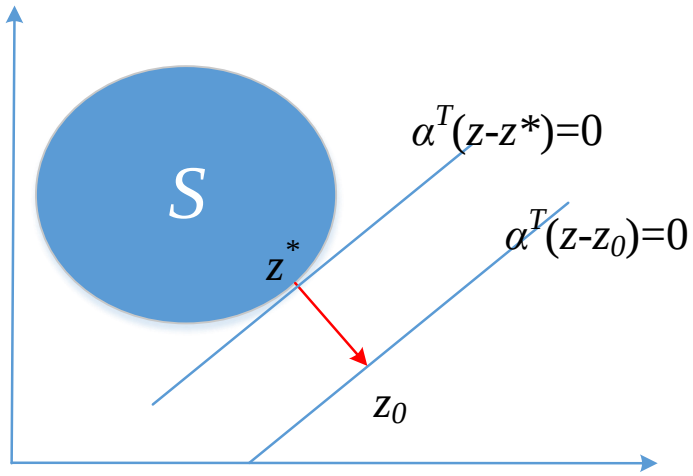

Figure 4.6. LSE-based SDP cut will add $\alpha^T(z - z^*) \leq 0$ as constraint to the SOCP problem

Based on LSE theory, for any optimal solution of SOCP relaxation z_0 belong to cycle C in a cycle basis, First, we will find the shortest distance from z_0 to the set S where z^*, and $\tilde{W}^*$ is the corresponding value found in S. Therefore, a small LSE optimization over a cycle in (4.59) will give us corresponding z^*, and $\tilde{W}^*$ for set S.

$$\begin{aligned} &\min_{z_i,\tilde{W}} \quad \|z_0 - z_i\|^2 \\ &st. \quad z_i = \text{Trace}(A_i\tilde{W}^T), i = 1, \cdots, 12 \\ &\qquad \tilde{W} \succeq 0 \end{aligned} \tag{4.59}$$

where, $\tilde{W}$ is a corresponding submatrix of W for cycle C in a cycle basis.

Based on LSE thorium, If the norm of $z_0 - z^*$ is zero, that means z_0 belongs to the SDP set and z_0 meets the requirement of cycle constraint. Therefore, $\alpha = z_0 - z^* = 0$ and no cuts will add to the SOCP relaxation problem. In the other hand, if z_0 does not belong to the SDP feasible region, then $\alpha \not\equiv 0$ and $\alpha^T(z - z^*) \leq 0$ inequality constraints will add to the original SOCP problem. This method will apply for every cycle in a cycle basis. Therefore,

in each iteration, several cuts will add to the original problem. Our studies show that even 3 to 4 iterations are enough to reach to a quality result for state estimation with SOCP relaxation. Based on all of the above discussion, the proposed joint optimization algorithm, can be summarized as follows:

Algorithm 7 Proposed joint state estimation and bad data detection algorithm for AC networks

Input AC network model
Calculate Ybus and Branch matrices for input system
Creat initial conditions and measurement matrix
Solve convex SCOP-based SE for finding initial guess for SE problem
for i=1 to number of iterations **do**
Solve joint algorithm and find the optimal solution for SOCP based SE
Separate cutting planes from each cycle in cycle basis by LSE-based SDP separation
Add cuts and resolve Joint optimization algorithm.
end for
If there are any measurements with bad data, remove the measurement and rerun the join optimization.

The coding of the proposed algorithm can be found in the appendix.

4.7 Case Studies

In this section, two categories of case studies are presented to show the effectiveness of the proposed simultaneous state estimation and bad data identification algorithm. The algorithm is programmed and implemented using CVX toolbox of the MATLAB [88]. MATLAB have been running on a Core2Duo, 3.00 GHz PC with 6.00 GB of RAM. MOSEK solver [89] is used for solving convex optimization. In each scenario of case studies, MATPOWER OPF results have been used as the true values of the measurements [90]. Noises were represented using random Gaussian distribution values with zero mean, and standard deviation of 0.01 pu for power and 0.005 pu for voltage is added to the true measurements.

Case studies are carried out in two different steps. In the first step, the proposed strengthened SOCP estimator with SDP cuts is tested on the IEEE-14, 30 and 118 bus systems as

well as 17 of NESTA test cases and the results are compared with those obtained from the estimator using SOCP only (without SDP cuts) [59]. In the next step, joint state estimation and bad data identification are tested. First, the proposed algorithm is tested in the presence of one or two corrupted measurements. Next, the algorithm is tested in the presence of multi bad data measurements.

4.7.1 Least Absolute Value State Estimation with Conventional Measurement Set

In this section, proposed algorithm was tested on IEEE 14, 30 and 118 test system. The results of the proposed estimator then compared to the classic SOCP relaxed optimization found in [59]. In order to make such comparison to be meaningful, the same approach was used for all of the test systems, e.g. In order to ensure the observability of the system, the conventional measurement sets were adapted from [91] and can be found in Table 1 in [59]. also, for IEEE 118 bus system, simple measurement set consist of (i)The real and reactive power flow for each end of transmission lines and (ii)Voltage magnitude at the slack bus. Equations (4.60)-(4.63) shows the performance indexes used to evaluate the proposed algorithm.

$$RMS-VE=\sqrt{\frac{\sum_{i=1}^{N}(V_i^{tr}-V_i^{e})^2}{N}} \tag{4.60}$$

$$RMS-AE=\sqrt{\frac{\sum_{i=1}^{N}(\delta_i^{tr}-\delta_i^{e})^2}{N}} \tag{4.61}$$

$$REL-VE=\max_{i=1,\dots,N}\left|\frac{V_i^{tr}-V_i^{e}}{V_i^{tr}}\right|\times 100 \tag{4.62}$$

$$REL-AE=\max_{i=1,\dots,N}\left|\frac{\delta_i^{tr}-\delta_i^{e}}{\delta_i^{tr}}\right|\times 100 \tag{4.63}$$

In equations (4.60)-(4.63), RMS-VE represents RMS voltage error in p.u, RMS-AE represents RMS angle error (rad), REL-VE represents maximum relative voltage error (%) and REL-VE presents maximum relative angle error(%) respectively. Note that in all the scenarios, in order to avoid division by zero in REL-AE and be able to have a meaningful comparison between the maximum relative voltage and the maximum relative angle, reference bus angle assumed to be 1 rad.

Table 4.5 shows the comparison between SOCP estimator and proposed LSE-SDP estimator. From table 4.5 for all three cases, the proposed LSE-SDP method significantly dominates SOCP estimator. The cost of using proposed method is its computational time. Since the algorithm needs to solve iteratively, its computational time is higher than SOCP estimator. For instance, for IEEE 14, IEEE 30 and IEEE 118 bus systems, SDP separation applied for four iterations and the computation time was 0.64, 1.11 and 5.83 (sec) respectively which was higher than 0.21 (sec), 0.26 (sec) and 0.64 (sec) SOCP's computational time reported in [59]. However, LSE-SDP's computational time still is in acceptable range since the SDP separation is applying for every cycle in a cycle basis. In all of the tested systems, our studies show that 2-4 iterations are enough to reach to an acceptable result.

4.7.2 The Effect of PMU Data on Static State Estimation

This section shows the effect of PMU data on static state estimation. Introducing PMU to the power system, enhance the sampling rate and accuracy of the measurement system. Not only, using PMU increase the sampling rate from one sample per every couple of minutes up to 60 sample per seconds, but also increases the accuracy of the measurement as well. Traditional SCADA system data usually contains 5% error. By introducing PMU the accuracy of the measurement increases to 1%.

In order to show the effect of the PMU sampled data on the state estimation algorithm, 5% Gaussian noise added to to the active and reactive power injection and transmission line flow for IEEE 14, 30 and 118 bus systems. The effect of SCADA system data compared to the previous finding in which PMU measurement is used. The results clearly show that high noise level in SCADA-based measurement affects estimation results significantly. The comparison between SCADA measurement base estimator and PMU based estimator can be found in Table 4.1.

Table 4.1. Comparison between SCADA-based and PMU-based SE

	PMU based Measurement				SCADA Based Measurement			
Network	RMS-VE	RMS-AE	REL -VE	REL -AE	RMS -VE	RMS -AE	REL -VE	REL -AE
IEEE14	6.46×10^{-4}	5.93×10^{-3}	0.04	0.47	0.0036	0.042	2.01	2.29
IEEE30	1.07×10^{-3}	3.27×10^{-3}	0.03	0.12	0.0124	0.0066	4.53	10.55
IEEE118	6.00×10^{-3}	1.59×10^{-3}	0.08	0.3	0.0014	0.0064	0.14	0.53

4.7.3 Robustness of LSE-SDP Estimator

This section presents robustness evaluation of the LSE-SDP estimator and answers the question of "how robust is the algorithm for handling big networks". In order to do that, LSE-SDP estimator was applied to the 17 state-of-the-art NESTA v0.6.0 AC transmission system test cases. Test cases start with the simple case of 3 buses to the complicated one with 1345 buses under typical operating condition (TYP). For each case, two different methods of estimation have been considered: i. Least Absolute value estimation (LAV) and ii. Least Square Error estimation(LSE). The comparison between two methods shows that as of expectation for most of the cases, LSE estimation dominated LAV estimator and reached to the more accurate results. However, it can be argued that results are very close to each other for both methods.

For better evaluation of the algorithm results, Maximum Voltage Error (MVE) and Maximum Angle Error (MVA) was added to existing performance indexes. The results are displayed in Table 4.6.

4.7.4 Performance of the Co-Optimization Algorithm against Noise and Single Bad Data

In order to compare the performance of the proposed method with LSE or LAV as objective functions, bad data will be injected. a single meter is assumed to be corrupted. For IEEE-14 bus system, bad data are added to the active and reactive power flow measurement of the line (5,6) while for the IEEE-30 system, active and reactive power injection at bus 1 contain bad data measurements. Also, for New-England-39, IEEE-57 and IEEE-118 bus systems, bad data randomly added to the active and reactive line flow measurements. In all cases, the bad data are simulated by multiplying the true measurement by 1.2. The measurement sets for IEEE-14 and IEEE-30 are adapted from [59], while for other cases, the measurements of line flows are distributed randomly among transmission lines.

4.7.4.1 Sensitivity of the Detection Threshold τ_1

In the case study on IEEE 14-bus system, we will inject data attack to a randomly selected line's real power and reactive power measurements. The attack vector obtained, and the identified attack vector are shown in the following tables: Tables 4.2 and 4.3. Note that there are total 122 measurements. The tables list only those meters with bad data greater than 0.1% pu. The left two columns present the bad data and their meter indices sorted by magnitudes. The right two columns present the identified bad data and the corresponding meters sorted by magnitudes.

It can be found that the identification of the attack vector o is dependent on the assumed threshold τ_1 value or the assumed l_1 norm of the attack vector. When the assumed value is

Table 4.2. The real bad data vector versus the identified bad data vector o ($\tau_1 = 1.34$)

Bad Data vector	ith meter	Identified o	ith meter
−0.0377	54	−0.0255	54
−0.0144	15	−0.0055	5
−0.0121	94	−0.0046	9
−0.0051	43	−0.0045	12
−0.0036	18	−0.0043	4
−0.0036	9	−0.0042	10
−0.0034	10	−0.0032	7
−0.0028	5	−0.0029	1
−0.0027	47	−0.0028	13
−0.0025	72	−0.0027	64
−0.0024	17	−0.0024	2
−0.0017	7	−0.0024	72
−0.0017	4	−0.0021	47
−0.0013	64	−0.0020	74
−0.0012	12	−0.0018	3
−0.0011	49	−0.0018	50
−0.0010	96	−0.0016	15

much greater than the real value, the detection algorithm can identify the meter with the greatest attack value. The identified attack o_i is of the same order of a_i. When the assumed value is smaller than the real value, the detection can identify the meter with the greatest attack value as well. However, the identified value is not of the same order of the real value.

The above test shows that the proposed joint algorithm is successful in identification of the meter with the worst attack. Further, the identified bad data is in the same order of the real bad data injection our estimation of the threshold is reasonable.

4.7.4.2 Monte-Carlo Simulation

For meaningful comparison between the proposed algorithm (joint state estimation and bad data detection) and the traditional LNRT method, SDP cut-based method is implemented for both LNRT-LAV and LNRT-LSE optimization. The performance metrics here are the RMS of angle error (RMS-AE), RMS of voltage error (RMS-VE), and the average

Table 4.3. The real bad data vector versus the identified bad data vector o ($\tau_1 = 0.08$)

Bad data vector	ith meter	Identified o	ith meter
−0.1586	57	−0.0137	57
−0.0424	97	−0.0103	97
−0.0108	63	−0.0063	43
−0.0059	43	−0.0031	7
−0.0052	64	−0.0031	13
−0.0042	7	−0.0027	69
−0.0041	13	−0.0027	44
−0.0038	18	−0.0019	45
−0.0031	45	−0.0017	3
−0.0027	44	−0.0015	1
−0.0023	69	−0.0010	64
−0.0018	70	−0.0010	11
−0.0014	47	−0.0009	23
−0.0012	28	−0.0008	47
−0.0012	23	−0.0006	28
−0.0012	71	−0.0005	71
−0.0011	34	−0.0005	51
−0.0010	49	−0.0004	76

Mean-Square Error ($MSE = ||x_k - \hat{x}_k||^2/N$, where $\hat{x}_k$ notates the estimated state variable vector) over 200 Monte Carlo runs. Table. 4.7 represents the result of the comparison. Note that, both LNRT and co-optimization algorithm successfully identified bad data in all cases. Also, the estimation result shows a slightly better performance of co-optimization compare to LAV and LSE in the presence of single bad data. Fig 4.7 shows the MSE index for each optimization algorithm over 200 Monte Carlo iterations. The computational time for each optimization algorithms can be found in Table 4.4. Although the joint state estimation and bad data detection algorithm seems a slightly slower in the Table, computational time for Largest Normalized Residue calculation needs to be added to the LAV and LSE optimizations time to make the comparison more meaningful.

For meaningful comparison between suggested algorithm and traditional LNRT method, LSE based SDP cut implemented for both LNRT-LAV and LNRT-LSE optimization. The

Table 4.4. Computational time for optimization algorithms

Cases	LSE	LAV	Co-opt.
IEEE 14	0.49	0.51	0.55
IEEE 30	1.01	0.98	1.04
New-England 39	1.26	1.40	1.46
IEEE 57	2.24	2.41	2.50
IEEE 118	4.62	5.22	5.22

performance metrics here are average RMS˙angle and RMS˙voltage in (4.60) and (4.61) together with average Mean-Square Error ($MSE = ||x_k - x_k^{tr}||_2/N$) over 200 Monte Carlo runs. Table. 4.7 represents the result of the comparison. Note that, both LNRT and co-optimization algorithm successfully identified bad data for all cases. Also, the estimation result shows a slightly better performance of co-optimization compare to LAV and LSE in the presence of single bad data. Fig 4.7 shows the MSE index for each optimization algorithm over 200 Monte Carlo iterations. The computational time for each optimization algorithms can be found in Table 4.4. Although co-optimization algorithm seems slightly slower in the Table, computational time for Largest Normalized Residue calculation needs to be added to the LAV and LSE optimizations time to make the comparison more meaningful. Besides, in our case studies for IEEE-14 and IEEE-30 bus systems, Jacobian matrix in LNRT algorithm was very close to the singularity, which shows in some scenarios, singular Jacobian matrix might happen.

4.7.5 Performance of the Proposed Algorithm Against Noise and Multiple Corrupted Measurements

In LNRT algorithm a threshold is set to find the outlier measurement. If any corrupted measurement is found, state estimation will be repeated after discarding this bad datum. This procedure continues until no bad datum can be identified. Co-optimization method uses the same procedure for identifying bad data and in fact, [77] claims that for single bad

data, the co-optimization algorithm in (4.42) with $\tau_0 = 1$ are equivalent to the LNRT test. However, the relationship of this method for multi bad data is unclear.

To further examine the performance of co-optimization algorithm compare to LNRT, scenarios with multiple corrupted measurements are designed for testing the algorithms on the IEEE and new-England case systems. The focus here is to observe the number of corrupted measurements which could be identified by co-optimization algorithm in the first iteration compare to the LNRT algorithm. Also, the effectiveness of the suggested method for recovering from multiple bad data is compared to LNRT algorithms in this section. Therefore, for each case study, the true measured value of the 10% of randomly selected measurements are multiplied by 1.2 to generate multiple bad data and LNRT and co-optimization algorithms are tested in the presence of those corrupted measurements.

Fig 4.8 represents the Mean Square Error of each algorithm for every iteration, while Fig 4.9 represents Percentage of corrupted measurements detection on the IEEE-30 bus system. Also, Table 4.8 lists the performance results obtained by each algorithm for every iteration. The results show a better performance of the co-optimization algorithm in the identification of the corrupted measurements. In some cases, LNRT methods were not able to identify any of the corrupted measurements, while the co-optimization algorithm found some of them. These results suggest that, although the computational time of the co-optimization algorithm is higher than LNRT, the number of times state estimation needed to rerun after discarding the bad datum would significantly decrease and thus the overall computational time of state estimation when the measurements contain multiple bad data could be decreased by using proposed algorithm.

4.8 Conclusion

A joint AC network state estimation and bad data identification algorithm is introduced in this chapter. The proposed algorithm uses the sparse matrix characteristic to identify bad

data. Sparse matrix based identification has been implemented for linear state estimation in the literature. Also, a new LSE base SDP cuts proposed in order to strengthen SCOP relaxation which can be weak for AC meshed power networks, due to the relaxation of feasibility constraint. the proposed algorithm uses LSE criteria to create valid inequality constraints in order to separate SOCP relaxation solution from SDP feasible region. The effectiveness of the algorithm verified by comparing the results with non-convex state estimator with SOCP based formulation. Also, the robustness of method tested on the 17 state-of-the-art NESTA v0.6.0 AC transmission system test cases. Numerical results from case studies demonstrate more accurate results in SOCP relaxed state estimation, successful implementation of the algorithm for the simultaneous state estimation and bad data identification and improved performance compared to largest normalized residue tests.

Table 4.5. Comparison of state estimator performance with a conventional measurement set and noise

Network	SOCP				LSE-SDP			
	RMS-VE	RMS-AE	REL-VE	REL-AE	RMS-VE	RMS-AE	REL-VE	REL-AE
IEEE14	2.77×10^{-3}	2.67×10^{-3}	0.43	0.85	7.54×10^{-5}	6.83×10^{-4}	0.01	0.05
IEEE30	4.25×10^{-3}	4.39×10^{-3}	0.88	1.39	7.10×10^{-4}	1.90×10^{-3}	0.03	0.09
IEEE118	2.62×10^{-3}	1.91×10^{-3}	0.61	0.72	1.40×10^{-3}	1.50×10^{-3}	0.03	0.07

Table 4.6. LSE-SDP state estimator performance for NESTA v0.6.0 test cases

Networks	Least Absolute Value Estimation						Least Square Error Estimation					
	MVE	MAE	RMS-VE	RMS-AE	REL-VE	REL_AE	MVE	MAE	RMS-VE	RMS-AE	REL-VE	REL_AE
NESTA_3lmbd	2.08×10^{-4}	1.10×10^{-3}	1.20×10^{-4}	8.50×10^{-4}	0.00	0.14	2.30×10^{-4}	9.00×10^{-4}	1.35×10^{-4}	7.30×10^{-4}	0.03	0.13
NESTA__4gs	2.30×10^{-4}	4.32×10^{-4}	1.62×10^{-4}	3.58×10^{-4}	0.02	0.05	1.61×10^{-4}	3.23×10^{-4}	1.08×10^{-4}	2.72×10^{-4}	0.01	0.04
NESTA__5pjm	2.80×10^{-3}	1.47×10^{-4}	2.70×10^{-3}	7.64×10^{-5}	0.26	0.01	1.90×10^{-3}	9.92×10^{-5}	1.90×10^{-3}	6.11×10^{-5}	0.18	0.01
NESTA__6ww	2.77×10^{-5}	1.98×10^{-4}	1.31×10^{-5}	1.00×10^{-4}	0.00	0.02	3.73×10^{-5}	1.61×10^{-4}	2.21×10^{-5}	1.11×10^{-4}	0.00	0.02
NESTA__14ieee	3.43×10^{-4}	1.97×10^{-4}	1.11×10^{-4}	1.01×10^{-4}	0.03	0.02	1.84×10^{-4}	3.51×10^{-4}	7.99×10^{-5}	2.22×10^{-4}	0.02	0.05
NESTA__24ieee	2.08×10^{-4}	1.60×10^{-3}	1.07×10^{-4}	6.52×10^{-4}	0.02	0.12	1.25×10^{-4}	9.40×10^{-4}	7.29×10^{-5}	3.94×10^{-4}	0.01	0.07
NESTA__29edin	1.40×10^{-3}	2.00×10^{-2}	1.30×10^{-3}	4.90×10^{-3}	0.13	1.36	1.10×10^{-3}	1.18×10^{-2}	4.06×10^{-4}	3.60×10^{-3}	0.10	1.09
NESTA__30as	1.88×10^{-4}	7.89×10^{-4}	6.47×10^{-5}	5.92×10^{-4}	0.02	0.1	1.01×10^{-4}	2.41×10^{-4}	5.27×10^{-5}	7.95×10^{-5}	0.01	0.03
NESTA__30fsr	3.51×10^{-4}	6.26×10^{-4}	2.63×10^{-4}	2.20×10^{-4}	0.03	0.07	1.77×10^{-3}	3.09×10^{-4}	1.55×10^{-3}	1.46×10^{-4}	0.17	0.03
NESTA__30ieee	3.17×10^{-4}	4.95×10^{-4}	1.39×10^{-4}	3.43×10^{-4}	0.03	0.06	1.65×10^{-4}	6.67×10^{-4}	9.56×10^{-5}	3.28×10^{-4}	0.02	0.09
NESTA__39epri	3.72×10^{-4}	1.20×10^{-3}	2.31×10^{-4}	6.07×10^{-4}	0.04	0.11	3.23×10^{-4}	1.20×10^{-3}	2.06×10^{-4}	3.94×10^{-4}	0.03	0.11
NESTA__57ieee	3.70×10^{-3}	1.50×10^{-3}	9.37×10^{-4}	3.76×10^{-4}	0.39	0.20	5.27×10^{-4}	4.54×10^{-4}	4.35×10^{-4}	2.57×10^{-4}	0.05	0.06
NESTA__118ieee	3.55×10^{-4}	9.64×10^{-4}	1.07×10^{-4}	3.53×10^{-4}	0.04	0.16	1.83×10^{-3}	1.25×10^{-3}	3.50×10^{-4}	4.87×10^{-4}	0.18	0.25
NESTA__162ieee	4.20×10^{-4}	1.49×10^{-3}	9.05×10^{-4}	3.95×10^{-3}	0.04	0.13	3.69×10^{-4}	1.34×10^{-3}	1.15×10^{-3}	3.31×10^{-3}	0.03	0.11
NESTA__189edin	5.37×10^{-4}	2.23×10^{-3}	2.25×10^{-4}	8.47×10^{-4}	0.06	0.19	1.80×10^{-3}	1.77×10^{-3}	3.12×10^{-4}	6.28×10^{-4}	0.20	0.19
NESTA__300ieee	4.80×10^{-3}	1.98×10^{-3}	6.98×10^{-4}	5.10×10^{-4}	0.47	0.19	6.60×10^{-4}	1.44×10^{-3}	1.29×10^{-4}	3.70×10^{-4}	0.07	0.14
NESTA_1354pegase	8.34×10^{-3}	1.36×10^{-3}	4.00×10^{-4}	2.88×10^{-4}	0.78	0.21	1.07×10^{-3}	1.41×10^{-3}	2.79×10^{-4}	2.36×10^{-4}	0.10	0.14

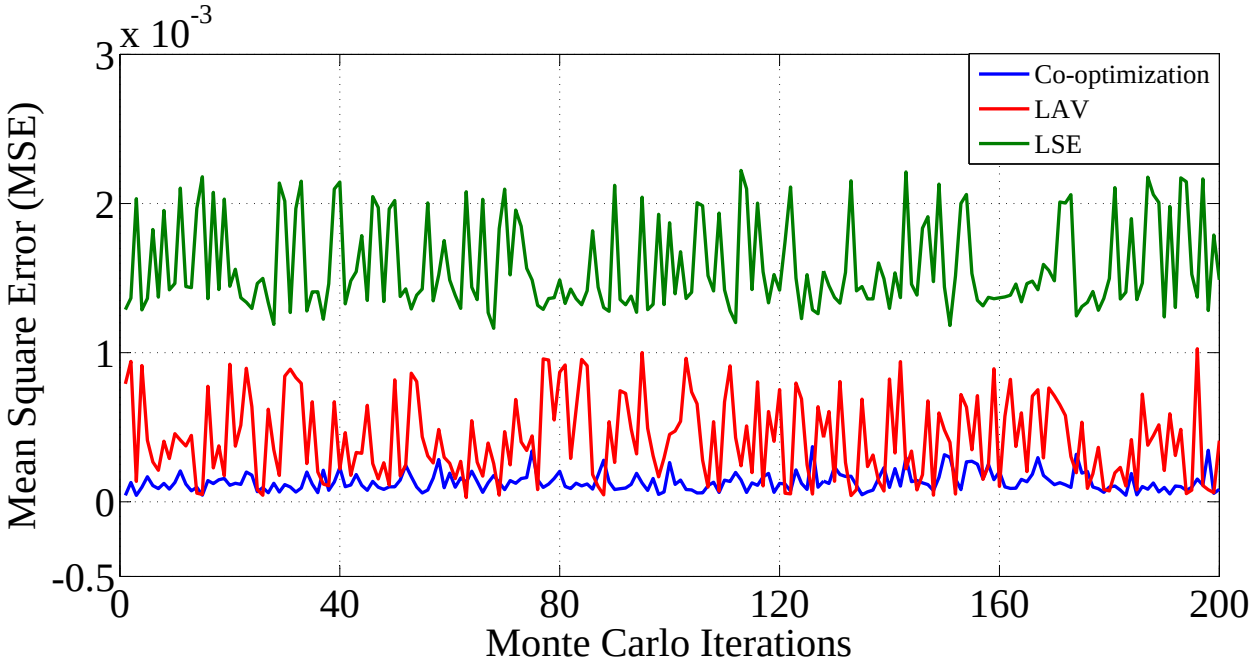

Figure 4.7. Mean Square Error(MSE) for the optimization algorithms on the IEEE-14 bus system over 200 Monte Carlo iterations in the presence of single bad data

Table 4.7. Performance comparison between co-optimization algorithm and LNRT method in the presence of noise and single bad data

Cases	LSE-LNRT			LAV-LNRT			Joint SE and bad data identification		
	MSE	RMS-AE	RMS-VE	MSE	RMS-AE	RMS-VE	MSE	RMS-AE	RMS-VE
IEEE 14	1.60×10^{-3}	0.0330	0.0034	4.21×10^{-4}	0.0079	0.0019	1.34×10^{-4}	0.0022	0.0020
IEEE 30	1.01×10^{-2}	0.0038	0.0017	6.30×10^{-3}	0.0043	0.0017	1.90×10^{-3}	0.0049	0.0015
New-England 39	1.35×10^{-4}	0.0047	0.0060	1.26×10^{-4}	0.0049	0.0042	1.21×10^{-4}	0.0042	0.0060
IEEE 57	1.35×10^{-4}	0.0047	0.0060	1.31×10^{-4}	0.0050	0.0043	9.68×10^{-5}	0.0042	0.0060
IEEE 118	6.54×10^{-5}	0.0092	0.0045	4.66×10^{-5}	0.0064	0.0033	5.09×10^{-5}	0.0062	0.0032

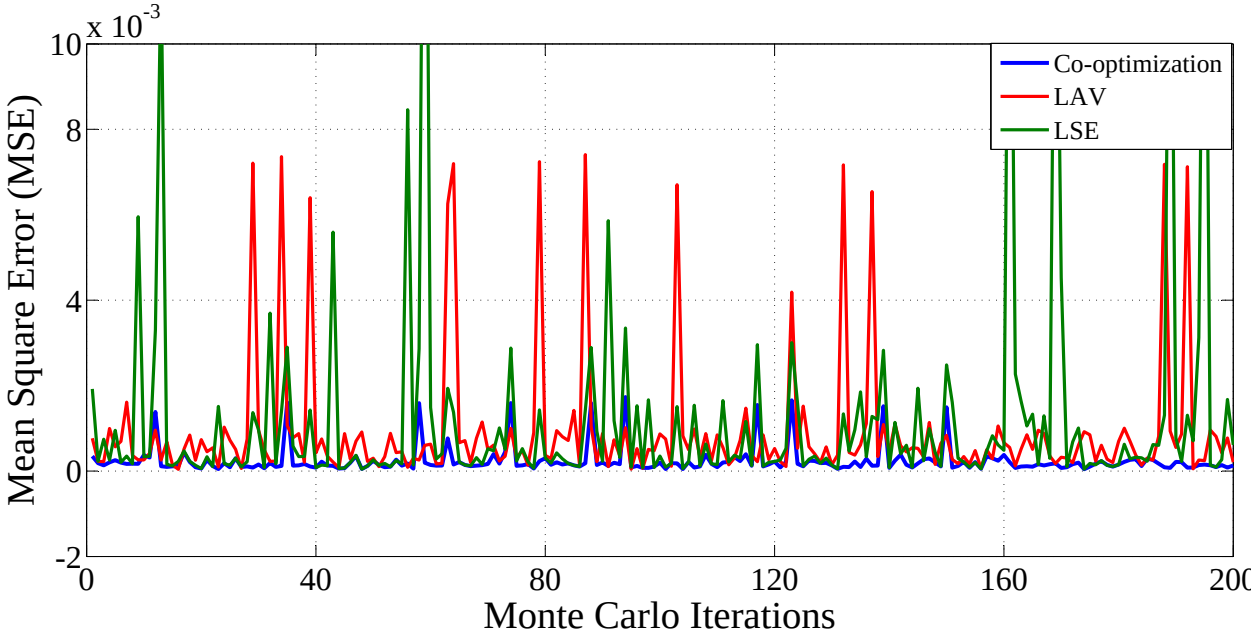

Figure 4.8. Mean Square Error (MSE) for the optimization algorithms on the IEEE-14 bus system over 200 Monte Carlo iterations in the presence of multiple bad data

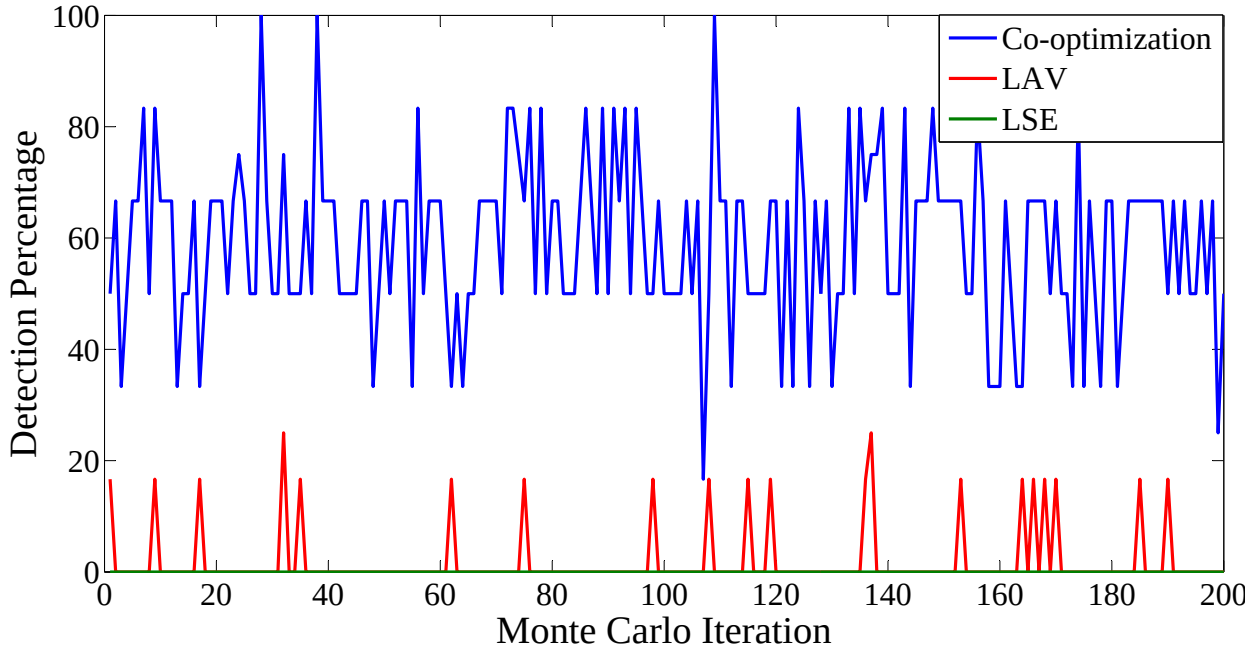

Figure 4.9. Percentage of corrupted measurements detection on the IEEE-30 bus system over 200 Monte Carlo iterations in the presence of multiple bad data

Table 4.8. Performance comparison between co-optimization algorithm and LNRT method in the presence of noise and multiple bad data

Cases	LSE-LNRT				LAV-LNRT				Co-optimization			
	Detection	MSE	RMS-AE	RMS-VE	Detection	MSE	RMS-AE	RMS-VE	Detection	MSE	RMS-AE	RMS-VE
IEEE 14	7.50%	8.90×10^{-3}	0.1925	0.0063	15.2%	4.50×10^{-3}	0.1040	0.0052	30.7%	5.30×10^{-4}	0.0084	0.0031
IEEE 30	0.00%	2.58×10^{-4}	0.0081	0.0023	0.00%	1.82×10^{-4}	0.0053	0.0034	8.95%	1.76×10^{-4}	0.0030	0.0027
New-England 39	13.9%	6.28×10^{-4}	0.0231	0.0107	26.5%	1.95×10^{-4}	0.0057	0.0062	32.5%	1.74×10^{-4}	0.0049	0.0087
IEEE 57	0.09%	1.75×10^{-4}	0.0106	0.0024	1.19%	1.78×10^{-4}	0.0030	0.0021	20.1%	7.31×10^{-5}	0.0028	0.0019
IEEE 118	0.98%	2.38×10^{-4}	0.0260	0.0050	5.17%	8.67×10^{-5}	0.0086	0.0037	23.33%	7.23×10^{-5}	0.0067	0.0036

CHAPTER 5

CONCLUSION AND FUTURE WORK

5.1 Conclusion

This dissertation conducted research in PMU based static and dynamic state estimation. In dynamic state estimation, recursive algorithm i.e. Kalman Filter, is used to estimate states and parameters of a synchronous generator using high rate PMU data. In static state estimation, new robust co-optimization algorithm is introduced for simultaneous state estimation and bad data detection. The dissertation brings incremental knowledge to the power systems and smart grid research area. Such incremental benefit is evidenced by the peer reviewed papers from this dissertation ([25] is published, [63] and [73] are under review). In particular, the dissertation research benefits are summarized in the following conclusions:

5.1.1 Dynamic State Estimation and Parameter Identification

For Dynamic state estimation, UKF is implemented for estimating states and parameters of a low-order synchronous generator model with both primary and secondary frequency control systems. The proposed method uses voltage magnitude and active power measurements as the inputs while it uses voltage angle, reactive power and frequency as the outputs. The inertia constant, damping coefficient, turbine-governor time constant, droop regulation as well as secondary frequency integrator unit gain will all be estimated. Both simulation data and real-world PMU data are used for case studies. In this part of the research, var-

ious techniques are implemented for improving proposed UKF algorithm. The techniques include:

- parameter conversion to increase parameter detection sensitivity.
- measurements interpolating to have a higher sampling rate to improve UKF convergence.

In the validation step, a low-order dynamic simulation model is constructed with the estimated parameters. Input data are fed into the model to generate output data. The generated output data will then be compared with the outputs from the measurements. The case studies demonstrate the feasibility of the proposed UKF estimation approach for system identification using PMU data. Through the proposed estimation method, a complex generator model can be emulated using a low-order generator with frequency controls. The case study on the real-world PMU data demonstrates the capability of the proposed UKF on identifying an equivalent generator model.

5.1.2 Robust AC Network Static State Estimation

A joint AC network state estimation and bad data identification algorithm is introduced in Chapter 4. The proposed algorithm uses the sparse matrix characteristic to identify bad data. Sparse matrix based identification has been implemented for linear state estimation in the literature. Also, a new LSE base SDP cuts proposed in order to strengthen SCOP relaxation which can be weak for AC mesh power networks, due to the relaxation of feasibility constraint. the proposed algorithm uses LSE criteria to create valid inequality constraints in order to separate SOCP relaxation solution from SDP feasible region. The effectiveness of the algorithm verified by comparing the results with non-convex state estimator with SOCP based formulation. Also, the robustness of method tested on the 17 state-of-the-art NESTA v0.6.0 AC transmission system test cases. Numerical results from case studies demonstrate more accurate results in SOCP relaxed state estimation, successful implementation of the

algorithm for the simultaneous state estimation and bad data identification and improved performance compared to largest normalized residue tests.

5.2 Future Research

The future research to continue this dissertation work can be presented as follows.

5.2.1 Subset Selection For Generator Model Identification

5.2.1.1 Background

Accurate estimation of the dynamic behavior of the synchronous machine has a great role in power system reliability analysis. Although nominal parameters of the machine are known, over the time these values will change due to the mechanical reasons such as repairs and aging. Such changing in the parameters of the synchronous machine can affect the actual response of the generator to the dynamic events when it is compared to its expected simulated response [92].

However, Research work shows that it's not efficient to estimate all the parameters of the generator. Some of the parameters are harder to estimate and can affect the accuracy of the estimation results. Instead, the most important parameter which has the most effect on the output of the system can be chosen to estimate. In this way, the estimation can be implemented in a more efficient and accurate way and thus it can produce more accurate results.

Section 3.5.3 of the dissertation, shows the difficulty of applying dynamic state estimation for a real-world system. From research results, it can be understood that the accuracy of the reactive power output and frequency estimation is not accurate enough. The reason can be the big difference between the fifth order of the classic dynamic model of the generator in compare to the high-order dynamic model of real-world generator. Besides, there are too

many of unknown parameters which have been tried to estimate with the UKF algorithm. Specifically, our practical experience shows that the estimation algorithm is highly sensitive to the change in X'_d and H. Therefore, it seems investigation on the sensitivity of the output to the parameters and use of subset selection algorithm can help improving the accuracy of estimation algorithm. Thus, subset selection will be used in future steps to select the most effective parameters on the output of the simplified model and then UKF will be used to estimate those selected parameters.

There are two major algorithms have been reported in the literature for subset selection: singular value decomposition method which was reported In [21] and [92] and trajectory sensitivity analysis which was reported in [93] and [94]. In the first method the diagonal elements of singular value decomposition of the sensitivity matrix show the most effective parameters on the output of the system while, in the second approach, trajectory sensitivity of the system to the change in the initial conditions and parameters will determine the most important parameters for the output. Based on the results of implementing UKF for the real-world system, there are still rooms for improvement in parameter estimation accuracy in order to get the better identification of the simplified dynamic model of the generator.

5.2.1.2 Subset Selection Based on Singular Value Decomposition of Sensitivity Matrix

Singular value decomposition (SVD) is the generalization of the eigen-decomposition of the positive semi-definite matrix. For any $m \times n$ matrix M, SVD can be written as follows:

$$M = U\Sigma V^* \tag{5.1}$$

where U and V are $m \times m$ and $n \times n$ unitary matrix respectively, while σ is a diagonal matrix with diagonal elements belong to the non-negative real number set. Based on SVD

theory, the non-zero singular value of M which can be found on the diagonal elements of Σ, represents the square roots of the eigenvalues of the MM^* matrix. In order to explain the usage of SVD theory on subset selection, consider generator dynamic equations in its state space model. Therefore, we will have the following equations:

$$\begin{cases} \dot{x} = Ax + Bu \\ Y = Cx + Du \end{cases} \tag{5.2}$$

Assume, $M = \{M_1, M_1, ..., M_n\}$ are the parameters of the generator. The sensitivity matrix of the system in 5.2 can be represented by the Jacobian matrix J of Y. Thus, sensitivity matrix elements can be written as follows:

$$J_{ij} = \frac{\partial Y_i}{\partial M_j} \tag{5.3}$$

If the measurement of system represented by $\hat{Y}$, LSE based parameters estimation, and its optimal solution can be written as follows:

$$\begin{cases} \hat{M} = \min \sum_{k=1}^{N} ||Y_k(M) - \hat{Y}_K(M)||_2^2 \\ \hat{M} = M_0 + (J^T J)^{-1} J^T r \end{cases} \tag{5.4}$$

where r represents error matrix associated with Y. By defining SVD of Jacobian matrix J and substitute it into the LSE optimal solution, the following equation can be found for estimated parameters $\hat{M}$:

$$J = U\Sigma V^T \tag{5.5}$$

$$\hat{M} = M_0 + \sum_{i=1}^{n} \frac{o_i v_i^T}{\sigma_i} r \tag{5.6}$$

where o_i and v_i are the i_{th} columns of U and V respectively, and σ_i is the ith singular values of matrix J. Equation (5.6) clearly demonstrates the relationship between output error and singular value of sensitivity matrix. Higher singular value shows a higher impact of the parameters on the output of the system. Therefore, parameters with highest singular value are the best candidate for parameter estimation.

5.2.1.3 Future Steps

In the future steps of the research, singular value decomposition of the sensitivity matrix would be implemented for the real-world PMU data to find the best subset of parameters for classic generator model. Then, parameter estimation would be carried out by using the identified subset of parameters while the other parameters assumed to be known. The main objective of this part of research should be to increase the accuracy of the simplified model. Therefore, The remaining steps for this task are:

- Defining classic model of generator in state space and find out its relevant sensitivity matrix
- Implement singular value decomposition algorithm for the sensitivity matrix on the reduced real-world system and find the subset of parameters to be estimated

5.2.2 Distributed State Estimation with ADMM

5.2.2.1 Background

The main challenge of the SE algorithms is the limitation of the number of measurements in power system. It is not possible to have a measurement on each bus or line of the power networks. Therefore, implementing centralized real-time SE for large-scale power network is practically infeasible due to the complexity of the system, limitation in the number of

measurement, the huge amount of data and privacy policies in deregulated environment. Therefore, Distributed Static State Estimation (DSSE) is introduced in the literature.

D-ES provide the ability to solve large-scale problem effectively by dividing the estimation to the local control areas. In each control area, local operator will gather its own measurement data and perform local state estimation with the exchange information of tie line measurements with the other control areas. Difference D-SE algorithm tries to achieve above objective and minimize the computational time as well as the amount of exchange data between areas.

One of the most widely used and effective distributed optimization algorithms is alternative direction method of multipliers (ADMM) [95]. ADMM has the same principle as dual decomposition, but the difference is an additional quadratic term in the dual variable of updating equation. ADMM specifically introduced to add the distributed platform implementation capability to the method of multiplier algorithm. In [96] and [97] ADMM used to implement distributed state estimation. Therefore, one of our research objectives is to implement new improved state estimation for distributed system by applying ADMM algorithm.

5.2.2.2 Dual Decomposition

A general optimization problem can be defined as follows:

$$\begin{aligned} f^* = f(\mathbf{x}^*) &= \min_{\mathbf{x}} f_(\mathbf{x}) \\ \text{subject to} \qquad & A\mathbf{x} = b \end{aligned} \tag{5.7}$$

where $\mathbf{x}^*$ is its optimal solution. Based on lagrangian relaxation technique, one can try to relaxes the minimization problem by transferring constraints to objective function as shown

in (5.8).

$$L(\mathbf{x};\lambda) = f(\mathbf{x}) + \lambda^T(A\mathbf{x} - b) \tag{5.8}$$

Lagrange dual function, $g(\lambda)$, is the greatest lower bound of $L(\mathbf{x};\lambda)$ can be defined as (5.9).

$$g^* = \max_{\lambda} \quad g(\lambda) = \inf_{\mathbf{x}} \quad L(\mathbf{x};\lambda) \tag{5.9}$$

Based on the duality theorem, solving dual problem will recover the optimal solution for primal problem as well. Dual decomposition theory suggests that if function $\mathbf{f}$ can be separated to the N functions such as $f(\mathbf{x}) = f_1(\mathbf{x}_2) + f_2(\mathbf{x}_2) + ... + f_N(\mathbf{x}_N)$, then one can separate its lagrangian relaxation as shown in (5.10) :

$$\begin{aligned} L(\mathbf{x};\lambda) &= \sum_{i=1}^{N} L_i(\mathbf{x}_i;\lambda) - \lambda^T b \\ L_i(\mathbf{x}_i;\lambda) &= f_i(\mathbf{x}_i) + \lambda^T A_i \mathbf{x}_i \end{aligned} \tag{5.10}$$

Therefore, dual decomposition can be separated into the N optimization and solve iteratively as shown in (5.11) and (5.12):

$$\mathbf{x}_i^{k+1} \;:=\; \text{argmin}_{\mathbf{x}_i}\; L_i(\mathbf{x}_i;\lambda^k), \qquad i = 1, ..., N \tag{5.11}$$

$$\lambda^{k+1} \;:=\; \lambda^k + \alpha^k(\sum_{i=1}^{N} A_i \mathbf{x}_i^{k+1} - b) \tag{5.12}$$

The dual decomposition algorithm can be solved in distributed parallelize way by first considering known λ^k from the last step and then solve N parallelize optimization in (5.11) to

find $\mathbf{x}_i^{k+1}$. Then update the dual variable in (5.12) to coordinate distributed optimizations in order to converge to the same global dual value Λ. The problems of the dual decomposition are often slow convergence and dependency to the lots of assumption [95].

5.2.2.3 Alternative Direction Method of Multiplier

The ADMM has been introduced to combined decomposability of dual decomposition method with the great convergence rate of the method of multiplier [95]. Assume optimization problem has the form of the following equation:

$$\begin{aligned} \min \quad & f(\mathbf{x}) + g(\mathbf{y}) \\ \text{s.t.} \quad & A\mathbf{x} + B\mathbf{y} = c \end{aligned} \tag{5.13}$$

Then ADMM augmented Lagrangian function, and its related iterations can be written as shown in (5.14)-(5.17) [95].

$$L_\rho(\mathbf{x}, \mathbf{y}, \lambda) = f(\mathbf{x}) + g(\mathbf{y}) + \lambda^T(A\mathbf{x} + B\mathbf{y} - c) + \frac{\rho}{2}||A\mathbf{x} + B\mathbf{y} - c||_2^2 \tag{5.14}$$

$$\mathbf{x}^{k+1} := \text{argmin}_{\mathbf{x}}\ L_\rho(\mathbf{x}, \mathbf{y}^k, \lambda^k) \tag{5.15}$$

$$\mathbf{y}^{k+1} := \text{argmin}_{\mathbf{y}}\ L_\rho(\mathbf{x}^{k+1}, \mathbf{y}, \lambda^k) \tag{5.16}$$

$$\lambda^{k+1} := \lambda^k + \rho(A\mathbf{x}^{k+1} + B\mathbf{y}^{k+1} - c) \tag{5.17}$$

Traditionally there are three major methods for solving ADMM : Gauss-Seidel method, Jacobian method, and Proximal Jacobian method. The difference between these methods comes from different approaches in parallelizing separated optimizations. Recently [98] showed that Gauss-Seidel and jacobian method could suffer from convergence problem. In Gauss-Seidel algorithm, each of distributed optimization blocks has to use an update from their last block and therefore they cannot be solved in parallelized manner. Also [98] shows

that Gauss-Seidel method may not be converged for large-scale systems. With the same approach, it is proven that the jacobian method is more likely to diverge than the Gauss-Seidel method due to its parallelized solving of optimization blocks. Therefore, the proximal jacobian algorithm has been proposed in [98] to solve the ADMM with the good convergence rate and guarantees its convergence to the global solution. Thus, in the future research, ADMM will be applied to the improved SE algorithm while proximal jacobian method will be used to solve it. Algorithm 8 shows proximal jacobian solver algorithm for ADMM based optimization [95].

Algorithm 8 Proximal Jacobian solver for ADMM

Initialize $\mathbf{x}_i^0$ and λ^0.
for k=0,1,... **do**.
Update $\mathbf{x}_i^{k+1}$ in parallel by:
$\mathbf{x}_i^{k+1} = \text{argmin}_{\mathbf{x}}\ f_i(\mathbf{x}_i) + \frac{\rho}{2}||A_i\mathbf{x}_i + \sum_{j\neq i} A_j\mathbf{x}_j^k - c + \frac{\lambda^k}{\rho}||_2^2 + \frac{1}{2}||\mathbf{x}_i - \mathbf{x}_i^k||_{p_i}^2$
Update $\lambda^{k+1} = \lambda^k - \gamma\rho(\sum_{i=1}^N A_i\mathbf{x}_i^{k+1} - c)$
S.t.
$0 \leq \gamma \leq 2$
$P_i \succ \rho(\frac{N}{2-\gamma} - 1)A_i^T A_i$
end for

5.2.2.4 Future Steps

In the future research, these steps have to be accomplished:

- Formulate improved state estimator with ADMM for distributed platform
- Implement distributed state estimator for IEEE case systems.
- Evaluate effectiveness of new improved estimator with comparing it to the existing estimator in literature

REFERENCES

[1] F. P. Commission *et al.*, "Prevention of power failure," *Volume I-Report of the Commission (Washington, DC: Government Printing Office: July, 1967)*, p. 7, 1967.

[2] A. Phadke, "Synchronized phasor measurements in power systems," *Computer Applications in Power, IEEE*, vol. 6, no. 2, pp. 10–15, April 1993.

[3] R. F. Nuqui, "State estimation and voltage security monitoring using synchronized phasor measurements," Ph.D. dissertation, Citeseer, 2001.

[4] N. Arghira, D. Hossu, I. Fagarasan, S. S. Iliescu, and D. R. Costianu, "Modern scada philosophy in power system operation-a survey," *University" Politehnica" of Bucharest Scientific Bulletin, Series C: Electrical Engineering*, vol. 73, no. 2, pp. 153–166, 2011.

[5] E. Farantatos, G. Stefopoulos, G. Cokkinides, and A. Meliopoulos, "Pmu-based dynamic state estimation for electric power systems," in *Power Energy Society General Meeting, 2009. PES '09. IEEE*, July 2009, pp. 1–8.

[6] Z. Huang, P. Du, D. Kosterev, and S. Yang, "Generator dynamic model validation and parameter calibration using phasor measurements at the point of connection," *Power Systems, IEEE Transactions on*, vol. 28, no. 2, pp. 1939–1949, May 2013.

[7] L. Fan and Y. Wehbe, "Extended kalman filtering based real-time dynamic state and parameter estimation using pmu data," *Electric Power Systems Research*, vol. 103, pp. 168–177, 2013.

[8] E. Ghahremani and I. Kamwa, "Dynamic state estimation in power system by applying the extended kalman filter with unknown inputs to phasor measurements," *Power Systems, IEEE Transactions on*, vol. 26, no. 4, pp. 2556–2566, Nov 2011.

[9] Ghahremani and I. Kamwa, "Online state estimation of a synchronous generator using unscented kalman filter from phasor measurements units," *Energy Conversion, IEEE Transactions on*, vol. 26, no. 4, pp. 1099–1108, Dec 2011.

[10] M. Ariff, B. Pal, and A. Singh, "Estimating dynamic model parameters for adaptive protection and control in power system," *IEEE Trans. Power Syst.*, vol. PP, no. 99, pp. 1–11, 2014.

[11] Y. Wehbe, "Model estimation of electric power systems by phasor measurement units data," *Graduate Theses and Dissertations*, 2012.

[12] S. van de Geer, "Least squares estimation," *Encyclopedia of Statistics in Behavioral Science*, vol. 2, pp. 1041–1045, 2005.

[13] H. W. Sorenson, "Least-squares estimation: from gauss to kalman," *Spectrum, IEEE*, vol. 7, no. 7, pp. 63–68, 1970.

[14] E. Wan, R. Van Der Merwe *et al.*, "The unscented kalman filter for nonlinear estimation," in *Adaptive Systems for Signal Processing, Communications, and Control Symposium 2000. AS-SPCC. The IEEE 2000.* IEEE, 2000, pp. 153–158.

[15] P. Yang, Z. Tan, A. Wiesel, and A. Nehora, "Power system state estimation using pmus with imperfect synchronization," *Power Systems, IEEE Transactions on*, vol. 28, no. 4, pp. 4162–4172, Nov 2013.

[16] K. Schneider, Z. Huang, B. Yang, M. Hauer, and Y. Nieplocha, "Dynamic state estimation utilizing high performance computing methods," in *Power Systems Conference and Exposition, 2009. PSCE '09. IEEE/PES*, March 2009, pp. 1–6.

[17] Z. Huang, P. Du, D. Kosterev, and B. Yang, "Application of extended kalman filter techniques for dynamic model parameter calibration," in *Power Energy Society General Meeting, 2009. PES '09. IEEE*, July 2009, pp. 1–8.

[18] Z. Huang, D. Kosterev, R. Guttromson, and T. Nguyen, "Model validation with hybrid dynamic simulation," in *Power Engineering Society General Meeting, 2006. IEEE*, 2006, pp. 9 pp.–.

[19] Z. Huang, K. Schneider, and J. Nieplocha, "Feasibility studies of applying kalman filter techniques to power system dynamic state estimation," in *Power Engineering Conference, 2007. IPEC 2007. International*, Dec 2007, pp. 376–382.

[20] K. Kalsi, Y. Sun, Z. Huang, P. Du, R. Diao, K. Anderson, Y. Li, and B. Lee, "Calibrating multi-machine power system parameters with the extended kalman filter," in *Power and Energy Society General Meeting, 2011 IEEE*, July 2011, pp. 1–8.

[21] M. Burth, G. C. Verghese, and M. VÉlez-Reyes, "Subset selection for improved parameter estimation in on-line identification of a synchronous generator," *Power Systems, IEEE Transactions on*, vol. 14, no. 1, pp. 218–225, 1999.

[22] M. Karrari and O. Malik, "Identification of physical parameters of a synchronous generator from online measurements," *Energy Conversion, IEEE Transactions on*, vol. 19, no. 2, pp. 407–415, June 2004.

[23] C. Lee and O. T. Tan, "A weighted-least-squares parameter estimator for synchronous machines," *Power Apparatus and Systems, IEEE Transactions on*, vol. 96, no. 1, pp. 97–101, Jan 1977.

[24] N. Zhou, D. Meng, Z. Huang, and G. Welch, "Dynamic state estimation of a synchronous machine using pmu data: A comparative study," *Smart Grid, IEEE Transactions on*, vol. PP, no. 99, pp. 1–1, 2014.

[25] H. G. Aghamolki, Z. Miao, L. Fan, W. Jiang, and D. Manjure, "Identification of synchronous generator model with frequency control using unscented kalman filter," *Electric Power Systems Research*, vol. 126, pp. 45–55, 2015.

[26] F. Schweppe and J. Wildes, "Power system static-state estimation, part i: Exact model," *Power Apparatus and Systems, IEEE Transactions on*, vol. PAS-89, no. 1, pp. 120–125, Jan 1970.

[27] F. C. Schweppe and D. B. Rom, "Power system static-state estimation, part ii: Approximate model," *power apparatus and systems, ieee transactions on*, no. 1, pp. 125–130, 1970.

[28] F. C. Schweppe, "Power system static-state estimation, part iii: Implementation," *Power Apparatus and Systems, IEEE Transactions on*, no. 1, pp. 130–135, 1970.

[29] A. Abur and A. G. Exposito, *Power system state estimation: theory and implementation*. CRC Press, 2004.

[30] A. Monticelli, "Electric power system state estimation," *Proceedings of the IEEE*, vol. 88, no. 2, pp. 262–282, 2000.

[31] F. Aminifar, M. Shahidehpour, M. Fotuhi-Firuzabad, and S. Kamalinia, "Power system dynamic state estimation with synchronized phasor measurements," *Instrumentation and Measurement, IEEE Transactions on*, vol. 63, no. 2, pp. 352–363, 2014.

[32] S. Wang, W. Gao, and A. S. Meliopoulos, "An alternative method for power system dynamic state estimation based on unscented transform," *Power Systems, IEEE Transactions on*, vol. 27, no. 2, pp. 942–950, 2012.

[33] C. Rakpenthai, S. Uatrongjit, and S. Premrudeepreechacharn, "State estimation of power system considering network parameter uncertainty based on parametric interval linear systems," *Power Systems, IEEE Transactions on*, vol. 27, no. 1, pp. 305–313, 2012.

[34] H. Sun, F. Gao, K. Strunz, and B. Zhang, "Analog-digital power system state estimation based on information theorypart i: Theory," *Smart Grid, IEEE Transactions on*, vol. 4, no. 3, pp. 1640–1646, 2013.

[35] J. Zhang, G. Welch, G. Bishop, and Z. Huang, "A two-stage kalman filter approach for robust and real-time power system state estimation," *Sustainable Energy, IEEE Transactions on*, vol. 5, no. 2, pp. 629–636, 2014.

[36] M. Nejati, N. Amjady, and H. Zareipour, "A new stochastic search technique combined with scenario approach for dynamic state estimation of power systems," *Power Systems, IEEE Transactions on*, vol. 27, no. 4, pp. 2093–2105, 2012.

[37] G. Valverde and V. Terzija, "Unscented kalman filter for power system dynamic state estimation," *IET generation, transmission & distribution*, vol. 5, no. 1, pp. 29–37, 2011.

[38] A. Al-Othman and M. Irving, "Uncertainty modelling in power system state estimation," in *Generation, Transmission and Distribution, IEE Proceedings-*, vol. 152, no. 2. IET, 2005, pp. 233–239.

[39] Y. Weng, Q. Li, R. Negi, and M. Ilic, "Semidefinite programming for power system state estimation," in *Power and Energy Society General Meeting, 2012 IEEE*. IEEE, 2012, pp. 1–8.

[40] Y. Weng, B. Fardanesh, M. D. Ilic, and R. Negi, "Novel approaches using semidefinite programming method for power systems state estimation," in *North American Power Symposium (NAPS), 2013*. IEEE, 2013, pp. 1–6.

[41] Y. Weng, Q. Li, R. Negi, and M. Ilic, "Distributed algorithm for sdp state estimation," in *Innovative Smart Grid Technologies (ISGT), 2013 IEEE PES*. IEEE, 2013, pp. 1–6.

[42] C. Lu, J. Teng, and W.-H. Liu, "Distribution system state estimation," *Power Systems, IEEE Transactions on*, vol. 10, no. 1, pp. 229–240, 1995.

[43] A. Sakis Meliopoulos and F. Zhang, "Multiphase power flow and state estimation for power distribution systems," *Power Systems, IEEE Transactions on*, vol. 11, no. 2, pp. 939–946, 1996.

[44] M. E. Baran and A. W. Kelley, "A branch-current-based state estimation method for distribution systems," *IEEE transactions on power systems*, vol. 10, no. CONF-940702–, 1995.

[45] H. Wang and N. N. Schulz, "A revised branch current-based distribution system state estimation algorithm and meter placement impact," *Power Systems, IEEE Transactions on*, vol. 19, no. 1, pp. 207–213, 2004.

[46] E. Manitsas, R. Singh, B. C. Pal, and G. Strbac, "Distribution system state estimation using an artificial neural network approach for pseudo measurement modeling," *Power Systems, IEEE Transactions on*, vol. 27, no. 4, pp. 1888–1896, 2012.

[47] M. Pau, P. A. Pegoraro, and S. Sulis, "Efficient branch-current-based distribution system state estimation including synchronized measurements," *Instrumentation and Measurement, IEEE Transactions on*, vol. 62, no. 9, pp. 2419–2429, 2013.

[48] R. Singh, B. Pal, and R. Jabr, "Choice of estimator for distribution system state estimation," *IET generation, transmission & distribution*, vol. 3, no. 7, pp. 666–678, 2009.

[49] D. A. Haughton and G. T. Heydt, "A linear state estimation formulation for smart distribution systems," *IEEE Transactions on Power Systems*, no. 28, pp. 1187–1195, 2013.

[50] R. Singh, B. Pal, and R. Jabr, "Distribution system state estimation through gaussian mixture model of the load as pseudo-measurement," *IET generation, transmission & distribution*, vol. 4, no. 1, pp. 50–59, 2010.

[51] Y. Deng, Y. He, and B. Zhang, "Branch-estimation-based state estimation for radial distribution systems," in *Power Engineering Society Winter Meeting, 2000. IEEE*, vol. 4. IEEE, 2000, pp. 2351–2356.

[52] F. Chowdhury, J. P. Christensen, and J. L. Aravena, "Power system fault detection and state estimation using kalman filter with hypothesis testing," *Power Delivery, IEEE Transactions on*, vol. 6, no. 3, pp. 1025–1030, 1991.

[53] L. Jia, R. J. Thomas, and L. Tong, "On the nonlinearity effects on malicious data attack on power system," in *2012 IEEE Power and Energy Society General Meeting*. IEEE, 2012, pp. 1–8.

[54] E. Handschin, F. C. Schweppe, J. Kohlas, and A. Fiechter, "Bad data analysis for power system state estimation," *Power Apparatus and Systems, IEEE Transactions on*, vol. 94, no. 2, pp. 329–337, 1975.

[55] A. Monticelli, F. F. Wu, and M. Yen, "Mutiple bad data identification for state estimation by combinatorial optimization," *Power Delivery, IEEE Transactions on*, vol. 1, no. 3, pp. 361–369, 1986.

[56] H. Zhu and G. B. Giannakis, "Robust power system state estimation for the nonlinear ac flow model," in *North American Power Symposium (NAPS), 2012*. IEEE, 2012, pp. 1–6.

[57] R. A. Jabr, "Radial distribution load flow using conic programming," *Power Systems, IEEE Transactions on*, vol. 21, no. 3, pp. 1458–1459, 2006.

[58] ——, "A conic quadratic format for the load flow equations of meshed networks," *Power Systems, IEEE Transactions on*, vol. 22, no. 4, pp. 2285–2286, 2007.

[59] R. Jabr and B. Pal, "Ac network state estimation using linear measurement functions," *Generation, Transmission & Distribution, IET*, vol. 2, no. 1, pp. 1–6, 2008.

[60] B. Kocuk, S. S. Dey, and X. A. Sun, "Strong socp relaxations for the optimal power flow problem," *ArXiv e-prints*, 2015.

[61] H. Hijazi, C. Coffrin, and P. Van Hentenryck, "Polynomial sdp cuts for optimal power flow," *arXiv preprint arXiv:1510.08107*, 2015.

[62] V. Kekatos and G. Giannakis, "Distributed robust power system state estimation," *Power Systems, IEEE Transactions on*, vol. 28, no. 2, pp. 1617–1626, 2013.

[63] Z. Miao, L. Fan, H. G. Aghamolki, and B. Zeng, "Least square estimation-based sdp cuts for socp relaxation of ac opf," *Automatic Control, IEEE Transactions on*, 2016 (Submitted).

[64] S. S. Haykin, S. S. Haykin, and S. S. Haykin, *Kalman filtering and neural networks*. Wiley Online Library, 2001.

[65] J. J. Hyun and L. Hyung-Chul, "Analysis of scaling parameters of the batch unscented transformation for precision orbit determination using satellite laser ranging data," *Journal of Astronomy and Space Sciences*, vol. 28, no. 3, pp. 183–192, 2011.

[66] S. Julier, "The scaled unscented transformation," in *American Control Conference, 2002. Proceedings of the 2002*, vol. 6, 2002, pp. 4555–4559 vol.6.

[67] S. Julier, J. K. Uhlmann, and H. Durrant-Whyte, "A new approach for filtering nonlinear systems," in *American Control Conference, Proceedings of the 1995*, vol. 3, Jun 1995, pp. 1628–1632 vol.3.

[68] S. Julier, J. Uhlmann, and H. Durrant-Whyte, "A new method for the nonlinear transformation of means and covariances in filters and estimators," *Automatic Control, IEEE Transactions on*, vol. 45, no. 3, pp. 477–482, Mar 2000.

[69] S. J. Julier and J. K. Uhlmann, "New extension of the kalman filter to nonlinear systems," in *AeroSense'97*. International Society for Optics and Photonics, 1997, pp. 182–193.

[70] H. Jouni and S. Simo, "Optimal filtering with kalman filters and smoothers. manual for matlab toolbox ekf/ukf," *Helsinki University of Technology, Department of Biomedical Engineering and Computational Science*, 2008.

[71] P. Kundur, N. J. Balu, and M. G. Lauby, *Power system stability and control*. McGraw-hill New York, 1994, vol. 7.

[72] D. Kosterev, "Hydro turbine-governor model validation in pacific northwest," *Power Systems, IEEE Transactions on*, vol. 19, no. 2, pp. 1144–1149, May 2004.

[73] H. G. Aghamolki, Z. Miao, and L. Fan, "Joint ac network state estimation and bad data identification using strengthened second-order conic programming relaxation," *Smart Grid, IEEE Transactions on*, 2016 (Submitted).

[74] ——, "A hardware-in-the-loop scada testbed," in *North American Power Symposium (NAPS), 2015*. IEEE, 2015, pp. 1–6.

[75] Y. Wehbe, L. Fan, and Z. Miao, "Least squares based estimation of synchronous generator states and parameters with phasor measurement units," in *North American Power Symposium (NAPS), 2012*. IEEE, 2012, pp. 1–6.

[76] L. Fan, Z. Miao, and Y. Wehbe, "Application of dynamic state and parameter estimation techniques on real-world data," *Smart Grid, IEEE Transactions on*, vol. 4, no. 2, pp. 1133–1141, 2013.

[77] O. Kosut, L. Jia, R. J. Thomas, and L. Tong, "Malicious data attacks on the smart grid," *IEEE Transactions on Smart Grid*, vol. 2, no. 4, pp. 645–658, 2011.

[78] H. Zhu and G. B. Giannakis, "Estimating the state of ac power systems using semidefinite programming," in *North American Power Symposium (NAPS), 2011*. IEEE, 2011, pp. 1–7.

[79] X. Bai, H. Wei, K. Fujisawa, and Y. Wang, "Semidefinite programming for optimal power flow problems," *International Journal of Electrical Power & Energy Systems*, vol. 30, no. 6, pp. 383–392, 2008.

[80] X. Bai and H.-Y. Wei, "Semi-definite programming-based method for security-constrained unit commitment with operational and optimal power flow constraints," *Generation, Transmission & Distribution, IET*, vol. 3, no. 2, pp. 182–197, 2009.

[81] S. Bose, D. F. Gayme, S. Low, and K. M. Chandy, "Optimal power flow over tree networks," in *Communication, Control, and Computing (Allerton), 2011 49th Annual Allerton Conference on*. IEEE, 2011, pp. 1342–1348.

[82] S. Sojoudi and J. Lavaei, "Physics of power networks makes hard optimization problems easy to solve," in *Power and Energy Society General Meeting, 2012 IEEE*. IEEE, 2012, pp. 1–8.

[83] A. Gomez Esposito and E. R. Ramos, "Reliable load flow technique for radial distribution networks," *Power Systems, IEEE Transactions on*, vol. 14, no. 3, pp. 1063–1069, 1999.

[84] W. Xu, M. Wang, J.-F. Cai, and A. Tang, "Sparse error correction from nonlinear measurements with applications in bad data detection for power networks," *Signal Processing, IEEE Transactions on*, vol. 61, no. 24, pp. 6175–6187, 2013.

[85] K. Mehlhorn and D. Michail, "Implementing minimum cycle basis algorithms," *Journal of Experimental Algorithmics (JEA)*, vol. 11, pp. 2–5, 2007.

[86] T. Kavitha, C. Liebchen, K. Mehlhorn, D. Michail, R. Rizzi, T. Ueckerdt, and K. A. Zweig, "Cycle bases in graphs characterization, algorithms, complexity, and applications," *Computer Science Review*, vol. 3, no. 4, pp. 199–243, 2009.

[87] H. J. Greenberg, "Greedy algorithms for minimum spanning tree," *University of Colorado at Denver*, 1998.

[88] M. Grant, S. Boyd, and Y. Ye, "Cvx: Matlab software for disciplined convex programming," 2008.

[89] A. MOSEK, "The mosek optimization toolbox for matlab manual, version 7.1 (revision 28)," *ht tp://mosek. com,(accessed on March 20, 2015)*, 2015.

[90] R. D. Zimmerman, C. E. Murillo-Sánchez, and R. J. Thomas, "Matpower: Steady-state operations, planning, and analysis tools for power systems research and education," *Power Systems, IEEE Transactions on*, vol. 26, no. 1, pp. 12–19, 2011.

[91] A. Abur and F. H. Magnago, "Optimal meter placement for maintaining observability during single branch outages," *Power Systems, IEEE Transactions on*, vol. 14, no. 4, pp. 1273–1278, 1999.

[92] Y. Wehbe and L. Fan, "Pmu-based system identification for a modified classic generator model," in *North American Power Symposium (NAPS), 2015*, Oct 2015, pp. 1–6.

[93] I. A. Hiskens and M. Pai, "Trajectory sensitivity analysis of hybrid systems," *Circuits and Systems I: Fundamental Theory and Applications, IEEE Transactions on*, vol. 47, no. 2, pp. 204–220, 2000.

[94] E. L. Geraldi, T. C. Fernandes, and R. A. Ramos, "Estimation of synchronous generator model parameters operating under unbalanced three-phase conditions," in *Power & Energy Society General Meeting, 2015 IEEE.* IEEE, 2015, pp. 1–5.

[95] S. Boyd, N. Parikh, E. Chu, B. Peleato, and J. Eckstein, "Distributed optimization and statistical learning via the alternating direction method of multipliers," *Foundations and Trends® in Machine Learning*, vol. 3, no. 1, pp. 1–122, 2011.

[96] S.-J. Kim, "Online power system state estimation using alternating direction method of multipliers," in *Power & Energy Society General Meeting, 2015 IEEE.* IEEE, 2015, pp. 1–5.

[97] H. Zhu and G. Giannakis, "Multi-area state estimation using distributed sdp for nonlinear power systems," in *Smart Grid Communications (SmartGridComm), 2012 IEEE Third International Conference on.* IEEE, 2012, pp. 623–628.

[98] W. Deng, M.-J. Lai, Z. Peng, and W. Yin, "Parallel multi-block admm with o (1/k) convergence," *arXiv preprint arXiv:1312.3040*, 2013.

APPENDIX A

LIST OF ABBREVIATIONS

μG	Micro-Grid
AC	Alternative Current
ADMM	Alternating Direction Method of multipliers
DC	Direct Current
DER	Distributed Energy Resources
DSE	Dynamic State Estimation
SSE	Static State Estimation
EPRI	Electric Power Research Institute
IEEE	Institute of Electrical and Electronics Engineers
IT	Information Technology
LNRT	Largest Normalize Residue Test
OPF	Optimal Power Flow
PMU	Phasor Measurement Unit
SDP	Semi-Definite Programming
SE	State Estimation
SOCP	Second Order Conic Programming
SSE	Static State Estimation
WAMC	Wide Area Measurement and Control

APPENDIX B

MATLAB CODE FOR JOINT OPTIMIZATION ALGORITHM

```
%% Define the system
mpc=nesta_case14_ieee;

%% Calulate System Matrices
[Ybus, Yf, Yt] = makeYbus(mpc);
%% Creat initial conditions and measurement matrix
Rp=ones(Nline,1);
Ip=zeros(Nline,1);
u(:,1)=ones(Nbus,1);
R(:,1)=ones(Nline,1);
I(:,1)=zeros(Nline,1);
delta(:,1)=zeros(Nbus,1);
Psch=(Pg-Pd);
Qsch=(Qg-Qd);

%% Solve convex SCOP based SE to find initial guess for SE problem

SE_coop_coop;

%% Run algorithm for number of iterations
```

```
for i=1:4

%% Solve joint algorithm and find the optimal solution for SOCP based SE

cvx_begin
variables R2(20,1) I2(20,1) u2(14,1) e(122,1) O(122,1)
 minimize norm(e,2)+Lambda*norm(O,1)
 subject to

 for it=1:Nbus
  G(it,it)*u(it)+sum(G(w,it).*R(r)-B(w,it).*I(r))+e(it)-O(it)==P(it);
 -B(it,it)*u(it)-sum(B(w,it).*R(r)+G(w,it).*I(r))+e(14+it)-O(14+it)==Q(it);
 end

 for k=1:Nline
    norm([R(k),I(k),(u(L(k,1))-u(L(k,2)))/2],2) <= (u(L(k,1))+u(L(k,2)))/2;
    g(k).*u(L(k,1))-g(k).*R(k)+b(k).*I(k14)+e(42+k)-O(42+k)==PFlow(k,1);
   -(b(k)+b_sh(k)/2).*u(L(k,1))
                      +b(k).*R(k)+g(k).*I(k)+e(62+k14)-O(62+k)==Qflow(k,1);
 end

%% Separate cutting planes by LSE-based SDP seperation

[alpha_i{1,it},aa_i{1,it},Z_i2{1,it}]=Cut_SDP(L,Ip,Rp,up,bus);
  for kk3=1:iii2
```

```
    for jj3=1:size(alpha_i2{1,kk3},2)
        alpha_i2{1,kk3}{1,jj3}*(Z2-Z_i2{1,kk3}{1,jj3}) <= 0;
    end
  end
cvx_end


end
```

APPENDIX C

REUSE PERMISSION OF PUBLISHED PAPERS IN CHAPTER 3

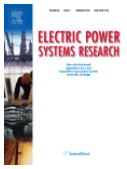

Title: Identification of synchronous generator model with frequency control using unscented Kalman filter

Author: Hossein Ghassempour Aghamolki,Zhixin Miao,Lingling Fan,Weiqing Jiang,Durgesh Manjure

Publication: Electric Power Systems Research

Publisher: Elsevier

Date: September 2015

Order Completed

Thank you for your order.

This Agreement between Hossein G Aghamolki ("You") and Elsevier ("Elsevier") consists of your license details and the terms and conditions provided by Elsevier and Copyright Clearance Center.

Your confirmation email will contain your order number for future reference.

Get the printable license.

License Number	3957281141776
License date	Sep 27, 2016
Licensed Content Publisher	Elsevier
Licensed Content Publication	Electric Power Systems Research
Licensed Content Title	Identification of synchronous generator model with frequency control using unscented Kalman filter
Licensed Content Author	Hossein Ghassempour Aghamolki,Zhixin Miao,Lingling Fan,Weiqing Jiang,Durgesh Manjure
Licensed Content Date	September 2015
Licensed Content Volume	126
Licensed Content Issue	n/a
Licensed Content Pages	11
Type of Use	reuse in a thesis/dissertation
Portion	full article
Format	both print and electronic
Are you the author of this Elsevier article?	Yes
Will you be translating?	No
Order reference number	
Title of your thesis/dissertation	PMU based States and Parameters Estimation in power system
Expected completion date	Dec 2016
Estimated size (number of pages)	100
Elsevier VAT number	GB 494 6272 12
Requestor Location	Hossein G Aghamolki ENB 322, 4202 E Fowler Ave Smart Grid Lab University of South Florida TAMPA, FL 33620 United States Attn: Hossein G Aghamolki

ABOUT THE AUTHOR

He obtained his Bachelor's degree and master's degree both in Electrical Engineering from Power and Water University of Technology in 2007 and Mazandaran University in 2010, respectively. He received his Ph.D. degree in Electrical Engineering from the University of South Florida, Tampa, FL in December 2016. He has worked as power market analyst at Iran Grid Management Company (Iran ISO), Tehran, Iran from 2008 to 2013. His research interests include power system analysis, modeling, dynamics, state estimation, and optimization as well as distributed optimization and control in smart grids.